Identification of subject-specific parameters of a Hill-type muscle-tendon model for simulations of human motion

Anke VAN CAMPEN

Jury:
Prof. dr. ir. J. Berlamont, voorzitter
Prof. dr. ir. J. De Schutter, promotor
Prof. dr. I. Jonkers, promotor
dr. ir. F. De Groote, co-promotor
Prof. dr. ir. G. Pipeleers
Prof. dr. ir. J. Vander Sloten
Prof. dr. ir. J. Swevers
Prof. dr. ir. M. de Zee
(Aalborg University)

Proefschrift voorgedragen tot
het behalen van de graad
van Doctor in de
Ingenieurswetenschappen

January 2014

D/2014/7515/7
ISBN 978-94-6018-783-4

Nobody said it was easy
No one ever said it would be so hard.

– Coldplay, *The Scientist*

General acknowledgments

I hereby thank in random order

For the main scientific support: Joris De Schutter and Friedl De Groote. For (partially) reading and (constructively) critisizing this manuscript: respective Members of the Jury. For the (emergency) support either scientific or technical: Steven Bellens, Tinne De Laet, Wilm Decre, Lode Bosmans, Amar Kumar Behera, Max Boegli, Keivan Zavari, Maarten Witters, and -last but not least- professor G. Jean-Pierre Merckx and Jan Thielemans too. For being the owners of a pair of (symbolic) running shoes: Anouk Bosmans, Goele Pipeleers, Joris, Wouter Dekeyser, Friedl, Keivan, Max, Maarten, Clara Verhelst, Myriam Verschuure. For being very helpfull secretaries: Lieve Notre, Karin Dewit and the others whose number has exponentially grown over the last year. For offering me, voluntary or unvoluntary, olives during lunch: mainly Max, but also Keivan. For being *good* master thesis students: Sam Van Rossom, Anneleen De Bruyn and Ward Vermeulen. For all that valuable small and BIG support at discrete instants in time considering the last lustrum of my life (mainly because I don't remember the previous five that well): Nina Van Campen and Wim Spaepen, Dirk Van Campen, Jesse Stroobants, Sabine Bervoet and Marc Pauwels, Marie-Paule Wijns, Frank Bastiaens, Robby Huygen. For those I forgot to mention: I'm sorry.
For being home when I come home: Maarten and Walter.

Anke$^{\circ\circ\circ}$

Abstract

Biomechanical analyses of human motion (e.g. gait) often rely on computer simulations based on musculoskeletal models. A musculoskeletal model describes how muscles produce force, how this force is transferred by the tendons to the skeleton, and how the skeleton moves as a result. The better a musculoskeletal model is in agreement with a certain subject/patient, the more reliable the outcomes of simulations will be. This is of huge importance when clinical decisions would be based on these simulations. A long term goal of the biomechanical society is to evolve to subject-specific modeling: creating a musculoskeletal model of any patient would obviously be beneficial. Yet, it is not straightforward to collect the information necessary to build these subject-specific models. Currently, most analyses are based on a generic model constructed using data collected in cadavers of old subjects. Musculoskeletal geometry can be extracted *in vivo* using Magnetic Resonance imaging, but it is not possible to determine the parameters describing the force generating capacity of the muscle-tendon (MT-) actuators *in vivo* in Hill-type models. Hence, these parameters should be obtained through optimization techniques which rely on experimentally obtained subject-specific information on the angle-moment relationship of specific muscle groups. This relationship typically results from dynamometer experiments.

It has been shown that dynamometer data contain information about the muscle-tendon parameters that are important to accurately simulate gait. This is the starting point of this thesis. The focus in this thesis is on the actuators of the knee joint. A first pair of contributions are made towards more accurate experimental measurements of the knee joint moment based on dynamometry. To this end, geometry-based knee axes of rotation and motion-based (functional) knee axes of rotation resulting from different algorithms are compared. The estimated axes' poses are validated based on imaging techniques. It resulted that motion-based axes better represent the actual knee joint axis than geometry-based axes. As a second contribution, an extended dynamometer setup allowing more accurate measurement of the knee angle-moment relationship has been developed:

segment kinematics are tracked based on (skin mounted) markers, while a load cell gives information on three dimensional (3D) reaction forces and moments. This allows us to perform a 3D inverse dynamic analysis to obtain the reaction moment in the knee joint. Calculations are based on a model of the lower limb in which the knee joint axis is defined as a motion-based axis. Knee moments resulting from the inverse dynamic analysis are compared to 2D dynamometer data. Maximum differences between the calculated moments and the moments as registered by the dynamometer were between 10Nm and 25Nm for isometric dynamometry, which shows the relevance of this contribution.

The third contribution is the description of the inter-dependency of the two most crucial (for a motion simulation point of view) muscle-tendon parameters for the knee joint actuators, being the tendon slack length and the optimal muscle fiber length. This finding turns out to be crucial for the fourth contribution of this thesis, being the development of an estimation method for these parameters.

The fourth contribution is the development and validation (in a simulation environment) of a method for the estimation of muscle-tendon parameters of the knee joint actuators based on isometric dynamometry. The algorithm aims at estimating the tendon slack length and the optimal muscle fiber length. The method relies on the use of *a priori* physiological knowledge to define a physiologically feasible set and constraints for the optimization. A new set of optimization variables is introduced which greatly improves the numerical condition of the optimization. The estimation method comprised a heuristic phase to determine the physiologically feasible set and the hot start for the non-linear constrained optimization problem. The optimization minimizes the difference between the experimentally obtained moment and the simulated moment. The influence of the initial guess and measurement noise was studied in simulation and compared to the performance of the method presented by Garner and Pandy (2003). The new method shows a low dependency on the initial guess, and outperformed the method of Garner and Pandy (2003) in terms of accuracy by at least one order of magnitude when parameters were estimated from noisy data.

A last contribution of the thesis describes the added value of subject-specific parameters for simulation of human movements based on two case studies. The subjects were power athletes, hence they belonged to a specific sub-group of the population. For both subjects four musculoskeletal models are constructed: a model with linearly scaled geometry and muscle-tendon parameters, a model with linearly scaled geometry and identified MT-parameters , a model with image-based geometry and linearly scaled MT-parameters, and finally a model with image-based geometry and identified MT-parameters. Three movements are evaluated for each model: isokinetic dynamometry at $30^\circ/s$,

a gait trial at 4km/h, and a countermovement jump. The dynamometry allowed us to investigate the effect of including subject-specific parameters of knee joint actuators on the level of the knee joint alone, whereas walking and jumping allowed us to study the influence of local improvements on other joints (as joints are linked by bi-articular muscles). The main finding of this study was that musculoskeletal modeling benefits more from including the subject-specific MT-parameters than from subject-specific geometric features. Also, the importance was more pronounced for the motions which require more force. It was also the first time that the performance of musculoskeletal models including image-based geometry and subject-specifically estimated MT-parameters has been evaluated.

Samenvatting

Biomechanische analyses van menselijke beweging (zoals bijvoorbeeld gaan) steunen vaak op computersimulaties dewelke steunen op musculoskeletale modellen. Een musculoskeletaal model beschrijft de krachtproductie in spieren, hoe deze spierkrachten via de pezen worden overgedragen op het skelet, en op welke manier het skelet hierdoor gaat bewegen. Hoe beter de specifieke eigenschappen van een patiënt beschreven zijn in het musculoskeletale model, hoe meer betrouwbaar de resultaten van de simulaties zullen zijn. Het belang hiervan is groot wanneer klinische beslissingen gebaseerd zouden worden op de simulaties. Biomechanici streven ernaar om op lange termijn te evolueren naar subject-specifieke modellering omdat het definiëren van een musculoskeletaal model van elke patiënt uiteraard ten voordele is van de patiënt zelf. Het is echter niet vanzelfsprekend alle informatie te verzamelen die nodig is om zulke subject-specifieke modellen op te stellen. Daarom zijn de meeste analyses nog steeds gebaseerd op een generisch model dat is opgesteld aan de hand van data van kadavers van oudere personen.

Daar waar musculoskeletale geometrie wel *in vivo* kan afgeleid worden uit magnetische-resonantiebeelden, is het erg moeilijk tot zelfs onmogelijk om *in vivo* de parameters van spier-peesmodellen, te achterhalen. Een manier om deze parameters te bepalen is door gebruik te maken van optimalisatietechnieken. Optimalisatietechnieken maken gebruik van experimenteel opgemeten subject-specifieke informatie over de moment-hoekrelatie van specifieke spiergroepen. Deze moment-hoekrelatie kan bijvoorbeeld bekomen worden via dynamometrie.

Er is reeds aangetoond dat dynamometriedata informatie bevatten over de spier-peesparameters dewelke de nauwkeurigheid van gangsimulaties het meeste beïnvloeden.

De twee eerste bijdragen zijn gemaakt met het oog op het bekomen van nauwkeurigere experimentele metingen van het kniemoment gebruikmakend van dynamometrie. Hiervoor werden geometriegebaseerde rotatie-assen en bewegingsgebaseerde (functionele) rotatie-assen berekend via verschillende algoritmes vergeleken. De geschatte poses van de assen zijn vervolgens gevalideerd

met beeldvormingstechnieken. De resultaten toonden dat de bewegingsgebaseerde assen een betere schatting opleverden dan geometrie-gebaseerde assen van de werkelijke knie-as. Daarnaast werd een uitgebreide dynamometer-testopstelling ontwikkeld dewelke toelaat nauwkeurigere metingen van de moment-hoekrelatie ter hoogte van het kniegewricht te bekomen. De testopstelling omvatte het registreren van de segmentale kinematica gebaseerd op huidmarkers terwijl een krachtsensorinformatie registreerde met betrekking tot drie-dimensionale reactiekrachten en -momenten. Dit liet ons toe een volledige 3D-inverse analyse uit te voeren om het reactiemoment in het kniegewricht te berekenen. De berekeningen zijn gebaseerd op een model van het been waarin het kniegewricht gedefinieerd is als een bewegingsgebaseerde as. Kniemomenten volgen uit de inverse dynamische analyse en werden vergeleken met de 2D-dynamometer data. Maximale verschillen tussen de berekende momenten en de geregistreerde momenten varieerden tussen 10Nm en 25Nm voor isometrische dynamometrie. Dit toont het belang van deze bijdrage aan.

De derde bijdrage in deze thesis is de beschrijving van de afhankelijkheid tussen de twee meest cruciale spier-peesparameters voor de actuatoren van het kniegewricht. Deze parameters zijn de optimale spiervezellengte en de pees-slacklengte (de lengte van de pees waarbij krachtoverdracht op het skelet begint). Deze bevinding is in eerste instantie belangrijk geweest voor de vierde bijdrage in deze thesis. De afhankelijkheid zou echter ook meer algemeen aangewend kunnen worden bij het schalen van spier-peesparameters.

De vierde bijdrage in deze thesis is de ontwikkeling en validatie (in een simulatie omgeving) van een methode voor de schatting van de spier-pees parameters van de actuatoren van het kniegewricht op basis van isometrische dynamometrie. Het algoritme tracht de pees slack-lengte en de optimale spiervezellengte te schatten. De methode steunt op *a priori* kennis met betrekking tot fysiologische eigenschappen van de spieren om een fysiologische oplossingsruimte en de beperkingen voor de optimalisatie te definiëren. De introductie van een nieuwe set van optimalisatievariabelen heeft geleid tot een betere numerieke conditie van de optimalisatie. Het schattingsalgoritme omvat een heuristiek waarmee de fysiologische oplossingsruimte en de warme start voor het niet-lineaire optimalisatieprobleem worden bepaald. De optimalisatie minimaliseert het verschil tussen synthetisch gereproduceerde experimentele gewrichtsmomenten en een model-gebaseerd gewrichtsmomenten. De invloeden van de beginschatting van de MT-parameters en meetruis zijn bestudeerd en de prestatie van het nieuwe algoritme is vergeleken met het algoritme zoals beschreven door Garner and Pandy (2003). Het nieuwe algoritme is slechts beperkt afhankelijk van de beginschatting en is in termen van nauwkeurigheid meer dan een grote orde beter dan het algoritme van Garner and Pandy (2003) wanneer de MT-parameters worden geschat op basis van ruizige data.

De laatste bijdrage van deze thesis licht de toegevoegde waarde van het gebruik van subject-specifieke spier-pees parameters toe voor simulaties van menselijke beweging op basis van twee cases. De subjecten waren kracthsporters en behoorden dus tot een specifieke subgroep in de populatie. Voor elk van hen werden vier musculoskeletale modellen opgesteld: een model waarvan de geometrie en de spier-pees parameters lineair geschaald waren, een model waarvan de geometrie gebaseerd was op beeldvorming en de spier-pees parameters lineair geschaald waren, een model waarvan de geometrie linear geschaald was en de spier-pees parameters van de actuatoren van de knie subject-specifiek geschat (functioneel geschaald), en een model waarvan de geometrie gebaseerd was op beeldvorming en waarvan de spier-pees parameters van de actuatoren van de knie subject-specifiek functioneel geschaald waren. Er werden drie bewegingen geëvalueerd: isokinetische dynamometrie aan een snelheid van 30°/s, gaan aan 4km/u, en een krachtsprong. De belangrijkste bevinding van deze studie was dat de simulaties doorgaans voordeel hebben bij de functionele schaling van spier-pees parameters. Het was de eerste keer dat de mogelijkheden van musculoskeletale modellen met beeldgebaseerde geometrie en functioneel geschaalde spier-pees parameters werden geëvalueerd tijdens dynamische simulaties.

Abbreviations and symbols

General abbreviations[1]

2D, 3D, 6D	two-, three-, or six-dimensional
(f)AoR	(functional) Axis of Rotion
BMI	Body Mass Index
CE	Contractile Element
CIA	Classic Inverse Approach
COM	Centre of Mass
DOF	Degree Of Freedom
EA	Equivalent Axis
EPI	transepicondylar axis
EMG	electromyography
FD	Forward Dynamics
FHA	Finite Helical Axis
Fim	Fisher information matrix
GaL	sphere fitting technique of Gamage and Lasenby [41]
GEO	geometry-based
GRF	Ground Reaction Force
ID	Inverse Dynamics
IK	Inverse Kinematics
ISB	International Society of Biomechanics

[1] General abbreviations are listed below. Those abbreviations appearing only locally are left out of this list.

M2D,M3D	moment resulting from 2D, 3D inverse dynamics
Mdyn	moment resulting from the dynamometer
MR(I)	Magnetic Resonance (Imaging)
MS	Musculoskeletal
MT	Muscle-tendon
MVC	Mean Voluntary Contraction
NLP	Non-linear Optimization Problem
PCSA	Physiological Cross Sectional Area
PE	Passive Element
PIA	Physiological Inverse Approach
RMS	Root Mean Square
ROM	Range of Motion
SARA	Axis transformation algorithm of Ehrig et al. [37]
STA	Soft Tissue Artefacts

General symbols[2]

$\underset{\sim}{(.)}$	prediction of (.)
$\widetilde{(.)}$	normalized (.)
$\alpha_{(\mathrm{opt})}$	(optimal) pennation angle
Δ (.)	change in (.)
$\delta_{\max}$	(maximum) distance to regression line
ϵ_{t}	tendon strain
$\tau_{(\mathrm{de})\mathrm{act}}$	(de)activation time constant
a	activation
$\mathrm{F}_{\mathrm{act}}$	active muscle force
$\mathbf{F}_{\mathrm{knee}}$	reaction forces at the knee
$\mathrm{F}_{\mathrm{m/t}}$	muscle/tendon force
$\mathrm{F}_{\mathrm{m}}^{\max}$	maximum isometric muscle force
F_{mt}	muscle-tendon force
$\mathrm{F}_{\mathrm{pas}}$	passive muscle force
$\mathbf{F}_{\mathrm{tc}}$	interaction force between tibia and crank
f_{v}	velocity-dependent force
$\mathrm{L}_{\mathrm{m}}^{(\mathrm{opt})}$	(optimal) muscle fiber length
L_{t}	muscle-tendon length
$\mathrm{L}_{\mathrm{t}(^{\mathrm{s}}}$	tendon (slack) length
m	mass
p	parameter
$\mathbf{q}$, $\dot{\mathbf{q}}$, $\ddot{\mathbf{q}}$	generalized position, velocity, acceleration
${}^{b}_{a}\mathbf{R}$	rotation/orientation from frame a to frame b

[2]General symbols are listed below. Those symbols appearing only locally are left out of this list.

$(\mathrm{M})\mathrm{S}^{e}_{(\mathrm{rel})}$	(relative) (Moment-) sensitivity
${}^{b}_{a}\mathbf{T}$	transformation from frame a to frame b
${}_{a}\mathbf{t}^{a,b}$	translation from frame b to frame a expressed in frame a
u	exciation
$\mathrm{v}_{\mathrm{m}}^{\max}$	(maximum) muscle contraction velocity
w_{m}	muscle width
$\mathbf{y}$	measurement output

$d = 1 \ldots D$	number of degrees of freedom included
$i = 1 \ldots I$	number of time instants
$j = 1 \ldots J$	number of muscles included
$k = 1 \ldots K$	number of experiments included
$p = 1 \ldots P$	number of parameters included
$s = 1 \ldots S$	number of segments included

MUSCLES

BFL/S	m. biceps femoris long/short head
Gas	m. gastrocnemius
GL/M	m. gastrocnemius lateral/medial
GRA	m. gracilis
HamLat/Med	lateral/medial hamstrings
RF	m. rectus femoris
SM	m. semimembranosus
SOL	m. soleus
ST	m. semitendinosus
TFL	m. tensor fascia latae
VI,VL,VM	m. vastus intermedius, lateralis, medialis

Table of contents

Chapter 1

Introduction

In this introduction biomechanical analysis of human motion is placed in a general framework, and the motivation for this research is given. Furthermore, an overview and the scope of the different chapters in this thesis are given.

1.1 Motivation

Biomechanical analysis for the evaluation of human motion is a valuable tool. The potential applications are very diverse. Probably the applications with the highest added value from a social point of view are the treatments of mobility impairments in order to enhance the individual's quality of life. Yet, up till now, the applicability is restricted to e.g. the design of prostheses or implementation techniques for prostheses (e.g. [45]) or to evaluate post-operatively the effect of skeletal reconstruction (e.g. [98]). Other applications are found in the field of sports and optimisation of sports performances. The tool is used to investigate and gain insight into the influence of orthotics or techniques on specific injuries (e.g. [36; 74]). Although in none of these clinically oriented applications biomechanical analyses are used to make predicitions, in one specific case the tool has been used for this purpose to solve an ethical issue: the specific case of South-African double transtibial amputee and blade runner Oscar Pistorius. Here, biomechanical scientists had to provide an answer to the question whether the blades would being an advantage when competing in regular competition.

This case is worth mentioning, because the different scientists made different conclusions [18; 108]. This is an illustration of the shortcomings in the field of biomechanicals as well as it is an illustration of the challenges biomechanical research faces to evolve from a useful tool to gain general insights in human motion to a valuable *and* a reliable tool for the evaluation of specific cases.

Typically, biomechanical analyses rely on musculoskeletal models which include the description of anatomical features and the description of physiological features. The anatomical features comprise the lengths of the actuators (muscle-tendon lengths), the moment arms, the geometry of the bones, and the lines of action of the actuators. The physiological features comprise description of how muscles produce force and how tendons transfer force. These days, many analyses are still based on the generic model presented by Delp et al. in 1990 [32]. This model represents an average adult male. The data to construct the model's features are extracted from a limited set of cadavers [16; 113]. Obviously, this model cannot provide accurate results for any analysis: both the anatomical as well as the physiological features depend on age, level of activity, and gender of the subject. To compensate for differences in length, often an anthropometric scaling of the different features to the length of the specific segments is done. However, aspects such as bone deformities are not captured, neither does morphologic scaling result in a good representation of the muscle and tendon characteristics [112]. Therefore, biomechanical researchers put many efforts in the development of methodologies which step-by-step allow them to construct subject-specific musculoskeletal models. The ambition of many biomechanical researchers is to come to a moment in time where virtual treatments can be performed based on personalized models. Accurate *a priori* evaluation of the outcome of an intervention would enable clinicians to work out optimal treatment plans. In the mean time, the quest to find methods to increase objective predictions continues. Much progress has already been made concerning the anatomic features (e.g. [84; 100]). Subject-specific definition of anatomic features relies on imaging techniques like magnetic resonance (MR) or computer tomography (CT). This thesis however focuses on describing subject-specific physiological features of muscles and tendons. The difficulty inherent to this aim is that most of these features cannot be obtained from *in vivo* nor from *in vitro* data. Therefore, identification techniques should be applied [62]. Until today, only Garner and Pandy in 2003 [42] and Lloyd and Besier also in 2003 [63] described a method for estimating the muscle-tendon paramters of muscles and tendons of the upper limb and lower limb based on individual strength data. The methods however have not been validated.

This thesis contributes to subject-specific modeling in biomechanical analysis by (i) designing an experimental setup to obtain a more accurate subject-specific angle-moment relationship of the knee joint (chapters 4 and 5), (ii) developing an algorithm for the estimation of the muscle-tendon parameters of the actuators of the knee joint in a simulation environment and comparing its performance to the performance of the algorithm of Garner and Pandy (2003), and (iii) validating the

outcomes of the algorithm using forward and inverse simulation techniques for different types of movement based on two case studies.

1.2 Chapter-by-chapter overview and contributions

Chapter 2: Muscle-tendon modeling and parameter estimation

This chapter explains the general concepts of muscle-tendon modeling and parameter estimation, in order to provide the required background for the remainder of this thesis. Furthermore, the relation between the remaining chapters is explained.

Chapter 3: Sensitivity of dynamic simulations of gait and dynamometer experiments to hill muscle model parameters of knee flexors and extensors

This chapter presents the results of a sensitivity analysis which relies on moment-angle relationships obtained by dynamometry. Dynamometry is a useful experimental setup, because muscle group specific angle-moment relationships can be obtained in a controlled way per individual. The study revealed that dynamometer experiments contain information on muscle-tendon (MT-) parameters. Also, an hierarchy is found in the MT-parameters. As the hierarchy was equivalent for dynamometry and dynamic simulations of gait, dynamometry can be used to obtain experimental data in order to identify the most sensitive parameters to enhance the accuracy of the simulations (further explained in chapters 6 and 7).

This chapter is based on my master thesis [29], and hence it is not a contribution of this thesis. However, it is the foundation for the work presented in the next chapters.

Chapter 4: Functional knee axis based on isokinetic dynamometry data: Comparison of two methods, MRI validation, and effect on knee joint kinematics

This chapter presents the first step towards obtaining more accurate dynamometer data. Experimental dynamometry typically faces problems when it comes to data accuracy. These problems result from the assumption that the moment generated around the joint axis of rotation corresponds to the measured moment around the axis of rotation of the dynamometer. This assumption does not hold for following two reasons: (i) the fixation between the dynamometer device and the body segments is not rigid, and (ii) the pose of the joint axis of rotation is not known. The consequences of the former are that the joint axis of rotation moves relative to the dynamometer axis of rotation,

and the pose of the joint axis of rotation is not known in time. The overall consequence is that the registered moment is not a good representation of the joint moment generated by the muscles around the joint axis of rotation and hence, the strength of the actuators.

In reality, the knee joint axis of rotation is an instantaneous axis i.e. its pose depends on the segmental kinematics and on the load (amount of force produced by the muscles and the external load) [109]. It is however not possible to estimate the joint axis of rotation instanteneously using conventional measurement techniques: kinematic data of the segments (being the postion of the tibia relative to the femur) are typically obtained by skin mounted markers which implies that the data are noisy due to soft tissue artefacts [22]. Alternatively, the joint axis of rotation can be determined based on bone geometry or for a certain range of motion.

The contribution in this thesis is that the validity of geometry-based axes and functional axes (which are motion-based axes) is verified. Many algorithms have already been presented for the estimation of functional knee axes of rotation, none of them have been validated on real data. Therefore, the best performing sphere fitting algorithm and axis transformation algorithm according to simulation studies are applied on real data. The validation relies on the comparison with the pose of equivalent axes which are calculated based on magnetic resonance images (MRI) of the knee in different knee flexion angles and hence, directly reflect the position of the bones.

Chapter 5: An extended dynamometer set-up to improve the accuracy of knee joint moment assessment

This chapter describes a new dynamometer setup which allows us to perform a full three dimensional (3D) inverse dynamic analysis resulting in an improvement of the accuracy of the experimental data for knee joint dynamics.

The contributions in this thesis are twofold. First, the introduction of the combination of 3D motion tracking and the 3D external forces and moments registration allows us to perform the inverse dynamic analysis. Second, the limb model contains a knee joint axis of rotation defined as a functional axis of rotation instead of a geometry-based axis of rotation.

Chapter 6: A new method for estimation of subject-specific muscle-tendon parameters of the knee joint actuators: a simulation study

This chapter describes the identifiability of the muscle-tendon parameters and a new estimation procedure to obtain two subject-specific muscle-tendon parameters per muscle being the optimal muscle fiber length and the tendon slack length. Here, the focus is on the subject-specific definition of the features of the actuators of the knee joint in a simulation environment.

By optimal experimental design, a trade-off between deterministically chosen experimental sets is made. To this end, the experimental cost has to be evaluated in light of the information on the actuators contained in the experiments. In addition, the use of different transformations of the muscle-tendon parameters as variables to be estimated is evaluated.

The estimation procedure is two-phased. In phase I, the feasible set and the initial guess for the non-linear optimisation problem in phase II is defined. In phase II, a constrained non-linear problem is solved by fitting simulated moments and synthetically generated joint moments (simulation of dynamometer experiments). An important feature of the estimation procedure is that the operating range of the muscles is preserved in combination with the use of subject-specific strength-information. The operating ranges are obtained from literature [26]. The strength information is obtained via (simulated) dynamometry experiments. The influence of the initial guess and measurement noise is quantified. The performance of the new algorithm and the algorithm presented by Garner and Pandy [42] are evaluated and compared.

Following contributions are made: (i) a new transformation of muscle-tendon parameters is proposed which enhances the numerical properties of the parameter estimation, and hence allows us to estimate the most crucial muscle-tendon parameters from a minimum set of experiments, (ii) a new estimation algorithm is proposed which performance is evaluated in a simulation environment, and (iii) the performance of the previously presented algorithm of Garner and Pandy [42] is evaluated in a simulation environment to allow a comparison between both methods.

Chapter 7: The added value of the estimation of subject-specific muscle-tendon parameters in musculoskeletal modeling of the knee joint actuators: two case studies

This chapter describes the validation of the parameter estimation procedure as described in chapter 6 on experimental data. To this end, the optimal muscle fiber lengths and tendon slack lengths of the most sensitive knee joint actuators according to De Groote et al. [29] are estimated based on five isometric dynamometer experiments. The input to the optimisation is: the muscle activations which are registered via surface electromyography (EMG), the total length of the actuators and the moment arms, and the remaining MT-parameters (maximum isometric muscle force, pennation angle, and maximum contraction velocity) which are adopted from the generic model [32]. Four musculoskeletal (MS-) models are evaluated for two subjects. The first model includes linearly scaled geometry and linearly scaled MT-parameter values [32; 33]. The second model includes image-based, hence subjec-specific, geometry [84] and linearly scaled MT-parameter values. The third model includes linearly scaled geometry and estimated MT-parameters for the knee joint actuators. The fourth model includes image-based geometry and estimated MT-parameter values for the knee joint actuators. The performances of the MS-models are studied for three conditions being isokinetic dynamometry at 30 °/s, treadmill walking at 4km/h, and countermovement jumping. A forward dynamic analysis is performed (only isokinetic dynamometry) resulting in a predicted knee joint moment which is compared to the experimentally obtained moment, and an inverse dynamic analysis is performed resulting in muscle activations which are compared to experimentally obtained activations.

The main contributions of this study are the evaluation of MS-models including subject-specifically estimated MT-parameters (of knee joint actuators), and the comparison of the performance of MS-models which are subject-specific to a smaller or a greater extent. It is the first time that MS-models including functionally scaled MT-parameters in combination with image-based geometry have been evaluated.

A general schematic overview is provided on the next page.

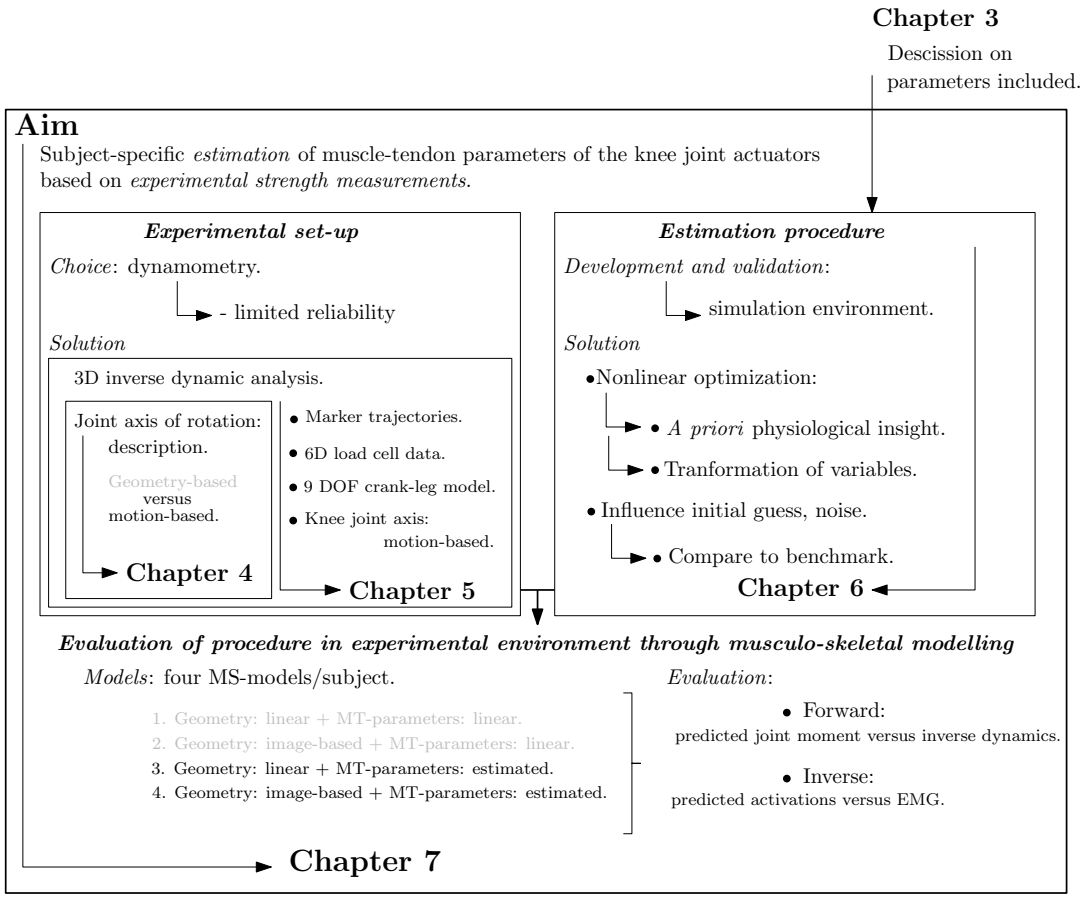
Chapter 3
Descission on
parameters included.
Aim
Subject-specific *estimation* of muscle-tendon parameters of the knee joint actuators based on *experimental strength measurements*.
Experimental set-up
Choice: dynamometry.
- limited reliability
Solution
3D inverse dynamic analysis.
Joint axis of rotation:
description.
Geometry-based
versus
motion-based.
Chapter 4
• Marker trajectories.
• 6D load cell data.
• 9 DOF crank-leg model.
• Knee joint axis:
motion-based.
Chapter 5
Estimation procedure
Development and validation:
simulation environment.
Solution
•Nonlinear optimization:
• *A priori* physiological insight.
• Tranformation of variables.
• Influence initial guess, noise.
• Compare to benchmark.
Chapter 6
Evaluation of procedure in experimental environment through musculo-skeletal modelling
Models: four MS-models/subject.
1. Geometry: linear + MT-parameters: linear.
2. Geometry: image-based + MT-parameters: linear.
3. Geometry: linear + MT-parameters: estimated.
4. Geometry: image-based + MT-parameters: estimated.
Evaluation:
• Forward:
predicted joint moment versus inverse dynamics.
• Inverse:
predicted activations versus EMG.
Chapter 7

Chapter 2

Background on musculoskeletal modeling and simulation, experimental design and experimental system identification

This chapter gives an introduction to muscle-tendon modeling, experimental design, and system identification. The section on muscle-tendon modeling first describes the function and structure of muscles and tendons, then describes different types of muscle-tendon models and modeling techniques. The section on experimental design first describes the concept of dynamometry, its advantages and shortcomings, then describes the concept of experimental design in light of dynamometry and parameter estimation. The last section discusses the basic principles of system identification.

2.1 Muscles and tendons from a physiological perspective

There are three types of muscles in the human body: smooth muscles (e.g. in the organs), cardiac muscles and skeletal muscles. What follows is mainly valid for skeletal muscles.

2.1.1 Muscle function

The function of muscles is twofold. On the one hand muscles produce force which induces motion or resists motion. On the other hand muscles produce heat as a result of their contractile activity to maintain the body temperature. The capacity of muscles to produce force is diverse and depends on the number of fibers, the cross-sectional area, and the pennation angle, which defines the orientation of the muscle fibers with respect to the tendon. In general, the higher the pennation angle, the more powerful a muscle is, because more fibers are arranged in parallel. In contrast, the parallel arrangement of muscle fibers allows larger changes in length. The calf muscle *m. gastrocnemius* is

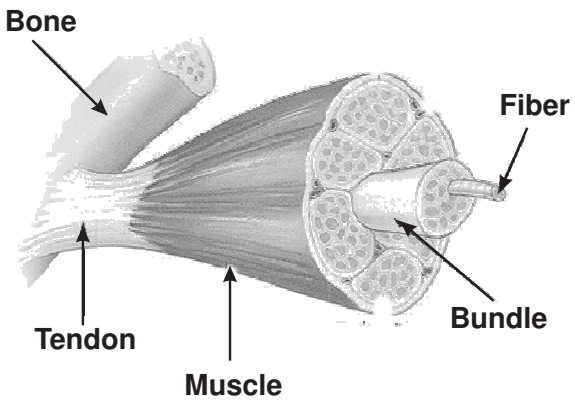

Figure 2.1: A muscle is attached to the bone by a tendon. Muscle fibers form muscle bundles. Muscle bundles and the extracellular matrix form the muscle (figure cfr. [17]).

a highly pennated muscle, whereas the fibers of *m. sartorius*, which supports hip motion and knee flexion, are parallel.

2.1.2 Cellular structure

Intracellular contractile proteins generate force in the muscle fibers. The proteins are arranged into so-called myofilaments which are grouped in bundles (myofibrils). The myofilaments are arranged in sarcomeres, which are the contractile units of a muscle. Sarcomeres contain thin actin filaments at the outer regions, and thick myosin filaments in the inner regions. The heads of the myosin form cross bridges with the actin. The contraction process relies on the interaction between actin and myosin (see figure 2.1).

2.1.3 Contractile process

The change occuring in muscle fiber length is a result of a change in the length of the sarcomeres. During muscle contraction, the myosin cross bridges attach to the actin filaments and flex towards the center of the sarcomere. The muscle shortens, and force is produced (if there is a resistance). Figure 2.2 is a schematic representation of a contracting muscle.

Muscle contraction is regulated by the concentration of calcium in the cytoplasma (the inside of the myofibrils), which enters (contraction) or leaves (relaxation) through the membrane. The binding between actin and myosin relies on the concentration of calcium. There are basically three

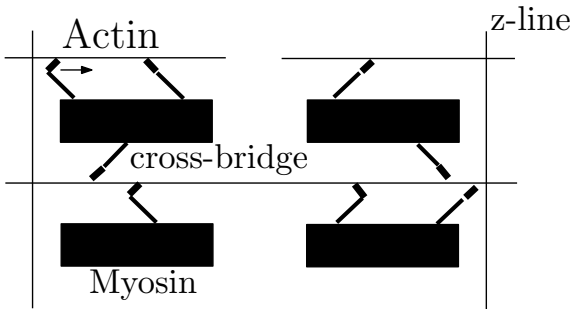

FIGURE 2.2: Schematic representation of a muscle fiber contracting. Actin and myosin filaments form cross-bridges. By flexing inwards the muscle shortens (figure cfr. [17]).

requirements for contraction: (i) interaction between actin and myosin, which is calcium regulated; (ii) the myosin heads have to flex inwards; and (iii) the system must convert chemical energy to mechanical energy.

Muscle contraction is initiated by the transmission of an action potential, an electrical signal which propagates through the nerves, from motor nerves to the muscle. This transmission causes a local depolarisation. The transmission takes place at the neuromuscular junction, which forms the connection between the neural system and the muscular system. The action potential triggers the influx of calcium, which causes the excitation of the muscle fibers.

2.1.4 Tendon function and structure

Tendons consist of fibrous connective tissue called collagen fibers. In contrast to muscles, tendons are not innervated, hence they are a passive structure. The main function of tendons is the transmission of the force produced in the muscles to the bones. This force transfer causes motion.

2.2 Muscle-tendon actuators from a modeling perspective

Muscle-tendon modeling aims at realistically representing muscle forces, hence changes in muscle fiber lengths, due to neural stimulations (muscle excitations). Neural stimulations trigger the influx (and efflux) of calcium, which concentration determines the amount of contraction in the muscle and the force transfer by the tendon to the skeleton. Hence, activation and contraction dynamics are described. Two main model-types are distinguished to describe muscle contraction: the Huxley-type models and the Hill-type models. First in this section, the activation dynamics are explained. Activation and contraction dynamics are the first two submodels in dynamic

musculoskeletal modeling.

2.2.1 Activation dynamics

Muscle fiber activation results from excitation by the central nervous system. The neural excitations determine the number of fibers which will activate, and the level of their activation. The excitation of a muscle is indicated by u. u is a dimensionless measure which reflects the relative number of fully excited muscles. u varies from 0, when a muscle is not excited, to 1, when a muscle is fully excited.

The activation of a muscle, indicated by a, is also dimensionless, and reflects the amount of force a muscle can produce. a varies from 0, when a muscle is not activated, to 1, when a muscle is fully activated. An excited muscle does not instantaneously produces force nor instantaneously stops producing force. Neural excitation of a fiber causes a passive Ca^{++} influx in the fiber. Ca^{++}-influx is a relatively fast process. Ca^{++} enables the muscle to contract. However, the influx of Ca^{++} introduces a time delay between excitation and contraction, because of a limited number of diffusion channels. τ_{act} describes the time delay. When stimulation stops, Ca^{++} is actively transported out of the muscle fiber. Again, there is a time delay between the decay in muscle excitation and the decay in muscle force. This time delay is described by τ_{deact}. As the efflux of Ca^{++} is a relatively slow process, τ_{deact} is larger than τ_{act}.

Hence, activation dynamics describe the transport of calcium through the cell membrane. Two frequently used models are the model of Zajac [120]:

$$\frac{\mathrm{d}a}{\mathrm{d}t} = \frac{1}{\tau_{\text{act}}}\ u - \frac{1}{\tau_{\text{deact}}}\ a + \left(\frac{1}{\tau_{\text{deact}}} - \frac{1}{\tau_{\text{act}}}\right)\ u\ a, \tag{2.1}$$

and the model of Raasch et al. [79]:

$$\frac{\mathrm{d}a}{\mathrm{d}t} = \begin{cases} (u-a)\ \left(\dfrac{u}{\tau_{\text{act}}} + \dfrac{1-u}{\tau_{\text{deact}}}\right) & u \geq a \\ \dfrac{u-a}{\tau_{\text{deact}}} & u < a. \end{cases} \tag{2.2}$$

Both models are nonlinear first-order differential equations. τ_{act} and τ_{deact} are assumed equal for all muscles. The latter model describes the influx and the efflux of Ca^{++} separately in contrast to the former model.

2.2.2 Huxley-type models

The Huxley model is a mechanistic model which is based on the cross bridge theory for contraction. Hence, the model tries to explain the biochemical reactions which underly the attachement and deattachement of actin and myosin. The base model is described in 1957 by Andrew Huxley [50]. Two states are defined to describe the system: either the cross-bridges are attached or the cross-bridges are de-attached. Each attached cross-bridge acts like a spring. The muscle force is then the sum of the contribution of all attached cross-bridges, represented by its stiffness multiplied by the displacement of the spring. Typically, the inputs to the model are the fraction of attached cross-bridges, the muscle fiber lengths and the contraction velocities. The model parameters are the muscle attachement and de-attachement rates. The model equations are partial differential equations which are typically computationally expensive to solve. In practice, the most common used Huxley model is the Distribution Model, which assumes that the spatial distribution of the cross-bridges is Gaussian. This leads to a computational simplification as the model equations are now ordinary differential equations.

Because the base Huxley model assumes a rigid attachement of the contractile elements to the attachement points on the bone, model extensions have been proposed (e.g. [114]) with an added serial elastic element in order to capture the elasticity of the tendon and the muscle itself.

Parameter estimation in cross-bridge models is a complicated problem. Therefore, these models are not often used in musculoskeletal modeling. van den Bogert et al. [107] compared the performance of a Huxley-type model to the performance of a Hill-type model for the simulation of running. Their conclusion was that the Hill-type model was better suited to describe muscle behaviour. The Huxley-type models are also used for studies at the level of single muscle fibers (e.g. [61]).

2.2.3 Hill-type models

The Hill model is a phenomenological model, describing a known relationship between input and output without trying to describe the biochemical mechanisms underlying muscle force production. The base model is described in 1938 by Hill [120]. Commonly, the Hill muscle model has three

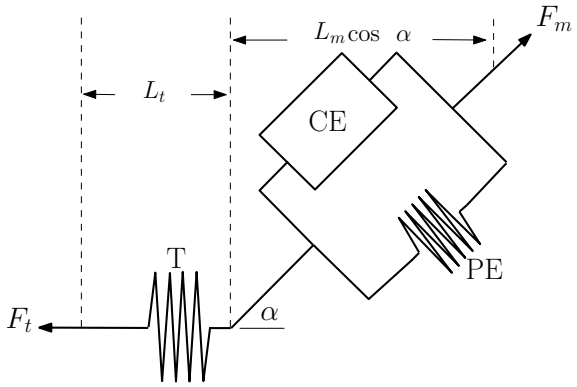

FIGURE 2.3: A schematic representation of the Hill-model. The tendon T is represented by a non-linear spring and has length L_{t}. The muscle is represented by a contractile element CE in parallel with a passive element PE and has length L_{m}. The pennation angle is α.

components: a nonlinear spring representing the tendon, a contractile element representing the active properties (actin-myosin interaction) of the muscle fibers, and a passive elastic element representing the passive properties of the muscle tissue. A schematic representation of the Hill-model is given in figure 2.2.3. The length of the muscle fiber is L_{m}, the length of the tendon is L_{t}, and the length of the muscle-tendon (MT-) actuator is L_{mt}. The angle between the orientation of muscle and tendon fibers is called the pennation angle α. The contraction velocity v_{m} of the muscle fiber is the change of the fiber length over time, i.e. $\dfrac{\mathrm{d}L_{\mathrm{m}}}{\mathrm{d}t}$.

Model parameters

In general, the properties of the muscles and the tendons are captured in four characteristcs describing the relation between the generated (muscle) or transferred (tendon) force in function of the fiber lenght or tendon strain, and the relation between the generated (muscle) force and the contraction velocity. The characteristics are dimensionless as they are scaled by five MT-parameters:

$F_{\mathbf{m}}^{\mathbf{max}}$ is the maximum isometric force a muscle can produce;

$L_{\mathbf{m}}^{\mathbf{opt}}$ is the fiber length at which the muscle produces maximum isometric force;

$v_{\mathbf{m}}^{\mathbf{max}}$ is the maximum contraction velocity of a muscle;

$\alpha_{\mathbf{opt}}$ is the pennation angle at optimal fiber length;

$L_{\mathbf{t}}^{\mathbf{s}}$ is the tendon slack length representing the tendon length at which force transfer starts, hence at which the tendon starts to act as a non-linear spring.

The values of the MT-parameters are muscle-dependent, and subject-specific. In general, the values of the parameters are obtained from cadaver studies [16; 112; 113] and are linearly scaled to the length of the segments [33].

Model parameters as determined by Delp et al. [32]

The frequently used lower limb model of Delp et al. [32] relies on the cadaver studies of [39; 113]. The five model parameters describing Hill-type MT-models are determined as follows:

$F_{\mathbf{m}}^{\mathbf{max}}$ equals the scaled physiological cross-sectional area of the muscle. The scaling factor is the muscle stress which is set to 25N/cm2 for young cadavers [113] and to 61N/cm2 for old cadavers [16]. The physiological cross-sectional area is derived from the muscle's volume.

$L_{\mathbf{m}}^{\mathbf{opt}}$ are derived from the raw fiber lengthts as reported by [113] which are scaled by the ratio of the optimal sarcomere length (2.8μm) as used by [32] and the optimal sarcomere length (2.2μm) as used by [113].

$v_{\mathbf{m}}^{\mathbf{max}}$ is derived from experimental force-length relationships at different fiber length. The maximum contraction velocity is defined at the optimal muscle fiber length [120].

$\alpha_{\mathbf{opt}}$ is measured as the angle formed by the muscle fibers with the line of force exerted by the muscle.

$L_{\mathbf{t}}^{\mathbf{s}}$ is initially chosen so that the muscle is slightly longer than the optimal fiber length at joint angles where passive moment start to develop. Because $L_{\mathrm{t}}^{\mathrm{s}}$ determines the joint angle where the muscle develops peak moment, $L_{\mathrm{t}}^{\mathrm{s}}$ is adapted so that the moment peaks at the corresponding angle obtained through dynamometer experiments (maximum voluntary contractions).

Model parameters as determined by Arnold et al. [7]

The more recently presented lower limb model of Arnold et al. [7] relies on the cadaver study (18 cadavers) of [112]. The five model parameters describing Hill-type MT-models are determined as follows:

$F_{\mathbf{m}}^{\mathbf{max}}$ is considered to be proportional to the physiological cross-sectional area of the muscle and a maximum isometric muscle stress of 61N/cm^2. The physiological cross-sectional area of the

muscle results from the muscle mass, the pennation angle, the density of the muscle and the fiber length.

$L_{\mathbf{m}}^{\mathbf{opt}}$ is calculated as the raw muscle fiber length of the muscle multiplied by the ratio of the optimal sarcomere length (2.7μm) and the mean sarcomere length of the respective muscle fiber.

$v_{\mathbf{m}}^{\mathbf{max}}$ is equivalent to [32].

$\alpha_{\mathbf{opt}}$ is measured as the angle between the fibers and the distal muscle tendon.

$L_{\mathbf{t}}^{\mathbf{s}}$ is determined according to [32].

Model parameters as determined by Modese et al. [69]

The London lower limb model relies on the single cadaver study of [56]. The five model parameters describing Hill-type MT-models are determined as follows:

$F_{\mathbf{m}}^{\mathbf{max}}$ is considered to be proportional to the physiological cross-sectional area of the muscle and a maximum isometric muscle stress of 37N/cm^2.

$L_{\mathbf{m}}^{\mathbf{opt}}$ is calculated as the actual muscle fiber length of a muscle-part multiplied by the ratio of the optimal sarcomere length (2.7μm) and the mean sarcomere length of the respective muscle fiber.

$v_{\mathbf{m}}^{\mathbf{max}}$ is not applicable as no force-velocity characteristics are implemented.

$\alpha_{\mathbf{opt}}$ is determined by calculating the angle of the direction of the muscle fibers and the estimated line of action of the muscle.

$L_{\mathbf{t}}^{\mathbf{s}}$ is set to the measurend length of the tendon.

Model parameters versus muscle-tendon anatomy

For α_{opt} and $F_{\text{m}}^{\text{max}}$ it is obvious that there is a direct relationship between the value of the parameter in the MT-model and the anatomy of the muscle as both can be measured (or can be related to measurable) anatomical features of the muscle-tendon actuator. This holds to a lesser extent for the value of $L_{\text{m}}^{\text{opt}}$, as a prediction of the optimal sarcomere length is needed (see e.g. [26; 60]). However

for $L_{\mathrm{t}}^{\mathrm{s}}$, there is no reflection of an anatomical feature into the determination of the parameter value, which in turn makes it impossible to obtain a physical measurement for the parameter value. As seen in the models of [7; 32], $L_{\mathrm{t}}^{\mathrm{s}}$ is the MT-parameter which is adapted so that the maximum joint moment is produced at a specified joint angle.

Model equations

Muscle contraction dynamics are described by a first order differential equation. The muscle activations are the inputs to the model. The MT-lengths L_{mt} are considered as known features as they follow from skeletal kinematics. The muscle fiber lengths or the muscle-tendon forces are the model states.
The total muscle force F_{m} is the sum of the active muscle force F_{act} and the passive muscle force F_{pas}:

$$F_{\mathrm{m}} = F_{\mathrm{act}}(a, L_{\mathrm{m}}, v_{\mathrm{m}}) + F_{\mathrm{pas}}(L_{\mathrm{m}}). \tag{2.3}$$

F_{act} depends on the activation a, the fiber length L_{m}, and the contraction velocity v_{m}:

$$F_{\mathrm{act}}(a, L_{\mathrm{m}}, v_{\mathrm{m}}) = a\ F_{\mathrm{m}}^{\max}\ f_{\mathrm{act}}^{\mathrm{l}}(\frac{L_{\mathrm{m}}}{L_{\mathrm{m}}^{\mathrm{opt}}})\ f_{\mathrm{act}}^{\mathrm{v}}(\frac{v_{\mathrm{m}}}{v_{\mathrm{m}}^{\max}}), \tag{2.4}$$

with $f_{\mathrm{act}}^{\mathrm{l}}$ the active force-length characteristic, and $f_{\mathrm{act}}^{\mathrm{v}}$ the active force-velocity characteristic. In case the muscle fiber velocity is zero, $f_{\mathrm{act}}^{\mathrm{v}}$ equals one.
F_{pas} only depends on the fiber length L_{m}:

$$F_{\mathrm{pas}}(L_{\mathrm{m}}) = F_{\mathrm{m}}^{\max}\ f_{\mathrm{pas}}^{\mathrm{l}}(\frac{L_{\mathrm{m}}}{L_{\mathrm{m}}^{\mathrm{opt}}}), \tag{2.5}$$

with $f_{\mathrm{pas}}^{\mathrm{l}}$ the passive force-length characteristic.
The tendon force F_{t} depends on the tendon strain ϵ_{t}:

$$F_{\mathrm{t}}(L_{\mathrm{t}}) = F_{\mathrm{m}}^{\max}\ f_{\mathrm{t}}^{\mathrm{l}}(\epsilon_{\mathrm{t}}). \tag{2.6}$$

L_{t} determines the tendon strain:

$$\epsilon_{\mathrm{t}} = \frac{L_{\mathrm{t}} - L_{\mathrm{t}}^{\mathrm{s}}}{L_{\mathrm{t}}^{\mathrm{s}}}. \tag{2.7}$$

The interaction between muscle and tendon is described as follows:

$$F_{\mathrm{t}} = F_{\mathrm{mt}}, \tag{2.8}$$

$$F_{\mathrm{t}} = F_{\mathrm{m}} \ cos\ \alpha, \tag{2.9}$$

$$L_{\mathrm{mt}} = L_{\mathrm{t}} + L_{\mathrm{m}} \ cos\ \alpha, \tag{2.10}$$

$$cos\ \alpha = \sqrt{1 - \left(\frac{w_{\mathrm{m}}}{L_{\mathrm{m}}}\right)^2}, \tag{2.11}$$

$$w_{\mathrm{m}} = L_{\mathrm{m}}^{\mathrm{opt}} \ sin\ \alpha_{\mathrm{opt}}. \tag{2.12}$$

w_{m} is the width of the muscle (the distance between proximal and distal aponeuroses, which are the transition from muscle to tendon) which is assumed to be constant.

Equations 2.3 to 2.12 are combined into the non-linear first order differential equation given as:

$$v_{\mathrm{m}} = f(L_{\mathrm{m}}, a, L_{\mathrm{mt}}), \tag{2.13}$$

or, equivalently:

$$\frac{\mathrm{d}L_{\mathrm{m}}}{\mathrm{d}t} = f_{\mathrm{v}}^{-1}(L_{\mathrm{m}}, a, L_{\mathrm{mt}}), \tag{2.14}$$

where f_{v}^{-1} is the inverse of f_{v}.

Model simplifications

The same dimensionless force-length-velocity and force-strain characteristics are used for all muscles and tendons. However, physiologically there are different muscles types with different dynamic characteristics. Also the tendons exhibit a higher (short tendons) or lower stiffness (long tendons).

Assumptions are made for reasons of simplicity. The dynamic behaviour of a muscle is assumed to be a representative upscale of the force production in a muscle fiber. The force production is assumed to depend on the activation (the input signal), the fiber length, and the contraction velocity.

The geometry of the muscle is simplified in three ways: within a muscle the muscle fibers are assumed to run in parallel in a plane from aponeurosis to aponeurosis. The muscle is attributed a particular area which is kept constant. This means that during contraction the tendons move along their axes which causes a change in the pennation angle.
Hence, compared to the biological muscles and tendons, the characteristics are generalisations and

the MT-models are simplifications [120].

Model alternatives

The Hill-model is often represented as in figure 2.2.3. However, some alternatives to this represention are also commonly used.

In this thesis, it has been opted to work with the model as presented in figure 2.2.3. The estimation procedure is based on isometric experiments, hence contraction velocity is zero. Millard et al. [68] indicate this model as the *equilibrium muscle-tendon model*. However, when performing dynamic simulations, equation 2.14 should be solved in order to find a unique solution for a given fiber length, and singularities occur when α equals 90°, and f_{v}^{-1}, a, and F_{act} equal 0.

Schutte [89] and Millard et al. [68] avoid the singularities by adding passive damping (a damper in parallel with the contractile element). The damped model is referred to as the *damped equilibrium model*. By choosing a low damping constant, the model generates similar force profiles as the equilibrium model [68].

In case the tendon is very stiff, the tendon strain is negligible. In this case, L_{m} directly results from equation 2.10, and v_{m} directly results from $\frac{\mathrm{d}L_{\mathrm{m}}}{d\mathrm{t}}(2.10)$, the muscle force can directly be calculated from equation 2.9. Millard et al. [68] refer to this mode as the *rigid-tendon musculoskeletal model*. Klein-Horsman et al. [56] also used this model, regardless of the tendon properties.

Model characteristics

Different approaches for the implementation of the model characteristics have been described. Figure 2.4 shows three different force-length-velocity characteristics. The model characteristics are according to Schutte [89], Thelen [99], and Millard et al. [68]. These characteristics are available through OpenSim, a software package for dynamic simulations of human motion [33] which is widely used (hence these characteristics are also widely used).

Active force-length

Active force - length curves are shown in figure 2.4a. Schutte [89] does not describe a mathematical formulation of the active-force length curve. Active force values corresponding to a given L_{m} are extracted by interpolation. Thelen [99] describes a Gaussian function (with an adaptable shape factor) which approximates the upscaled force-length characteristics of sarcomeres. A Gaussian

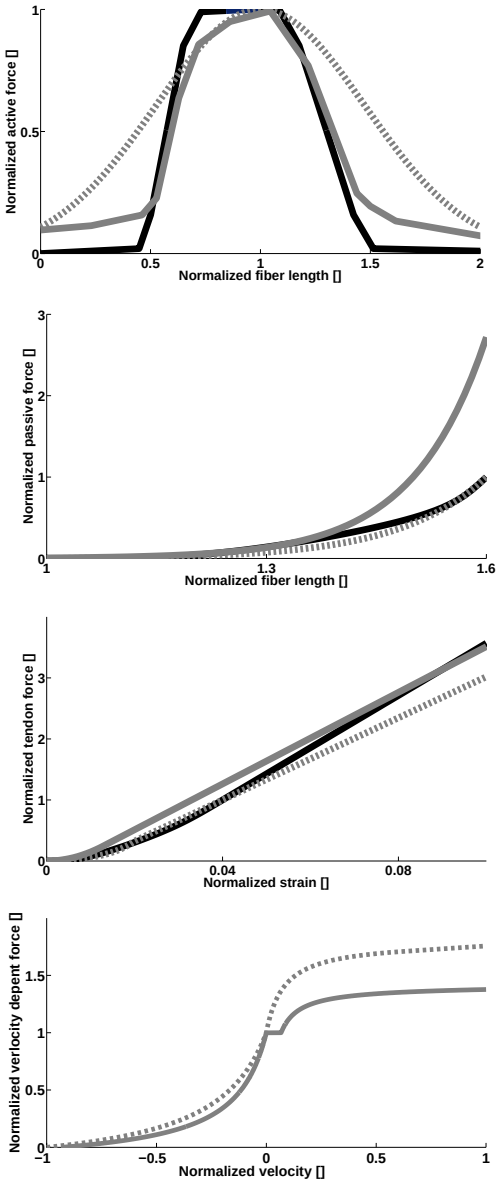

Figure 2.4: Force-length-velocity characteristics from top to bottom: active force - length, passive force - length, tendon force - strain, and active force velocity are shown. The characteristics according to Schutte [89] are in solid grey, according to Thelen [99] are in dashed grey, and according to Millard et al. [68] are in solid black.

rather than a piecewise polynomial is used for numerical reasons. Millard et al. [68] describe the active force-length characteristic as an upscaled sarcomere force-length characteristic, but so that it is continuous in its second detivative by applying Bezier splines.

Passive force - length
Passive force - length curves are shown in figure 2.4b. The passive-force length characteristic is described by an exponential function. Schutte [89] describes an exponential function with passive muscle strain at maximal isometric force of 0.5 (which is related to the stiffness of a muscle). Thelen [99] describes an hyperbolic-like function with an adaptable passive muscle strain at maximal isometric force which is generically set to 0.6. Shape factors in both descriptions are equal. Millard et al. [68] describe a curve using Bezier-points so that the curve of Thelen is approximated as closely as possible with continuous second derivatives.

Tendon force - strain
Tendon force - strain curves are shown in figure 2.4c. Schutte [89] describes a piecewise function which is zero whenever the tendon strain ϵ_t is smaller than or equal to zero, which is quadratic for the region in which the tendon acts as a non-linear spring ($\epsilon_t < 0.013$), and linear for the remaining values of ϵ_t. Thelen [99] also describes a piecewise function with an hyperbolic-like part when ϵ_t is smaller than or equal to 0.04, and with a linear part otherwise. At the amount of strain smaller or equal to 0.04, one unit of normalized force is generated in the tendon. Millard et al. [68] fit a curve with continuous second derivative on the curve of Thelen so that the slope at strain 0.04 is equal, and the curves match as closely as possible for all strains smaller than 0.04.

Active force - velocity
Active force - velocity curves are shown in figure 2.4d. Schutte [89] and Thelen [99] provide different analytical descriptions of the function based on experimental data. The formulations comprise a concentric part and an eccentric part. Millard et al. [68] describe the Thelen-curve so that the second derivative is continuous.

In this thesis, the implementation according to Millard et al. [68] has been chosen, because (i) these characteristics have a continuous second derivative which is beneficial for the estimation procedure as will be explained later, and (ii) the curves are validated on experimental data ([67], [117]). Additionnally, the implementation allows for easy adaptations of the characteristics to e.g. aging. However, here, the generic implementation [68] has been used.

2.3 Skeleton dynamics

In dynamic musculoskeletal modeling, contraction dynamics is the second submodel out of three. The first submodel describes the activation dynamics, which relates muscle excitation to muscle activation. The third submodel describes the skeleton dynamics which relates muscle forces and external forces to the motion of the skeleton.

Skeleton dynamics describe the dynamic relation between internal and external forces acting on the skeleton and the resulting motion. In case of gait, the external forces are the ground reaction forces and moments acting on the foots, and gravity. The internal forces are the muscle-tendon forces and the passive forces resulting from stretching soft tissues as ligaments.
The skeleton equations of motion then become [24]:

$$M(\mathbf{q})\ \ddot{\mathbf{q}} + c(\mathbf{q}, \dot{\mathbf{q}}) + g(\mathbf{q}) + R(\mathbf{q})\ \mathbf{F}_{\mathrm{mt}} + E(\mathbf{q}, \dot{\mathbf{q}}) = 0, \tag{2.15}$$

with $\mathbf{q}$, $\dot{\mathbf{q}}$, $\ddot{\mathbf{q}}$ the generalized coordinates, velocities and accelerations, describing the motion of the body segments along the $1...D$ degrees of freedom, $M(\mathbf{q}) \in \mathbb{R}^{D\times D}$ the generalized inertia matrix, $c(\mathbf{q}, \dot{\mathbf{q}}) \in \mathbb{R}^{D}$ the vector of generalized coriolis and centrifugal forces, $g(\mathbf{q}) \in \mathbb{R}^{D}$ the vector of generalized gravitational forces, $R(\mathbf{q})\ \mathbf{F}_{\mathrm{mt}}$ the joint moments formed by the product of the moment arms $R(\mathbf{q}) \in \mathbb{R}^{D\times J}$ (with $j = 1 \dots J$ the number of actuators) and the muscletendon forces $\mathbf{F}_{\mathrm{mt}} \in \mathbb{R}^{J}$, and $E(\mathbf{q}, \dot{\mathbf{q}}) \in \mathbb{R}^{D}$ the vector of generalized external forces and moments.

2.4 Dynamic motion simulations

In this section the data acquisition and data processing for dynamic simulations of motion are described. Dynamic motion analyses comprise data aqcuisition, scaling, inverse kinematics, and inverse or forward dynamics. In this word, dynamic motion analyses is used to validate MS-models which include subject-specifically estimated MT-parameters (see also chapter 7).

2.4.1 Data acquisition

In general, data acquisition comprises registration of marker trajectories, external forces, and muscle activations. Specific analyses also obtain bone and muscle geometric data from imaging, e.g. MRI, and muscle specific strength information through e.g. dynamometry for calibration of MT-parametes [38].

Marker trajectories

Typically, skin-mounted markers are placed on anatomical landmarks to measure the motion of body segements. Markers are either active in case they emit light, or passive in case they reflect light. Camera systems, e.g. Vicon (Vicon Motion Systems Ltd. UK) or Krypton (Krypton Electronic Engineering n.v.), register the 3D-trajectories of the markers which reflect the motion of the bones.

External forces

During gait or jumping or any motion where only the feet make contact with the environment, the ground reaction forces between the supporting foot (both feet in case of double support) are measured using force plates.

Electromyography

Electromyography (EMG) allows us to obtain information on the excitation signal. To this end, surface electrodes are placed above the skin on top of the muscle of interest. The placement of the electrodes is crucial, as it determines which motor units will contribute to the recorded signal. This implies that the EMG signal of a specific muscle can be biased by neigbouring motor units of other muscles [73]. Also, EMG is only applicible to superficial muscles.

The raw EMG signals need processing as they are very noisy. First, the EMG signal is high-pass filtered, the cut-off (Nyquist frequency) frequencies are function of the sample frequency (Nyquist

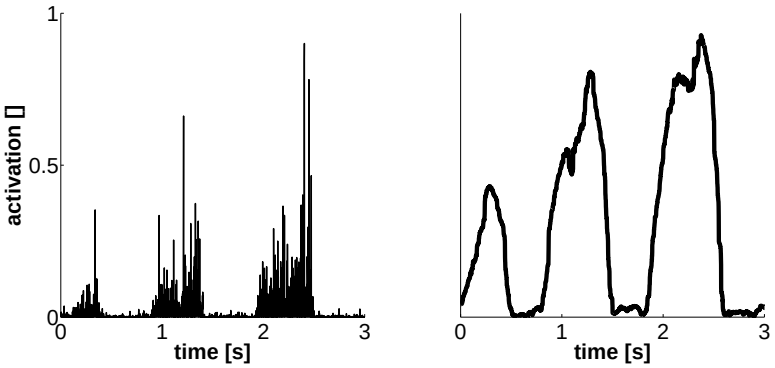

Figure 2.5: A rectified unfiltered EMG signal is shown left, a filtered and scaled EMG signal is shown right.

frequency = sample frequency/2). Second, the EMG signal is rectified and the root mean square over a certain window is calculated. Third, the EMG signal is low-pass filtered.

For validation of muscle activations, EMG signals are often scaled. However, there is no consensus about which technique should be used for scaling. In this thesis, the normalization is relative to the maximum signal values within a recorded motion. This is called the *peak dynamic method*, but this choice is open for discussion. Alternatively, signals can be scaled by the peak EMG from an isometric or isokinetic mean voluntary contraction (MVC) (*isometric/isokinetic MVC method*) or by a mean value recorded during a motion (*mean dynamic method*), (see e.g. [19; 43]).

In this thesis, activation dynamics are neglected when EMG recordings are used for validation purposes. Hence, it is assumed that the recorded signals are muscle activation. This is a simplification, as the activation dynamics basically act as a low-pass filter which introduces a delay between neural excitation and muscle activation [75].

2.4.2 Scaling

Scaling refers to the adaptation of a generic MS-model (e.g. [7; 32]) to the subject's anthropometry. Scaling is applied to MS-geometry, and to MT-parameters.

Musculoskeletal geometry

A common approach for scaling of geometry is based on a static measurement of skin mounted markers. Markers are mounted on anatomical landmarks, and hence reflect the segmental lenghts. The MS-model is scaled according to a scaling factor which is the ratio of the distance between the skin-mounted markers and the model markers. This is called anthropometrical scaling.

Imaging techniques allow to adapt musculoskeletal geometry, for example muscle paths, hence moment arms and actuator lengths (e.g. [84; 100]), according to subject-specific information extracted from the images.

MT-parameters

Cadaver studies [16; 112; 113] provide generic values for the MT-parameters in generic models [7; 32]. Calibration or scaling of these parameters is one of the big issues in biomechanical research [38].

In general, linear scaling of the generic values is applied to adapt the MT-parameter values. Hence, the ratio between the lengths of the respective segments of the generic model and the subject's model is applied to the values of the MT-parameters of the actuators spanning the segments. However, it has been shown that this linear scaling does not maintain the muscle's operating range, i.e. the joint angles at which a muscle delivers force [115]. Winby et al. [115] showed that anthropometric methods which preserve the operating length perform best.

Functional scaling is an alternative method for anthropometric scaling which aims at reflecting the subject-specific force generating capacities. Two methods have been published previously. Garner and Pandy [42] estimated the optimal fiber length and the tendon slack length for each actuator of the upper limb based on isometric dynamometry (see section 2.5). Lloyd and Besier [63] focussed on obtaining the tendon slack lengths together with three parameters related to activation dynamics (to adapt the scaling of the muscle activations) and two parameters which regulate the relative strength between flexors and extensors. However, neither of these approaches studied (i) the sensitivity of the experimental set to the parameters, nor (ii) the identifiability of the parameters. Additionnaly, the inaccuracy of the experimental protocol was ignored and the validations have not been performed properly. Yet, these are important issues in parameter estimation (see 6.2.3).

2.4.3 Inverse Kinematics

Inverse kinematics (IK) is the estimation of joint kinematics (position, velocity, acceleration) based on marker trajectory data, which for human motion analysis are obtained through skin-mounted markers. If the tracked body segment is rigid, the segment's pose (orientation and location) can be directly calculated from a minimum set of three non-collinear points (markers). Obviously, body segments are non-rigid. What we want to obtain, is the pose of the bone from the skin-mounted markers. Between the bone and the markers there are muscles and other soft tissues such as fat, which move relative to the bone. As a consequence, the trajectories as obtained from the skin-mounted markers are biased by the motion of these intermediary tissues. This error source is referred to as soft tissue artefacts (STA) [57]. Additional errors are instrumental errors (related to the accuracy of the camera system) [23], but STA are the most critical. STA are in the range of centimeters [3], which is easily one order of magnitude larger than the range of instrumental errors. STA have a systematic component, they are subject-dependent and task-specific.

Different techniques have been developed to reduce the sensitivity of IK to instrumental errors and STA ([21; 28; 64; 96]). In this thesis, IK is performed through a Kalman smoothing algorithm [28]. The main drawback of the other techniques is that only part of the trajectories is used to estimate joint kinematics at a time instant whereas Kalman smoothing calculates the estimates (generalized coordinates) at each time instant based on the whole trajectory, a process model and a measurement model. The process model predicts the expected time evolution of the generalized coordinates. To guarantee a smooth motion, it is assumed that the fourth derivative of the generalized coordinates is constant. This is based on the *a priori* knowledge that the acceleration of the segement cannot change abruptly. The model errors introduced by this assumption, are taken into account by the process noise. The measurement model relates the joint kinematics to the measured marker trajectories. The measurement model is based on a biomechanical model with a number of degrees of freedom (DOFs). Each marker in the model is weighted to indicate its reliability: the more the marker position is corrupted by STA, the lower the weight. The higher the weight, the more the estimate is based on the measurement model.

2.4.4 Inverse and Forward Dynamics

Inverse dynamics (ID) refer to the calculation of joint reaction forces and moments using equation 2.15 for a recorded motion with generalized coordinates $\mathbf{q}$ and generalized external forces $E(\mathbf{q}, \dot{\mathbf{q}})$.

Forward dynamics (FD) refer to the calculation of the motion resulting from a given time-trajectory of the excitations u, initial values of the activations, initial positions and velocities of the generalized coordinates, and MT-forces for each actuator. The motion is obtained by integration of the activation, contraction, and skeleton dynamics.

2.4.5 Muscle-tendon force calculation

The human body contains more actuators than degrees of freedom, hence the body is overactuated. This means that an infinite number of combinations of muscle-tendon forces can generate the joint moments underlying a given motion. As it is hardly possible to measure individual MT-forces *in vivo*, techniques have been developed to calculate the MT-forces based on a MS-model. Typically, an optimization problem with a certain goal criterion is solved, which assumes that muscle force distribution results from the optimisation of a performance criterion. In general, the solution approaches are either inverse or forward.

Inverse approach

An inverse approach solves an optimisation problem (e.g. [4], but there are many other references) which is often a static optimisation problem. The optimisation is called static because it starts from joint reaction moments, and the MT-forces are calculated at discrete time instants. No time-dependency is taken into account which makes the approach numerically efficient, but which does not allow to take muscle physiology (activation and contraction dynamics) into account. ID underlies the static optimisation, as MT-forces are calculated so that the resulting joint moment matches the ID result. The optimisation problem can be represented as follows:

The goal criterion is the sum of the activations at a time instant t_i to a power n:

$$\min \sum_{j=1}^{J} (a_j(t_i))^n, \tag{2.16}$$

or equivalently if $n = 2$ [80]

$$\min \sum_{j=1}^{J} \|a_j(t_i)\|_2 , \tag{2.17}$$

and if $n = \infty$ [1]

$$\min \sum_{j=1}^{J} \|a_j(t_i)\|_{\infty} . \tag{2.18}$$

Squaring the activations penalizes high activations and rewards low activations. The rationale behind this is that humans try to be as energetically efficient as possible, hence try to activate their muscles as little as possible. Alternatively stated, the higher the norm, the more muscles are activated.

The optimisation variables are the activations of every muscle j at every time instant i. Alternatively, MT-forces can be chosen as optimisation variables, because when assuming that the MT-actuators are ideal force generators, activations and MT-forces are related by $F_{\mathrm{m}}^{\max}$, the maximal isometric force a muscle can produce:

$$F_{\mathrm{mt}} = F_{\mathrm{m}}^{\max} \, a. \tag{2.19}$$

As a consequence, the goal criterion can also be restated as [80]:

$$min \sum_{j=1}^{J} \left(\frac{F_{\mathrm{mt},j}(t)}{F_{\mathrm{m},j}^{\max}} \right)^n . \tag{2.20}$$

The constraints impose that the muscle forces are larger than or equal to zero, and that the estimated joint moments, which result from the estimated MT-forces and the moment arms according to the geometry of the MS-model, match the ID joint moments.

Inverse Physiological Approach

General inverse approaches neglect muscle physiology in favor of calculation time. Obviously, this modeling error influences the results of the optimisation. Therefore, De Groote et al. [30] developed the *physiological inverse approach* (PIA) which combines the numerical efficiency and the inclusion of the muscle physiology.

The approach of the PIA is that a large-scale optimisation problem is solved from which MT-forces, activations, and excitations result at discrete time instants while skeleton dynamics are imposed as a penalty function. This turns the goal criterion into a bi-objective criterion which allows deviations between the predicted joint moments, and the joint moments resulting from the ID. Activation dynamics are imposed by a set of linear equalities and inequalities obtained via a

nonlinear transformation of variables [30]. The contraction dynamics are imposed at each discrete time instant by discretizing and linearizing the Hill-model which allows us to calculate an activation and update the current activation iteratively until the optimum activation, the activation minimizing the goal criterion, is reached.

In this thesis, the PIA is used for MT-force calculations.

Forward approach

A forward approach solves a large-scale optimisation problem for the global time trajectory of a given motion at once. At each iteration, muscle excitations are updated. As activation dynamics couples muscle excitations and activations, contraction dynamics couple activations and MT-forces, and skeleton dynamics couple MT-forces and the resulting motion, a set of nonlinear differential equations has to be integrated each iteration. Hence, calculations are time expensive (see e.g. [4]) without guarantee that the global optimum is reached. The optimisation problem can be presented as follows:

The goal criterion is a physiologically inspired criterion which often aims at minimizing the metabolic energy consumption [80].

The optimisation variables are the excitations of every actuator j at every time instant i.

The constraints impose activation dynamics, contraction dynamics, and skeleton dynamics as equality constraints, bounds on the optimisation variables as inequality constraints.

2.5 Dynamometry

Dynamometry refers to a set-up for strength assessment of selective muscle groups. The set-up is used for rehabilitation, training, and research purposes. Figure 2.6 shows a Biodex dynamometer (Biodex 3 Medical Systems, Inc., New York, USA). For this thesis, a dynamometer set-up is used for the acquisition of subject-specific strength profiles of the right knee joint actuators being mainly quadriceps, the muscle group on the frontside of the thigh, and mainly hamstrings, the muscle group on the backside of the thigh.

Figure 2.6: A standard Biodex dynamometer [14].

The convenience of dynamometry is that the relation between joint moment and joint angle can be measured in a controlled way. The experimental conditions are either isometric or isokinetic. Isometric indicates that the joint angle is fixed, hence the actuator lengths are constant. Isokinetic indicates that the joint angle changes at a constant velocity. The muscle contractions are either concentric or eccentric. During a concentric contraction the muscle is shortening. During an eccentric contraction the muscle is lengthening. When strength profiles of a certain muscle group

are acquired, they are influenced by the position of other joints. For example, when the strength of the quadricps is measured, the position of the hip joint should remain fixed (or be known) as the rectus femoris is a bi-articular muscle spanning both hip and knee. Hence, its position on the force-length characteristic and thus its force generating capacity is determined by both hip and knee angle. As the regular fixations are chest belts, it is not obvious to guarantee that other joints apart from the joint of interest maintain their position.

Much research has been performed related to the validity and reliability of dynamometer experiments. The main findings are summarized below.

2.5.1 Validity

The validity of the set-up refers to the accuracy of the measurements. Drouin et al. [34] studied the validity of a dynamometer by using calibrated weights during isometric and isokinetic measurements. They concluded that the results of the dynamometer are valid. This is in agreement with my own findings, performing similar experiments (results not published). In fact, this type of experiments shows that the dynamometer correctly registers the moment exerted around the dynamometer's axis of rotation and that the dynamometer correctly takes gravitional effects into account.

2.5.2 Reliability

The reliability of the setup refers to the extent the measurements are repeatable, and the desired data are obtained. Among many others Sole et al. [95], Lund et al. [65], and Impellizzeri et al. [51] studied the reliability of dynamometers for knee extension and flexion. Reliability is categorized as being *relative* or *absolute*.

The relative reliability indicates to which degree an individual maintains its position in a sample with repeated measurements and is therefore also referred to as between-subjects measure [9]. It is quantified by Intra Class Correlation coefficients (ICC) [88]. ICC's are reported to be high by all three studies. The relative reliability is often used for large-scale clinical follow-up studies: e.g. how does the strength of the population relates before and after training?

The absolute reliability indicates to which degree the repeated measurements vary for an individual and is therefore also referred to as within-subject measure [9]. It is quantified for example by the standard deviation of the measurements (relative to the mean of the measurements). Lund et al. [65] and Impellizzeri et al. [51] reported both values between 7% and 20%. Whereas the

former claims the measurements are highly reliable, the latter states that is not straightforward to judge based on these results whether the reliability is high. Indeed, a value may be acceptable for rehabilitation studies, but might fail for training programs. Accuracy of experiments, as wanted for this thesis, is quantified by the absolute reliability.

To complete this discussion on reliability, some attention is dedicated to gravitational and inertial effects, learning effect, fatigue and settings of the dynamometer which are also issues of concern.

Gravitational effects

Gravitational effects are compensated by the dynamometer through a calibration where the segmental weight is determined in a passive condition at a chosen position. For example Biodex corrects for gravity throughout the range of motion by applying a sine function. Inertial effects have been reported to be minor [55]. This is in agreement with our own results.

Learning effect

Learning effect explains the apparant improvement of strength in time, which is a result from accomodation of the subject with the experiment. However, Lund et al. [65] report that during their experimental session, no effect of learning was observed. They attributed this to the fact that good instructions were given and a learning phase was added to the protocol. Impellizzeri et al. [51] report a learning effect for the hamstrings' peak moment to some extent, and attribute this to the fact that while seated, the force-length relationship common during gait is not respected.

Fatigue

Fatigue refers to the decay in strength which can be linked to a decay in the maximum activation by the amplitude of the EMG signal [13]. Bilodeau et al. [13] describe a progressive increase in the EMG amplitude with increasing muscle force and clear decrease in amplitude with fatigue. Sagnier [82] report a decay of 10% in quadriceps and hamstrings strength after ten consequetive repetitions (velocity 180 °/s).

Dynamometer settings

The impact of dynamometer settings including position (e.g. height) of the seat, alignment of the dynamometer axis of rotation and the joint axis of rotation, tightness of the fixation belts,

positioning of other joints have been no subject of papers as far as I am aware. Yet, they all influence the data as recorded by a standard setup. For example, fixation of the body segments prevents them from moving relative to the dynamometer and to each other because otherwise the alignment of the axes of rotation is disturbed and an offset is introduced which is not accounted for. However, fixation cannot be too tight, as this will influence muscle contraction. Apart from the fixation, the alignment is an issue. Considering the knee joint for simplicity, Assume perfectly rigid fixation, a strict alignment between the dynamometer axis of rotation and the joint axis of rotation is impossible as the former is a fixed axis in time and space whereas the latter is an instantaneous axis which pose is not accurately known because the pose is instantaneous [109]. The next section will come back to this. It is also common practice to align the axis based on palpable geometric features. Joints as the knee rely on ligaments and muscles to guide the kinematics such that rotation is achieved without undesirable translation [109]. Later on in this thesis (chapter 4), it is shown that bone geometry is not a good nor the best representation of the actual knee joint axis.

Altogether, clinicians and researchers who rely on experimental dynamometer data should be aware that the measurement data as given by the dynamometer in its regular setup do not reflect the moments muscles generate around the joint axis, but the moment generated around the dynamometer axis of rotation. In every situation where the alignment between joint axis and dynamometer axis is not maintained, joint moment and dynamometer moment do not correspond. Some extended setups have been described in literature. Kaufman et al [55] used a load cell to obtain reaction forces and moments, Arampatzis et al. [5] tracked the positions of the markers mounted on femur, tibia and crank, and Tsaopoulos et al. [101] used fluoroscopy to obtain the positions of the bones. A solution to assess more accurate joint moments is presented in chapters 4 and 5.

2.6 Knee joint

Figure 2.7 shows an MR-image representing a knee joint. Figure 2.8 shows some conventional terms to indicate anatomical directions and motions.

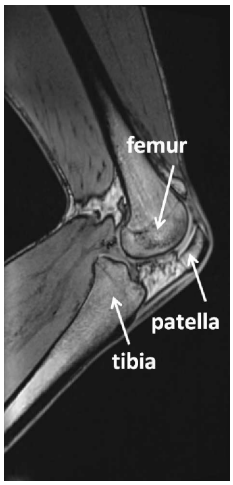

Figure 2.7: An MR-image of the knee joint. The bones composing the joint are the femur, the tibia, and the patella.

2.6.1 The knee joint from a physiological perspective

The joint comprises the patello-femoral joint between the patella and the lower end of the femur (thigh), and the tibio-femoral joint between the femoral condyles (further refered to as epicondyles) and the two menisci resting on the tibial (lower leg) plateau. The menisci are concave cartilogeneous structures which disperse friction. Ligaments in and around the joint guide the joint kinematics. The ligaments prevent hyperextension and secure the articulating bones. The main motion of the knee joint is flexion (bending of the knee) and extension (stretching of the knee), but there are also some smaller rotational (ab/adduction, internal/external rotation) motion components.

Joint mechanics

What follows, is valid for the tibio-femoral joint.

Assume a knee joint which is extending, e.g. when a person is sitting and stands up. What

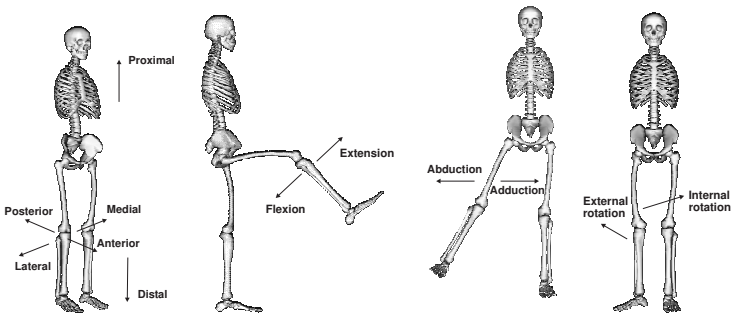

FIGURE 2.8: From left to right (i) the terms used for anatomical directions, (ii) flexion and extension of the knee joint, (iii) abduction and adduction (illustrated for hip joint), and (iv) internal and external rotation (illustrated for hip joint) are illustrated [33].

happens in the joint is the following: the epicondyles start making a backward sliding movement followed by a rolling movement, which brings the epicondyles into full contact with the menisci. At the last 20° of extension (hence near full extension), the tibia rotates externally, which is a consequence of the asymmetry in the knee joint (the lateral epicondyle is wider in the front than in the back). The medial articulating surface is longer, hence the lateral movement stops before the medial movement. This phenomenon is known as the screw home mechanism. During flexion, the joint axis of rotation moves backwards.

Axis of rotation

The axis of rotation (AoR) is defined as a set of points on a bone which have no velocity relative to the other bone at a given time instant. For human motion analysis, internal forces, moment arms and moments are expressed with respect to the joint axis of rotation. This stresses the importance of the defination of this axis. In general the knee joint axis of rotation is defined as the line connecting the epicondyles [32]. As a result, the AoR is fixed in time and space. However, as mentioned before, the femur makes a roll-back motion relative to the tibia. This implies that the AoR is not fixed. The pose of the AoR depends on the flexion angle, but also on the loading due to muscle and external forces [109]. In fact, the knee joint axis of rotation is an instanteneous axis of rotation describing the displacement between femur and tibia at every instant in time [22; 92; 109].

2.6.2 Knee joint from a modeling perspective

Given the complexity of the knee joint, modelling of the joint is not straightforward. Different modeling approaches for the knee joint are finite helical axis [22; 92; 109], planar displacing axis [119], and functional axis of rotation (e.g. [37; 41; 66]). Before going into these modelling approaches, some background is provided on the calculation of 3D kinematics for those readers who are not familiar with this matter.

3D kinematics

A rigid body in a 3D space has six degrees of freedom. This means that the body can translate along three (orthogonal) axes and rotate about three (orthogonal) axes to move from one position to another. The motion of one body relative to another body is described equivalently with three translations and rotations. To describe the motion of a rigid body, frames are attached to the body as illustrated in figure 2.9. Hence, whenever the displacement of the frames is known, the displacement of the body is known.

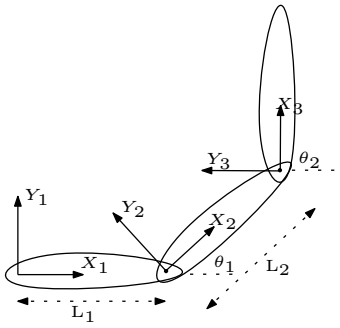

Figure 2.9: Each body has been assigned a local frame. By rotating frame XY_3 with θ_1 and θ_2 around Z_1, and translate it with L_1 along X_1 and $L2$ along X_2, frame XY_3 coincides with frame XY_1.

Transformation matrices

A transformation matrix $\mathbf{T}$ is a way to describe the relative position and orientation (pose) of a frame b with respect to a frame a:

$$ {}^{b}_{a}\mathbf{T} = \begin{pmatrix} {}^{b}_{a}\mathbf{R} & {}_{a}\mathbf{t}^{a,b} \\ 0_{1x3} & 1 \end{pmatrix}, \tag{2.21} $$

with ${}^{b}_{a}\mathbf{R}$ the orientation matrix of b with respect to a, and $t^{a,b}$ the position vector of b with respect to a expressed in a.

Considering figure 2.9, two transformations are needed to express the pose of link 3 in the frame of link 1: ${}^{3}_{2}\mathbf{T}$ describes the transformation from body 3 in frame 3 to frame 2, ${}^{2}_{1}\mathbf{T}$ describes the transformation from body 2 in frame 2 to frame 1, hence the transformation from body 3 in frame 3 to body 3 in frame 1 is ${}^{3}_{1}\mathbf{T} = {}^{2}_{1}\mathbf{T}\ {}^{3}_{2}\mathbf{T}$.

Composition of rotations

Relative rotation can be expressed by only three angles. In case the rotations take place around the axis of the moving frame, these values are called Euler angles. Assume that the rotation of frame b with respect to frame a is described by a rotation θ_{x} around the X-axis, followed by a rotation θ_{y} around Y-axis and eventually θ_{z} around the Z-axis, then the total rotation around the axis of the moving frame is expressed as:

$$ {}^{b}_{a}\mathbf{R} = \mathbf{R}(Z, \theta_{\mathrm{z}})\ \mathbf{R}(Y, \theta_{\mathrm{y}})\ \mathbf{R}(X, \theta_{\mathrm{x}}). \tag{2.22} $$

Otherwise, if the rotation takes place around the axis of the fixed frame, these values are called roll, pitch and yaw for which the total rotation is expressed as:

$$ {}^{b}_{a}\mathbf{R} = \mathbf{R}(X, \theta_{\mathrm{x}})\ \mathbf{R}(Y, \theta_{\mathrm{y}})\ \mathbf{R}(Z, \theta_{\mathrm{z}}). \tag{2.23} $$

Anatomical reference frames

In human motion analysis, an anatomical reference frame is defined for each body segment. The frames are attached to the bones. The orientation and location of the frames is according to the conventions of ISB (International Society of Biomechanics) [118]. In theory, the location and orientation can be chosen randomly. However, a random choice does not allow to clinically interpret the motions. Figure 2.10 shows the anatomical frames for tibia and femur. For the tibia, the origin of the frame is placed at the middle of the transepicondylar axis, the Y-axis connects the middle of the transepicondylar axis and the middle of the malleolar axis, the Z-axis coincides with the transepicondylar axis, the X-axis completes the right-handed frame. For the femur, the origin of the frame is placed at the hip joint center of rotation, the Y-axis is along the femur shaft in the plane defined by the hip center of rotation and the transepicondylar axis, the Z-axis coincides with the transepicondylar axis, the X-axis completes the right-handed frame.

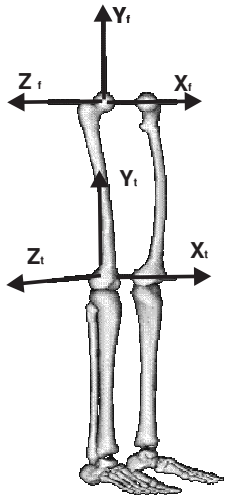

Figure 2.10: Illustration of the anatomical reference frames for femur ($_f$) and tibia ($_t$).

Finite helical axis

A finite helical axis (FHA) describes a finite displacement between two rigid bodies, here the displacement between femur and tibia. According to Chasles' theorem the displacement of a rigid body between two time instants can be described by a rotation around an axis and a translation along the same axis. FHA's are an approximation of instanteneous axes of rotation. FHA is calculated based on the registered position of at least three points fixed on each body. Knee joint axes of rotation can be expressed in the femoral or tibial reference frame.

The orientation and position of the FHA is calculated from the rotational part of the total transformation. The transformations can be obtained by the algorithms of Soderkvist [94] or De Groote et al. [28] via the generalized coordinates resulting from the segmental measurement models.

Whenever only data on the axis' pose at discrete time instants is available, the displacement of the bodies is described by an equivalent axis.

The theory as descibred above is valid for rigid bodies, hence for the displacements of the bones. Actual bone displacement as input for the FHA calculations can be obtained via markers placed on bone pins [109] or dynamic imaging techniques [92]. However, when using skin-mounted markers the kinematic data are corrupted by STA as explained in section 2.4. Cheze et al. [22] report that no accurate results are obtained whenever the two positions are not sufficiently distinct (about

25°). They suggest to model the knee joint axis of rotation as a mean axis between two distinct joint positions.

Models for axis displacement

Yamaguchi and Zajac [119] describe a planar model of the knee. The knee joint axis is modeled as a transepicondylar axis which translates in anterior-posterior direction and proximal-distal direction as a function of the flexion angle. The orientation of the axis remains constant. The reference position is according to the position of the transepicondylar axis when femur and tibia are aligned (zero knee flexion). This planar model is widely used as it e.g. defines the knee joint in the generic model of Delp et al. [32]. The functions describing the translations are shown in figure 2.11.

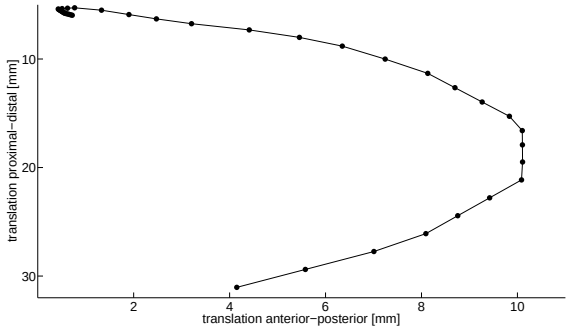

FIGURE 2.11: Planar knee joint model by Yamaguchi and Zajac [119]. Displacements in proximal-distal directions are shown in function of the anterior-posterior displacement of the axis of rotation.

For gait and jump simulations in this work, this planar knee joint model is used (see chapter7).

Walker described an alternative spatial knee joint model [111]. Therefore, five degrees of freedom were described in function of the knee flexion angle based on experimental data: internal rotation, ab/dduction, and translation along X-, Y-, Z-axis. This model allows to model abnormal motions of the knee joint.

Functional axis

A functional axis of rotation (fAoR) is the axis of rotation that best explains a recorded motion over a certain range. There are two main techniques to calculate functional axes of rotation.

Transformation techniques (e.g. [37; 87]) rely on 3D rigid body mechanics, and therefore can make use of anatomical coordinate systems.

Transformation technique

The transformation technique assumes that the axis of rotation is stationary in each local reference frame. As the axis is defined by its position and its orientation, a transformation should map the local points of the AoR's on both segments onto the same global points. Positions of tibial markers and femoral markers are input. Again, [28] or [94] can be applied to obtain the transformation matrices.

Transformation methods solve for the line best fitting both local sets of points.

Fitting technique

The circle fitting technique assumes that the markers move in circles relative with respect to the axis of rotation, and that the circle centers define the functional axis of rotation. Therefore, the distance from the registered marker positions to the center of the circles lying on the fAoR should equal the circle radius. Equivalently, the velocity vector resulting from the rotation of the marker around the axis of rotation should be perpendicular to the orientation of the axis of rotation.

Fitting techniques solve for the axis which best minimizes the deviations from the circles.

In this thesis, the functional axes of rotation are calculated according to Ehrig et al. [37] and Gamage and Lasenby [41]. This choice was based on the findings of MacWilliams [66] and Ehrig et al. [37] that these algorithms were respectively the best performing transformation and fitting techniques in simulation: when noise was applied to all markers the deviation from the actual axis was less than 1cm in the simulation environment.

2.7 System identification

Parameter estimation is the experimental determination of parameter values that govern the behaviour of a model. It is part of system identification which involves experimental design and data acquisition, model selection, parameter estimation, and model validation [62].

2.7.1 Optimal experiment design

Experiment design involves making choices so that the data become maximally informative subject to the constraints inherent to the experimental set-up [62]. For the dynamometer experiments, the constraints are that the excitation of the system (the muscles) is hard to control, and the number of experiments is limited. Therefore, it should be verified whether the experiments of interest contain information on the parameters. Additionally, it should be verified whether it is possible to extract parameter values from the experiments. The former can be studied by a sensitivity analysis, the latter can be studied by an identifiability study.

Sensitivity analysis

Model predictions depend differently on different parameters. Hence, it is more crucial to improve the accuracy of the values of the parameters with the highest influence on the model predictions. A senstivity analysis evaluates the influence of a parameter on the model prediction and allows to obtain a hierarchy in the parameters with respect to the experiments.
The local sensitivity S^e of an experiment e to a parameter p is calculated as follows:

$$S^e = \frac{\partial \widehat{\mathbf{y}}}{\partial p}, \tag{2.24}$$

with $\widehat{\mathbf{y}}$ the model prediction for a certain experiment, and $p = 1...P$ a model parameter.
The relative sensitivity S^e_{rel} is defined as:

$$S^e_{\text{rel}} = \frac{\Delta \widehat{\mathbf{y}}/\widehat{\mathbf{y}}}{\Delta p/p}, \tag{2.25}$$

with $\Delta \widehat{\mathbf{y}}$ the change in the model prediction due to the change Δp in the model parameters.

For non-linear models, sensitivities might depend on the nominal parameter value. Hence, ideally, the sensitivity to the parameters should be determined for a number of nominal parameters

spanning the whole parameter space. Techniques for sampling of the parameter space rely on the relative likelyhood that a parameter has a certain value. Examples are the computationally demanding Monte Carlo Analysis [12], which generates combinations of parameter values, or Latin Hypercube Sampling, which divides the parameter space in equal intervals [12].

Identifiability study

Identifiability of parameters relies on data quality (including how the system is excited) and data quantity. The importance lies in making a trade-off between the amount of information and the experimental burden. In this thesis, humans are performing the experiments. Hence, because of fatigue the experimental burden is an issue, and the amount of excitation is limited.
For simple problems, the identifiability of parameters can be checked visually by drawing the contours of the objective function. Locally optimum solutions become visible, and the shapes of the contours give information on the identifiability of a parameter. A valley-like shape typically indicates a poor identifiability.

However, in an n-dimensional parameter space, contour plots are not as straightforward to interpret. The richness of the experiments can then be quantified by the Fisher information matrix Fim which gives the expected value of the observed information for the estimated value $\widehat{p}$ [110]:

$$\text{Fim} = E\left[\left(\frac{\partial\widehat{\mathbf{y}}(p)}{\partial p}\right)^T P_v^{-1}\left(\frac{\partial\widehat{\mathbf{y}}(p)}{\partial p}\right)\right]|_{\widehat{p},} \tag{2.26}$$

$$= E\left[\underbrace{\left(\frac{\partial\widehat{\mathbf{y}}(p)}{\partial p}\right)^T \left(P_v^{-1}\right)^{\frac{1}{2}}}_{a}\left(P_v^{-1}\right)^{\frac{1}{2}}\left(\frac{\partial\widehat{\mathbf{y}}(p)}{\partial p}\right)\right]|_{\widehat{p}} \tag{2.27}$$

with P_v^{-1} the uncertainty on the measurements expressed in terms of covariance. The inverse of Fim reflects the covariance on $\widehat{p}$.

By a singular value decomposition of expression a in equation 2.27, the best identifiable part of the parameter space is extracted [110]. The singular values indicate the number of identifiable parameter combinations. The number of parameters is deduced from the singular values: whenever there is a jump in the decrease between two consecutive singular values, the number of identifiable parameter combinations is the number of singular values before the jump.The larger the singular value, the better the identifiability of the respective parameter combination, which is defined by the singular vector. Typically, all singular values close to zero show low identifiability. The identifiability is valid for the chosen nominal parameter values as the Fim is deduced from

equation 2.25.

Scaling

The parameters of interest do not necessarily have the same units, nor are they in the same order of magnitude. Scaling of parameters makes the parameters independent of their units [110]. Obviously, scaling influences the numerical values of the singular values, and hence the interpretation of the identifiability.

Scalarization of Fim

Often a scalar measure of the Fim is used to judge the identifiability of parameters. Scalarizations rely on the eigenvalues of the Fim. The three most popular scalarizations are [12; 15]:

- The D-criterion which maximizes (minimizes) the determinant of the Fim (the inverse of Fim):

$$\text{D-crit} = \max \det(\text{Fim}) = \min \det(\text{Fim}^{-1}), \tag{2.28}$$

  det(.) calculates the product of the eigenvalues of (.).

- The E-criterion which maximizes (minimizes) the minimum (maximum) eigenvalue $\lambda_{\min(\max)}$ of the Fim (the inverse of Fim):

$$\text{E-crit} = \max \lambda_{\min}(\text{Fim}) = \min \lambda_{\max}(\text{Fim}^{-1}). \tag{2.29}$$

- The A-criterion which maximizes (minimizes) the trace of the Fim (the inverse of Fim):

$$\text{A-crit} = \max \text{tr}(\text{Fim}) = \min \text{tr}(\text{Fim}^{-1}). \tag{2.30}$$

  tr(.) calculates the sum of the eigenvalues of (.).

The criteria can be interpreted in terms of the confidence region. The D-criterion minimizes the volume of the confidence region. The E-criterion minimizes the length of the major axis of the confidence region. The A-criterion minimizes the dimensions of the enclosing box on the confidence region. A geometrical visualisation of the criteria is provided in figure 2.12.

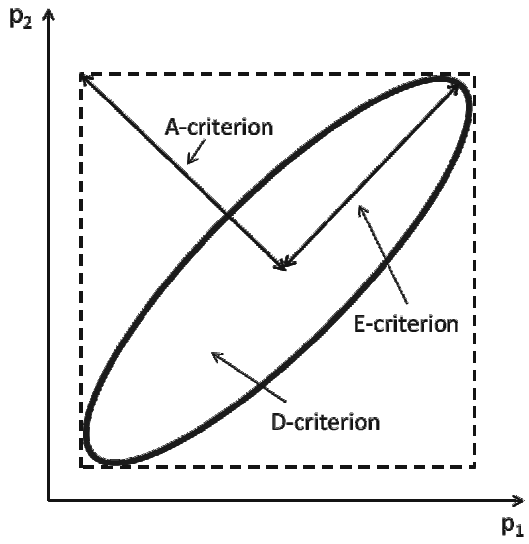

Figure 2.12: In a 2D space, the confidence region is given as an ellipse. The enclosing box is shown in dotted lines. D-, E, and A-criteria are indicated.

2.7.2 Parameter estimation

Model selection

In case the parameters in a model have no physical meaning, but are just adjusted to fit the data, a set of models is often available from which the best model has to be selected. In this work, the model is constructed based on physical insight into the MT-complex. In case of MT-models, the parameters have a physical interpretation. Hence, no model selection was performed. Or equivalently, it is correct to state that the model selection is done based on physical insight.

Estimation procedure

The aim of the estimation procedure is to minimize the error $\boldsymbol{\epsilon}(p)$ between a measured output $\mathbf{y}$, and a predictor sequence $\widehat{\mathbf{y}}(p)$ [62]:

$$\min_{p} \quad \boldsymbol{\epsilon}(p) = \mathbf{y} - \widehat{\mathbf{y}}(p). \tag{2.31}$$

Typically, the estimation procedure is formulated as an optimisation problem. The solution approach can be local or global. The estimation problem can be linear or non-linear (and when non-linear, convex or non-convex).

Definition of optimisation problems

An optimisation problem describes an objective function $f_o(\mathbf{x}) : \mathbb{R}^n \to \mathbb{R}$ which value has to be minimized, a set of optimisation variables $\mathbf{x} \in \mathbb{R}^n$, and a set of constraints which can be equality constraints $\mathbf{c}_i(\mathbf{x}) : \mathbb{R}^n \to \mathbb{R}$ or inequality constraints $\mathbf{g}_i(\mathbf{x}) : \mathbb{R}^n \to \mathbb{R}$:

$$\min_{\boldsymbol{x}} \quad f_o(\mathbf{x}) \quad , \tag{2.32}$$

$$\text{s.t.} \quad \mathbf{c}_i(\mathbf{x}) = 0 \qquad i = 1...n_{\text{eq}}, \tag{2.33}$$

$$\mathbf{g}_i(\mathbf{x}) = 0 \qquad i = 1...n_{\text{ineq}}, \tag{2.34}$$

with $n_{\text{(in)eq}}$ the number of (in)equality constraints. The solution corresponds to the vector $\mathbf{x}$ that yields the smallest value of the objective function of all points that satisfy the constraints. The feasible set represents the set of all variables $\mathbf{x}$ that satisfy the constraints of the problem.

Convex versus non-convex problems

An optimisation problem is convex when the objective function and the inequaltity constraints are convex in the optimisation variables, and the equality constraints are linear. A convex function is defined as follows [15]:

$$f(\alpha\mathbf{x} + \beta\mathbf{y}) \leq \alpha f(\mathbf{x}) + \beta f(\mathbf{y}), \tag{2.35}$$

for all $\alpha, \beta \in \mathbb{R}$, $0 \leq \alpha, \beta$, $\alpha + \beta = 1$. Geometrically, the inequality means that the line between any two points on the graph, lies above the graph. Hence, the curvature of the graph is positive. For convex optimisation problems every locally optimal point is globally optimal. Hence, any local optimum is also the global optimum. The main challenge in convex optimisation is recognizing the problem rather than solving it. Efficient solution approaches exist (e.g. interior point methods) to solve convex problems with a limited number of iterations [15].

A special group of convex problems are linear problems of which the objective function and constraints are linear.

An optimisation problem is non-linear (non-convex) if the objective function and constraints are

non-linear, but not known to be convex or known to be non-convex. Typically, these optimisation problems suffer from local optima. No simple solution approach is available for this kind of problems. The challenge regarding non-linear problems once the formulation is done, is solving the problem by e.g. providing/finding a good initial guess close to the optimal solution, and the choice of the algorithm.

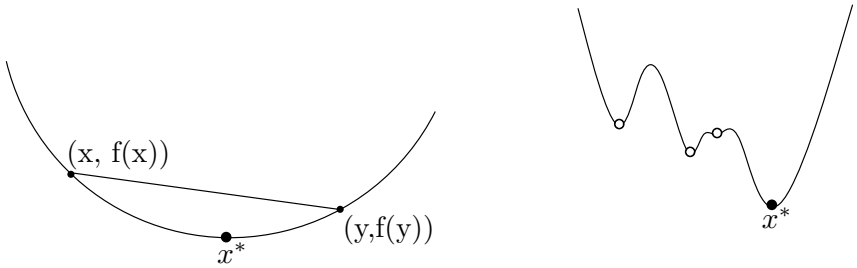

Figure 2.13: Geometric illustration of a convex function (left) and a non-linear (non-convex) function (right). The global optima are indicated with black disks, the local optima are indicated with circles.

Figure 2.13 illustrates the difference between a convex problem and a non-linear (non-convex) problem.

Global versus local optimisation

A global optimisation approach aims at finding the global optimum by searching the complete parameter space. Global optimisation methods generate and include randomness in the optimisation procedure e.g. in the search procedure. Popular global optimisation techniques are genetic algorithms and simulated annealing, which mimic natural phenomena (e.g . [70]). The main drawback of these global optimisation techniques is that they are time expensive. Although it might be garantueed that the true solution is found, the amount of time needed might be unrealistically large, which in real life *might involve let's say a 1000 of years (-Stephen Boyd).*

A local optimisation approach aims at finding a solution to the problem that is locally optimal. Hence, the solutions results in the smallest error in the goal function compared to all possible feasible solutions that are near. There is however no guarantee that the lowest possible value of the goal function has been obtained [15]. Local optimisation techniques rely on analytical properties of the problem (curvature information). Many algorithms assume second order continuity [76].

Model validation

Model validation aims at evaluating the performance of the model. Typically, it is verified whether the model can reproduce recorded data, hence whether the model is valid for its purpose. In this thesis, system identification is applied on the complete muscle-tendon model describing the contraction dynamics. Validation of the MT-model on its own is not possible. Therefore, in this thesis the performance of the musculoskeletal model including the MT-model is evaluated. In biomechanical motion analysis, model validation is often done by comparing recorded muscle activations by EMG and predicted muscle activations in the dynamic simulation.

2.7.3 Solution approach

The objective of this thesis was to determine the parameters of the Hill-model based on subject-specific data for the calculation of subject-specific muscle-tendon forces. Therefore, following steps have been taken:

1. Experimental data are obtained via dynamometry. To enhance data quality, a conventional dynamometer has been extended with motion tracking and external force registration. These extra data allow us to perform a full 3D inverse dynamic analysis. Hence, a more accurate estimate of the moment generated by the muscles around the joint axis of rotation is obtained. The joint axis of rotation in the knee model is defined by a functional axis of rotation instead of a geometry-based axis of rotation. The performance of functional axes versus geometry-based axes has been validated.

2. An estimation procedures is developed to solve the non-linear optimization problem from which subject-specific MT-parameter values are obtained by mapping experimental dynamometer data to MS-model predictions. The solution approach is a local non-linear optimization. Therefore, a lot of attention is paid to problem formulation, obtaining a good initial guess, and defining the feasible set.

3. The calculated MT-parameters are validated based on isokinetic dynamometry, walking and jumping by comparing estimated muscle activations to experimentally obtained muscle activations. For the isokinetic experiments, also the predicted joint moments are obtained by performing forward dynamic analysis.

Chapter 3

Sensitivity of dynamic simulations of gait and dynamometer experiments to Hill muscle model parameters of knee flexors and extensors

Abstract[1]

We assessed and compared sensitivities of dynamic simulations to musculotendon (MT) parameters for gait and dynamometer experiments. Our aim with this comparison was to investigate whether dynamometer experiments could provide information about MT-parameters that are important to reliably study MT-function during gait. This would mean that dynamometer experiments could be used to estimate these parameters. Muscle contribution to the joint moment (MT-moment) rather than relative MT-force primarily affects the resulting gait pattern and moment measured by the dynamometer. In contrast to recent studies, therefore, we assessed the sensitivity of the MT-moment, rather than the sensitivity of the relative MT-force. Based on sensitivity of the MT-moment to a parameter perturbation, MT-parameters of the knee flexors and extensors were classified in three categories: low, medium, and high. For gait, classification was based on the average sensitivity during a gait cycle. For isometric and isokinetic dynamometer experiments, classification was based on the highest sensitivity found in the experiments. The calculated muscle contributions to the knee moment during gait and dynamometer experiments had a high sensitivity to only a limited number o fMT-parameters of the knee flexors and extensors, suggesting that not all MT-

[1]This chapter has been published as a full article in *Journal of Biomechanics*: F. De Groote, A. Van Campen, I. Jonkers, J. De Schutter. Sensitivity of dynamic simulations of gait and dynamometer experiments to Hill muscle model parameters of knee flexors and extensors. 2010, vol. 43, pp. 1876-1883. Only minor changes concerning notational consistency and lay-out have been performed.

parameters need to be estimated. In general, the highest sensitivity was found for tendon slack length. However, for some muscles the sensitivity to the optimal fibre lengthorthemaximalisometricmuscleforcewasalsohighormedium.Theclassificationofthe individual MT-parameters for gait and dynamometer experiments was largely similar. We therefore conclude that dynamometer experiments provide information about MT-parameters important to reliably study MT-function during gait, so that subject-specific estimates of MT-parameters could be made based on dynamometer experiments.

3.1 Introduction

Direct measurement of musculotendon (MT) forces during motion is currently infeasible. MT-force distribution is therefore calculated from a dynamic musculoskeletal model comprising activation, contraction, and skeleton dynamics. Activation dynamics [59] describe the nonlinear relation between muscle excitation and muscle activation based on the activation and deactivation time constants, τ_{act} and τ_{deact}. Contraction dynamics describe the nonlinear relation between muscle activation and MT-force. The commonly used Hill model is based on five muscle-specific parameters: tendon slack length $L_{\mathrm{t}}^{\mathrm{s}}$, optimal muscle fibre length $L_{\mathrm{m}}^{\mathrm{opt}}$, maximal isometric muscle force $F_{\mathrm{m}}^{\mathrm{max}}$, optimal pennation angle α_{opt}, and maximal muscle fibre velocity $v_{\mathrm{m}}^{\mathrm{max}}$. Skeleton dynamics relate MT-forces and external forces to the resulting motion based on the musculoskeletal geometry. Hence, the accuracy of any analysis based on the dynamic musculoskeletal model depends, in part, on the MT-parameters describing activation and contraction dynamics.

State of the art analyses are based on a generic set of MT-parameters sourced from the literature. However, parameters reported in the literature vary widely (for an overview see [91]) and must often be compiled from different sources. These parameters are thus not subject-specific, although muscle properties are known to vary with age, gender and activity level [16; 39]. Therefore, the aims of this study are twofold: to investigate (1) which MT-parameters of the knee extensors and flexors have a considerable effect on the calculated MT-force distribution during gait and (2) whether it is feasible to make a subject-specific estimate of these MT-parameters based on dynamometer experiments measuring the anglemoment relation at the knee.

The effect of MT-parameters on the calculated MT-force distribution during gait has been investigated previously. Scovil and Ronsky (2006) studied the sensitivity of a forward simulation of gait and running to the parameters of a Hill-type muscle model. Redl et al. (2007) studied the

sensitivity of a static optimisation procedure to calculate the MT-force distribution underlying gait to $L_{\mathrm{t}}^{\mathrm{s}}$, $L_{\mathrm{m}}^{\mathrm{opt}}$, and muscle physiological cross-sectional area (PCSA), which is proportional to $F_{\mathrm{m}}^{\mathrm{max}}$. Both studies evaluated sensitivity using the ratio between the relative change in MT-force and the relative change in the MT-parameter. Both studies showed the highest sensitivity to $L_{\mathrm{t}}^{\mathrm{s}}$, a smaller sensitivity to $L_{\mathrm{m}}^{\mathrm{opt}}$, and a small sensitivity to PCSA during gait.

These studies, however, do not demonstrate which MT-parameters are important to analyse gait reliably for two reasons. Firstly, sensitivities reported by [91] were averaged over 14 muscles, but [81] have shown large differences between the sensitivities of four muscle groups, indicating the need to assess sensitivity in muscles individually. Secondly, both [91] and [81] investigated the relative effect of parameter perturbations on the MT-force production. However, it is the absolute muscle contribution to the joint moment (not the relative MT-force), which primarily affects the resulting motion. This follows from the human bodys equations of motion in which the absolute MT-forces appear in a product with the muscle moment arms. In our study, therefore, we investigated which MT-parameters of the knee extensors and flexors affected the calculated MT-force distribution during gait, by assessing sensitivity in individual muscles at the joint moment level.

Estimating MT-parameters based on dynamometer experiments is only feasible if these parameters affect the measured anglemoment relation. The effect of MT-parameters on the isometric anglemoment relation has been investigated by [49], who found that $L_{\mathrm{t}}^{\mathrm{s}}$ and $L_{\mathrm{m}}^{\mathrm{opt}}$ have a profound influence on the joint angle at which an actuator develops peak isometric force. Out et al. (1996) investigated the sensitivity of the isometric momentangle relation at the ankle to MT-parameters of m. soleus (SOL), m. gastrocnemius lateralis (GL), and m. gastrocnemius medialis (GM). They found that the maximal moment and the angle at which this maximal moment is delivered are most sensitive to $L_{\mathrm{t}}^{\mathrm{s}}$. However, [49] did not report the effect of individual MT-parameters and [77] only studied the ankle plantar flexors. The effect of MT-parameters on the isokinetic anglemoment relation has not yet been investigated.

In our study, we simultaneously assessed the effect of the MT-parameters of knee flexors and extensors on the individual muscle contributions to the knee moment during gait and on the measured anglemoment relation during isometric and isokinetic dynamometer experiments. To quantify this effect we introduced a new sensitivity measure. The calculated sensitivities during gait determined a ranking in the MT-parameters. MT-parameters with higher sensitivity require higher accuracy to reliably calculate muscle contributions to the joint moment.

Different analysis methods imply different relations between the MT-force distribution and the MT-parameters, and hence may result in different sensitivities. To evaluate how parameter sensitivity depends on the applied method, we determined sensitivities for muscle contributions calculated using three analysis methods: a forward simulation (cfr. [91]), a static optimisation (cfr. [81]), and a dynamic optimisation. The calculated sensitivities were then used to help answer the two research questions we have raised: (1) which MT-parameters of the knee extensors and flexors need to be accurately known to analyse the individual muscle contributions to the knee moment during gait (i.e. which MT-parameters have a high sensitivity during gait) and (2) do these MT-parameters affect the isometric or isokinetic anglemoment relation measured using dynamometry (i.e. do these MT-parameters also have a high sensitivity during at least one of the dynamometer experiments)?

3.2 Methods

3.2.1 Dynamic musculoskeletal model

The body model comprised eight segments and had 19 degrees of freedom (DOF) (see figure 3.1). Each leg was articulated by 43 muscles. Activation dynamics were described by a first order model [79] with $\tau_{\text{act}} = 11ms$ and $\tau_{\text{deact}} = 68ms$ [116]. Contraction dynamics were described by the Hill model (see figure 2.2.3)([90; 120]). The MT-specific parameters $L_{\text{m}}^{\text{opt}}$, L_{t}^{s}, $F_{\text{m}}^{\text{max}}$, α_{opt} and $v_{\text{m}}^{\text{max}}$, scaled the generic, dimensionless model.

3.2.2 Experimental setup and input data

Experimental data was collected for three subjects (26.5y, ±1.5): one male and one female recreational runner, and one male elite runner. Instrumented gait analysis was performed using a 3D motion capture system (Krypton, Metris) and a synchronised force plate (Bertec, Columbus, OH, USA). A modified Cleveland Clinic marker protocol was used (38 markers).

Each subject was tested in a Biodex Dynamometer (Biodex Medical Systems). Firstly, isometric knee flexion and extension moments during maximal voluntary contraction were measured at knee flexion angles of 15 °, 30 °, 60 °, 90 °, and 105 °, with 0 ° corresponding to full extension. Secondly, maximal voluntary knee flexion and extension moments were measured over the full range of motion of the knee at constant velocities of 60 °/s, 90 °/s, and 180 °/s. All experiments were

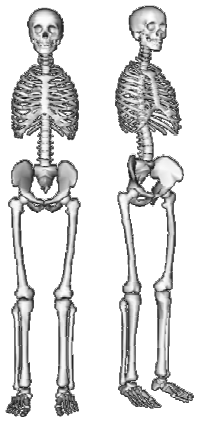

FIGURE 3.1: The body model. The body model comprised eight segments: a head - arms - trunk (HAT) segment, the pelvis, left and right thigh, lower leg and foot [32]. The model had 19 degrees of freedom (DOF): spherical joints connected the HAT-segment to the pelvis and the pelvis to the thighs. The knee joints were modelled as sliding hinges [119]. The ankle joints were modelled as simple hinges (metatarsal joints were not included in the model). The remaining six DOF corresponded to the position and orientation of the pelvis.

repeated at two different hip angles: a high flexion between 60 ° and 70 ° and a low flexion between 40 ° and 50 °, with 0 ° corresponding to full extension. The ankle was fixed in the neutral position by a rigid ankle foot orthosis.

Musculoskeletal models, scaled to each subject's dimensions, were generated using OpenSim [33] based on marker information collected during a static trial. The MT-parameters of the scaled musculoskeletal models were taken as the nominal values (see table 3.1). For each gait trial, joint kinematics and joint moments were calculated based on the measured ground reaction forces and marker trajectories by subsequently applying (1) a Kalman smoothing algorithm [28] for inverse kinematics and (2) an inverse dynamic analysis [33]. During the dynamometer experiments, joint kinematics and moments were measured directly. The moment arms of the MT-actuators during gait and the dynamometer experiments were calculated based on the scaled musculoskeletal model and the kinematic input.

3.2.3 Calculation of MT-force distributions

We assumed maximal static contraction of the agonists and complete relaxation of the antagonists during the isometric experiments. Activations of knee flexors were therefore 1 and activations of

knee extensors 0, when a knee flexor moment was exerted and vice versa when a knee extensor moment was exerted. Corresponding MT-forces were calculated using the Hill model.

The MT-force distribution during gait and the isokinetic experiments was calculated using two optimisation methods: the 'classical' inverse approach (CIA) ([4; 25]) and the physiological inverse approach (PIA) ([30; 78]). Both methods enforce the MT-force distribution to be consistent with the joint moments using the instantaneous moment arms of the MT-actuators. However, they differ in the way the performance criterion is minimised and muscle physiology is imposed.

CIA solves at each recorded time instant $i = 1 \dots I$ a static optimisation problem minimising the sum of squared activations of all muscles j, while constraining the MT-forces by:

$$F_{ij} = a_{ij}\ F_{ij}^{\max} \quad \text{for } j = 1 \dots J, \tag{3.1}$$

where muscle activations a_{ij} must lie between 0 and 1, minimal and maximal activation respectively, and $F_{ij}^{\max}$ denotes the instantaneous maximal MT-force, calculated from the force-length-velocity curve and the kinematic input [4].

PIA solves a dynamic optimisation problem minimising the sum of squared activations of all muscles over all time instants. Muscle activations are constrained to comply with activation dynamics. Contraction dynamics are imposed by a linearized Hill-model, neglecting muscle fibre contraction speed [30].

Activations and MT-forces were calculated by CIA and PIA for the 43 muscles in the model during the full gait cycle and for the 13 knee flexors and extensors during the isometric experiments. Nominal MT-forces were obtained based on the musculoskeletal model with nominal parameters. Perturbed MT-forces were obtained based on the musculoskeletal model in which each MT-parameter of the knee flexors and extensors was alternately perturbed by $\pm 5\%$. τ_{act}, τ_{deact}, and the normalized muscle fibre velocity $\frac{v_{\text{m}}^{\max}}{F_{\text{m}}^{\max}}$ was perturbed in all muscles simultaneously, since these parameters are not muscle-specific [120]. Perturbing MT-parameters influences the constraints of the optimisation underlying the MT-force calculation in both CIA and PIA.τ_{act}, τ_{deact} only influence PIA.

3.2.4 Forward simulation of the Hill-model

Nominal activations calculated using PIA were input to a forward simulation that calculates the corresponding MT-forces by integrating the contraction dynamics. Using nominal MT-parameters

TABLE 3.1: Nominal parameter values for three subjects

	$F_{\mathrm{m}}^{\max}$			$L_{\mathrm{t}}^{\mathrm{s}}$			$L_{\mathrm{m}}^{\mathrm{mopt}}$			α_{opt}		
Muscle	S1	S2	S3	S1	S2	S3	S1	S2	S3	S1	S2	S3
BFL	896	896	896	0.110	0.113	0.112	0.316	0.338	0.335	0.000	0.000	0.000
BFS	804	804	804	0.167	0.181	0.181	0.086	0.093	0.093	0.400	0.401	0.400
GRA	162	162	162	0.337	0.368	0.366	0.121	0.132	0.131	0.050	0.052	0.050
GL	683	683	683	0.057	0.072	0.074	0.336	0.425	0.440	0.140	0.140	0.140
GM	1558	1558	1558	0.053	0.067	0.069	0.345	0.436	0.450	0.300	0.297	0.300
RF	1169	1169	1169	0.114	0.116	0.114	0.311	0.316	0.310	0.087	0.087	0.090
SAR	156	156	156	0.510	0.539	0.536	0.099	0.103	0.103	0.000	0.000	0.000
SM	1288	1288	1288	0.078	0.083	0.082	0.349	0.372	0.368	0.260	0.262	0.260
ST	410	410	410	0.190	0.210	0.209	0.245	0.267	0.266	0.090	0.087	0.090
TFL	233	233	233	0.095	0.098	0.097	0.425	0.437	0.433	0.050	0.052	0.050
VI	1365	1365	1365	0.087	0.088	0.086	0.136	0.138	0.135	0.050	0.052	0.050
VL	1871	1871	0.1871	0.084	0.086	0.084	0.157	0.160	0.158	0.090	0.087	0.090
VM	1294	1294	1294	0.089	0.091	0.089	0.126	0.128	0.126	0.090	0.087	0.090

Nominal parameter values for the three test subjects (S1, S2, S3). These nominal parameters are obtained by scaling the generic musculoskeletal model [32] to the test subject's dimensions based on marker information collected during a static trial. Scaled musculoskeletal models are generated using OpenSim [33]. The maximal muscle fibre velocity is given by: $v_{\mathrm{m}}^{\max} = 10/s\ L_{\mathrm{m}}^{\mathrm{opt}}$ for all muscles.

in the Hill model yielded nominal forces, while alternately perturbing each MT-parameter of the knee flexors and extensors by ±5% yielded perturbed MT-forces.

3.2.5 Sensitivity analysis

Scovil and Ronsky [91] and Redl et al. [81] evaluated sensitivity using:

$$S^e_{ijp} = \frac{(F_{\mathrm{per},ij} - F_{\mathrm{nom},ij})/F_{\mathrm{nom},ij}}{(p_{\mathrm{per},p} - p_{\mathrm{nom},p})/p_{\mathrm{nom},p}} \tag{3.2}$$

where S^e_{ijp} was the sensitivity of muscle j to parameter p at time instant i, $p_{\mathrm{nom},p}$ and $p_{\mathrm{per},p}$ were the nominal and perturbed values of parameter p, and $F_{\mathrm{n}om}, ij$ and $F_{\mathrm{per},ij}$ were the nominal and perturbed values of muscle force j at time instant i. Our definition of sensitivity differed in two ways. Firstly, we evaluated the muscle contribution to the joint moment instead of the MT-force, since the joint moment determines propulsion during gait and it is also the measured quantity during dynamometer experiments. Secondly, we used an absolute instead of a relative measure, since a large relative change in a muscle contributing only little to the joint moment hardly affects the gait pattern or the measured moment. The resulting sensitivity measure was:

$$MS^e_{ijp} = \left| \frac{(M_{+\Delta p,ij} - M_{-\Delta p,ij})/2}{\Delta p_p / p_{\mathrm{nom},p}} \right|, \tag{3.3}$$

where $\Delta p_p / p_{\mathrm{nom},p}$ was the relative parameter perturbation, $M_{-\Delta p,ij}$ and $M_{+\Delta p,ij}$ were the perturbed contributions of muscle j to the knee moment at time instant i when parameter p was perturbed by respectively $-\Delta p_p$ and $+\Delta p_p$. Individual muscle contributions to the knee moment, the MT-moments, were calculated by multiplying the MT-forces by the moment arm of the MT-actuator with respect to the knee. Hence, a MS^e_{ijp} of 100Nm could be interpreted as a parameter perturbation of 10, changing the moment by 10Nm.

We determined sensitivity to the MT-parameters of m.rectus femoris (RF), m. tensor fasciae latae (TFL), m. vastus intermedius (VI), m. vastus lateralis (VL), m. vastus medialis (VM), m. biceps femoris caput longum (BFL), m. biceps femoris caput breve (BFS), m. gracilis (GRA), m. gastrocnemius lateralis (GL), m. gastrocnemius medialis (GM), m. sartorius (SAR), m. semimembranosus (SM), and m. semitendinosus (ST). For the isometric experiments, we determined sensitivity to each MT-parameter of the maximal MT-moment predicted by the Hill-model. For the isokinetic experiments and gait, we determined sensitivity to each MT-parameter for the

MT-moment calculated using (1) CIA, (2) PIA, and for the MT-moment predicted from (3) forward simulation of the Hill-model.

For the isokinetic experiments, the maximal during the experiment

$$MS^e_{jp} = \max_i \quad MS^e_{ijp}, \tag{3.4}$$

is reported. For gait, the time average of MS^e_{ijp},

$$MS^e_{jp} = \frac{1}{I}\sum_{i=1}^{I} MS^e_{ijp}, \tag{3.5}$$

is reported. Sensitivities were averaged over the three subjects.

The calculated sensitivities during gait determined a ranking in the MT-parameters. MT-parameters with higher sensitivity require higher accuracy to reliably calculate muscle contributions to the joint moment. To facilitate the interpretation of the results, we adopted the following sensitivity classification. We classified MT-parameters with respect to their sensitivity during gait as low ($MS^e_{jp} < 5$Nm), medium ($5\text{Nm} \leq MS^e_{jp} < 10$Nm), and high ($10\text{Nm} \leq MS^e_{jp}$). The moment exerted by both knee flexors and extensors averaged over a gait cycle is in the order of 5Nm. This means that to determine the muscle contribution to the joint moment with an accuracy of 10%, MT-parameters with medium or high sensitivity need to be known with an accuracy of at least 10% or 5% respectively.

During dynamometer experiments, maximal knee torques were measured, whereas during gait, knee torques were submaximal. We therefore adopted different bounds to classify sensitivities from the dynamometer experiments. We classified the MT-parameters with respect to the highest found in the isometric and isokinetic experiments as low ($MS^e_{jp} < 50$Nm), medium ($50\text{Nm} \leq MS^e_{jp} < 10$Nm), and high ($100\text{Nm} \leq MS^e_{jp}$). A change of 10Nm can be distinguished from measurement errors as reported by [65; 95; 97]. This means that a change in an MT-parameter with medium or high sensitivity by at least 20% or 10% respectively is measurable.

3.3 Results

Figure 3.2a, 3.3a, 3.4a show MS^e_{jp} to $L^{\mathrm{s}}_{\mathrm{t}}$, $L^{\mathrm{opt}}_{\mathrm{m}}$, and $F^{\mathrm{max}}_{\mathrm{m}}$ respectively for the different analyses during gait. Sensitivity to $L^{\mathrm{s}}_{\mathrm{t}}$ (figure 3.2a) is high for RF, VI, VL, BFL, GL, GM, and SM for PIA and the forward simulation, and for VI, VL, VM, GL, GM, and SM for CIA. Sensitivity to $L^{\mathrm{s}}_{\mathrm{t}}$ (figure 3.2a) is medium for TFL, VM, and ST for PIA and the forward simulation. Sensitivity to $L^{\mathrm{opt}}_{\mathrm{m}}$ (figure 3.3a) is medium for RF, VI, and VL for PIA and the forward simulation, and for VM for CIA. Sensitivity to $L^{\mathrm{s}}_{\mathrm{t}}$ and $L^{\mathrm{opt}}_{\mathrm{m}}$ of the other muscles and to $F^{\mathrm{max}}_{\mathrm{m}}$ (figure 3.4a), τ_{act} , τ_{deact} , α_{opt}, and $v^{\mathrm{max}}_{\mathrm{m}}$ of all muscles was low.

Figures 3.2b, 3.3b, 3.4b show MS^e_{jp} to $L^{\mathrm{s}}_{\mathrm{t}}$, $L^{\mathrm{opt}}_{\mathrm{m}}$, and $F^{\mathrm{max}}_{\mathrm{m}}$ for the different analyses of the dynamometer experiments. The patterns of MS during gait (figures 3.2a, 3.3a, 3.4a) resemble the patterns of MS during the dynamometer experiments (figures 3.2b, 3.3b, 3.4b). Table 3.2 illustrates the similarities in the classification for the case of PIA. Sensitivity to 16 MT-parameters is high or medium for gait. Fourteen of these 16 parameters are in the same or higher class for the dynamometer experiments. On the other hand, the sensitivity to $L^{\mathrm{s}}_{\mathrm{t}}$ of TFL and GL is medium and high for gait, but low and medium for the dynamometer experiments, respectively.

For each MT-parameter, table 3.3 reports the isometric and isokinetic experiment with the highest MS^e_{jp}. This shows that for different MT-parameters, maximal sensitivities result from a wide range of experiments.

Although standard deviations of MS^e_{jp} showed larger variability between test subjects for gait than for the dynamometer experiments (see figures 3.2 to 3.4), the classification of the MT-parameters for the individual subjects was similar.

MT-moments calculated based on PIA or a forward simulation often had a higher sensitivity to $L^{\mathrm{s}}_{\mathrm{t}}$, $L^{\mathrm{opt}}_{\mathrm{m}}$, and $F^{\mathrm{max}}_{\mathrm{m}}$ than MT-moments calculated based on CIA (figures 3.2 to 3.4).

3.4 Discussion

We assessed and compared sensitivities of dynamic simulations to MT-parameters for gait and for dynamometer experiments. The higher the sensitivity to an MT-parameter during gait, the more accurate this MT-parameter needs to be known to analyse gait accurately.

TABLE 3.2: Classification of the MT-parameters

		RF	TFL	VI	VL	VM	BFL	BFS	GRA	GL	GM	SAR	SM	ST
L_t^s	Gait													
	Dynamometer													
L_m^{opt}	Gait													
	Dynamometer													
F_m^{max}	Gait													
	Dynamometer													

Classification of the MT-parameters of the knee flexors and extensors with respect to their sensitivity during gait and dynamometerexperiments.Results are shown for PIA. If the classification was different for the isometric and isokinetic experiments, the highest class was selected. A high sensitivity is indicated in dark gray, a medium sensitivity in light gray, and a low sensitivity in white. Sixteen MT-parameters have a high or medium sensitivity during gait. Fourteen of these 16 parameters are in the same or a higher class for the dynamometer experiments. On the other hand, the sensitivity to L_t^s of TFL and GL is medium and high for gait, but low and medium for the dynamometer experiments, respectively.

Table 3.3: Dynamometer experiments with the highest sensitivity

a. Experiment with highest sensitivity to tendon slack length													
	RF	TFL	VI	VL	VM	BFL	BFS	GRA	GL	GM	SAR	SM	ST
Isometric dynamometry	H30	H15	H15	H15	H15	L15	H60	L90	H30	H30	L105	L15	L15
Isokinetic dynamometry													
CIA	H180	H90	H60	H60	H60	H90	H90	L180	H90	H60	H180	H90	H90
PIA	H180	H60	H60	H60	H60	H60	H90	H90	H60	H60	H60	H60	H60
simulation	H180	H60	H60	H60	H60	H60	L60	H90	H60	H60	H60	H60	H60
b. Experiment with highest sensitivity to optimal muscle fiber length													
	RF	TFL	VI	VL	VM	BFL	BFS	GRA	GL	GM	SAR	SM	ST
Isometric dynamometry	L30	L15	H30	H30	H30	L15	H60	L90	H15	H30	H105	L15	L15
Isokinetic dynamometry													
CIA	H60	H90	H90	H180	H60	H60	H90	H90	H180	H60	H180	H60	H180
PIA	H60	H90	H60	H60	H60	H60	H90	H60	H60	H60	H60	H60	H60
simulation	H60	H60	H60	H60	H60	H60	L60	H60	H60	H180	H60	H60	H60
c. Experiment with highest sensitivity to maximal isometric muscle force													
	RF	TFL	VI	VL	VM	BFL	BFS	GRA	GL	GM	SAR	SM	ST
Isometric dynamometry	L30	L30	H30	H30	H30	H15	H30	H60	H15	H15	L90	H30	L60
Isokinetic dynamometry													
CIA	H90	H90	H90	H90	H60	L60	L60	H90	H60	H60	L60	H60	H90
PIA	H90	L60	H60	H60	H90	H60	L60	H90	H60	H60	H90	H60	H90
simulation	H90	L60	H60	H60	H60	H60	L60	H60	H60	H60	H60	H60	H60

The isometric and isokinetic dynamometer experiments with the highest sensitivity MS^e_{jp} to (a) tendon slack length, (b) optimal muscle fibre length, and (c) maximal isometric force (c): H refers to a high hip flexion, L refers to a low hip flexion, the number indicates the knee flexion [°] in case of the isometric experiments and the knee angular velocity [$^\circ/s$] in case of the isokinetic experiments.

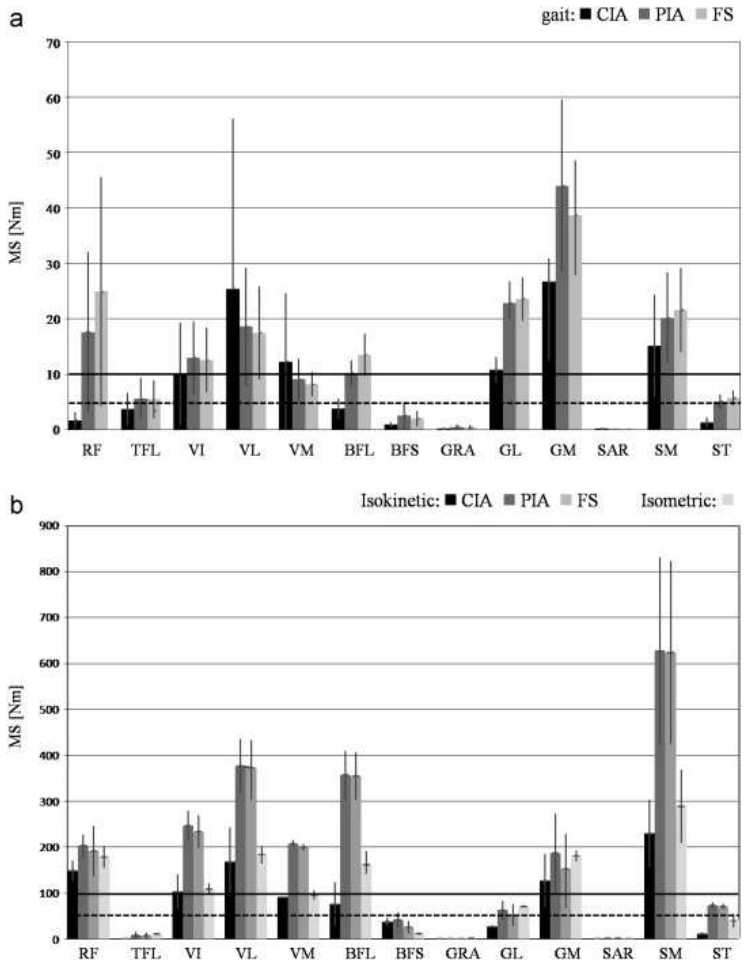

FIGURE 3.2: Sensitivities MS^e_{jp} [Nm], averaged over the test subjects, and standard deviation, of knee extensors to tendon slack length are shown. Knee extensors are m.rectus femoris (RF), m. tensor fasciae latae (TFL), m. vastus intermedius (VI), m. vastus lateralis (VL), and m. vastus medialis (VM). Knee flexors are m. biceps femoris caput longum (BFL), m. biceps femoris caput breve (BFS), m. gracilis (GRA), m. gastrocnemius lateralis (GL), m. gastrocnemius medialis (GM), m. sartorius (SAR), m. semimembranosus (SM), and m. semitendinosus (ST). For the isometric experiments (a, lightest grey), the sensitivity of the maximal muscle contribution to the isometric knee moment predicted by the Hill-model is given. For the isokinetic experiments (a) and gait (b), three different sensitivities are given: the sensitivity of the muscle contributions to the knee moment calculated based on CIA (black) and PIA (dark grey), and the sensitivity of the muscle contributions to the knee moment predicted from forward integration of the Hill-model (FS) (light grey). Standard deviation is indicated with †. According to the classification, the straight line (-) at 100Nm in (a) and 10Nm in (b) indicates the high sensitivity-level ; the dashed line (–) at 50Nm in (a) and 5Nm in (b) indicates the medium sensitivity-level.

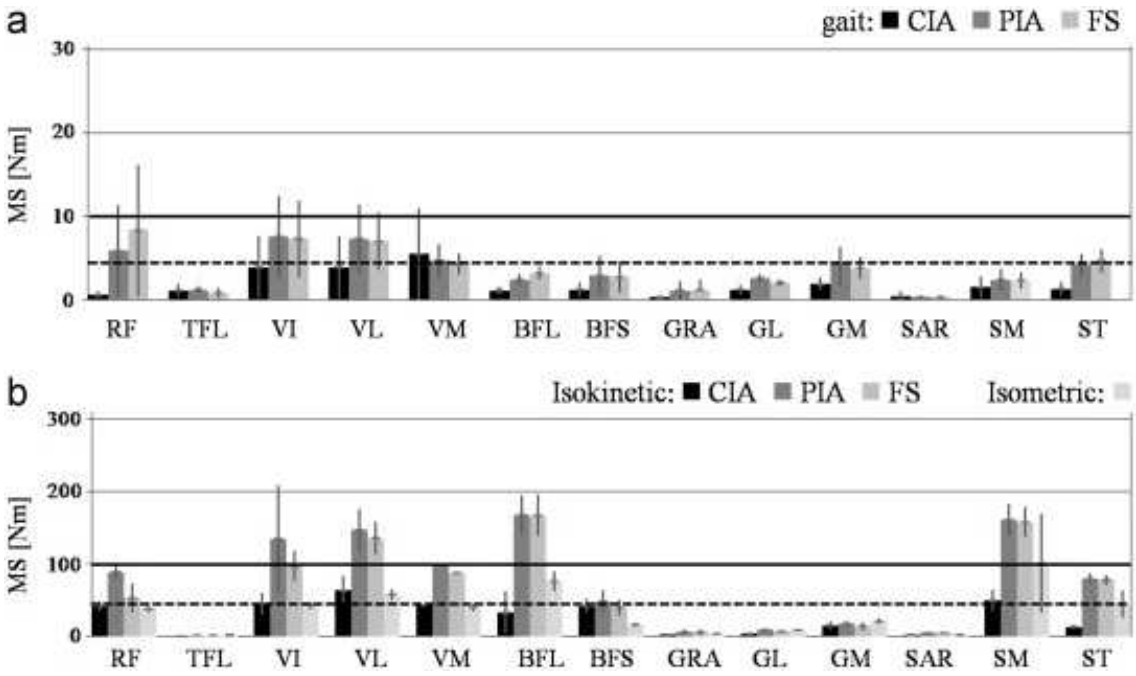

FIGURE 3.3: Sensitivities MS^e_{jp} [Nm], averaged over the test subjects, and standard deviation, of knee extensors to optimal muscle fibre length. Knee extensors are m.rectus femoris (RF), m. tensor fasciae latae (TFL), m. vastus intermedius (VI), m. vastus lateralis (VL), and m. vastus medialis (VM). Knee flexors are m. biceps femoris caput longum (BFL), m. biceps femoris caput breve (BFS), m. gracilis (GRA), m. gastrocnemius lateralis (GL), m. gastrocnemius medialis (GM), m. sartorius (SAR), m. semimembranosus (SM), and m. semitendinosus (ST). For the isometric experiments (a, lightest grey), the sensitivity of the maximal muscle contribution to the isometric knee moment predicted by the Hill-model is given. For the isokinetic experiments (a) and gait (b), three different sensitivities are given: the sensitivity of the muscle contributions to the knee moment calculated based on CIA (black) and PIA (dark grey), and the sensitivity of the muscle contributions to the knee moment predicted from forward integration of the Hill-model (FS) (light grey). Standard deviation is indicated with †. According to the classification, the straight line (-) at 100Nm in (a) and 10Nm in (b) indicates the high sensitivity-level ; the dashed line (–) at 50Nm in (a) and 5Nm in (b) indicates the medium sensitivity-level.

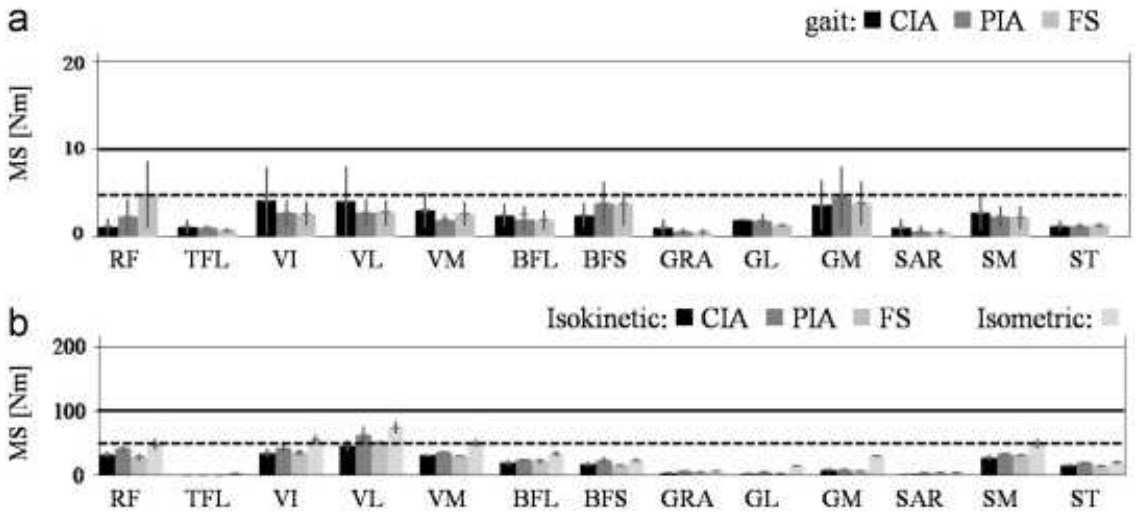

FIGURE 3.4: Sensitivities MS^e_{jp} [Nm], averaged over the test subjects, and standard deviation, of knee extensors to maximal isometric force are shown. Knee extensors are m.rectus femoris (RF), m. tensor fasciae latae (TFL), m. vastus intermedius (VI), m. vastus lateralis (VL), and m. vastus medialis (VM). Knee flexors are m. biceps femoris caput longum (BFL), m. biceps femoris caput breve (BFS), m. gracilis (GRA), m. gastrocnemius lateralis (GL), m. gastrocnemius medialis (GM), m. sartorius (SAR), m. semimembranosus (SM), and m. semitendinosus (ST). For the isometric experiments (a, lightest grey), the sensitivity of the maximal muscle contribution to the isometric knee moment predicted by the Hill-model is given. For the isokinetic experiments (a) and gait (b), three different sensitivities are given: the sensitivity of the muscle contributions to the knee moment calculated based on CIA (black) and PIA (dark grey), and the sensitivity of the muscle contributions to the knee moment predicted from forward integration of the Hill-model (FS) (light grey). Standard deviation is indicated with †. According to the classification, the straight line (-) at 100Nm in (a) and 10Nm in (b) indicates the high sensitivity-level ; the dashed line (–) at 50Nm in (a) and 5Nm in (b) indicates the medium sensitivity-level.

The higher the sensitivity to an MT-parameter during a dynamometer experiment, the more this parameter affects the measured angle-moment relation and hence, the more information the angle-moment relation contains about this parameter.

Comparing sensitivities during gait and dynamometer experiments allowed us to determine whether dynamometer experiments could provide information about the MT-parameters important to reliably study MT-function during gait. Similar sensitivity patterns for gait and dynamometer experiments would indicate that the MT-parameters which need to be known accurately to reliably analyse gait affect the isometric or isokinetic angle-moment relation measured. To help compare sensitivity patterns, MT-parameters were classified based on the effect of a parameter perturbation on the muscle contribution to the joint moment.

The sensitivity analysis showed that calculated MT-moments during gait had a high or medium sensitivity to only a limited number of MT-parameters of the 13 knee flexors and extensors (figures 3.2a, 3.3a and 3.4a), suggesting that not all muscle parameters need to be estimated. In agreement with [91] and [81], the sensitivity to $L_{\mathrm{t}}^{\mathrm{s}}$ was higher than the sensitivity to $L_{\mathrm{m}}^{\mathrm{opt}}$, and the sensitivity to $L_{\mathrm{m}}^{\mathrm{opt}}$ was higher than the sensitivity to $F_{\mathrm{m}}^{\mathrm{max}}$. However, our study revealed large differences between muscles in the effect on the muscle contribution to the joint moment when perturbing $L_{\mathrm{t}}^{\mathrm{s}}$ and $L_{\mathrm{m}}^{\mathrm{opt}}$ (figures 3.2 and 3.3). Furthermore, our definition of sensitivity revealed the lesser importance of knowing MT-parameters of TFL, GRA and SAR, as expected from the low MT-force production of these muscles.

Dynamometer experiments thus provide information about the majority of the MT-parameters that need to be accurately known to reliably calculate the MT-moment distribution during gait. However, MT-moments of TFL and GL are less sensitive to $L_{\mathrm{t}}^{\mathrm{s}}$ during dynamometer experiments than during gait. MT-length of TFL and peak MT-length of GL and the corresponding maximal isometric forces are higher during gait than during the isokinetic experiments. Since TFL and GL are bi-articular muscles, their MT-length is not only influenced by knee flexion, but also by hip and ankle position respectively. Hence, a way to obtain information about $L_{\mathrm{t}}^{\mathrm{s}}$ of TFL and GL is by changing the position of the test subject in the dynamometer.

To be useful for parameter estimation, dynamometer experiments need to contain information about the MT-parameters. However, accurate estimation of various MT-parameters also requires sufficient information in the dynamometer experiments. Our results showed that for different MT-

parameters, maximal sensitivities result from a wide range of experiments (table 3.3). Varying the hip angle during the dynamometer experiments resulted in a higher sensitivity to some MT-parameters, therefore, providing a means of collecting more information.

Garner and Pandy [42] estimated $L_{\mathrm{t}}^{\mathrm{s}}$, $L_{\mathrm{m}}^{\mathrm{opt}}$, and $F_{\mathrm{m}}^{\mathrm{max}}$ for all upper limb muscles based on isometric dynamometer experiments. Our study demonstrates that the measured isometric and isokinetic knee moments are only sensitive to a limited number of MT-parameters of the knee flexors and extensors. Consequently, it is not feasible to estimate $L_{\mathrm{t}}^{\mathrm{s}}$, $L_{\mathrm{m}}^{\mathrm{opt}}$, and $F_{\mathrm{m}}^{\mathrm{max}}$ of all knee flexors and extensors based on the studied set of dynamometer experiments. Furthermore, isokinetic dynamometer experiments are necessary to obtain information about $L_{\mathrm{m}}^{\mathrm{opt}}$ of RF, VI, and VM, three parameters having a medium sensitivity for gait, but a low sensitivity for the isometric dynamometer experiments (figure 3.3).

Sensitivity depends on the method used to calculate MT-forces: the sensitivity of MT-moments calculated based on PIA or a forward simulation to MT-parameters is higher than the sensitivity of MT-moments calculated based on CIA. A plausible explanation is that the dynamic musculoskeletal model is highly simplified in CIA. Using CIA, the Hill model is only used to calculate the instantaneous maximal MT-force. The ranking of the MT-parameters with respect to their sensitivities during gait, however, is similar for the three different analyses.

The higher inter-subject variability of MS_{jp}^{e} for gait than for dynamometer experiments was due to the higher variability in the kinematics. During dynamometer experiments, subjects were in a predefined position. Similarity of classification of the muscle specific MT-parameters, however, reinforced our conclusions.

In summary, the calculated muscle contributions to the knee moment during gait and dynamometer experiments had a high sensitivity to only a limited number of MT-parameters of 13 knee flexors and extensors. In general, the highest sensitivity was found to $L_{\mathrm{t}}^{\mathrm{s}}$. However, for some muscles the sensitivity to $L_{\mathrm{m}}^{\mathrm{opt}}$ or $F_{\mathrm{m}}^{\mathrm{max}}$ was also considerable. The ranking of the specific muscle MT-parameters with respect to their sensitivity during gait and dynamometer experiments was largely similar. We therefore conclude that the angle-moment relation measured by dynamometer experiments contains information about MT-parameters necessary to reliably analyse gait. Our study thus demonstrated the feasibility of subject-specific estimates of MT-parameters being made based on dynamometer experiments.

Acknowledgements

The support of the following projects is gratefully acknowledged: project G.0395.09 of the Research Foundation - Flanders, K.U.Leuven's Interdisciplinary Research Program IDO/07/12, and K.U.Leuven-BOF EF/05/006 Center-of-Excellence Optimization in Engineering.

Chapter 4

Functional knee axis based on isokinetic dynamometry data: comparison of two methods, MRI validation, and effect on knee joint kinematics

Abstract[1]

This paper compares geometry-based knee axes of rotation (transepicondylar axis and geometric center axis) and motion-based functional knee axes of rotation (fAoR). Two algorithms are evaluated to calculate fAoRs: Gamage and Lasenby's sphere fitting algorithm (GaL) and Ehrig et al.'s axis transformation algorithm (SARA). Calculations are based on 3D motion data acquired during isokinetic dynamometry. AoRs are validated with the equivalent axis based on static MR-images. We quantified the difference in orientation between two knee axes of rotation as the angle between the projection of the axes in the transversal and frontal planes, and the difference in location as the distance between the intersection points of the axes with the sagittal plane. Maximum differences between fAoRs resulting from GaL and SARA were 5.7° and 15.4 mm. Maximum differences between fAoRs resulting from GaL or SARA and the equivalent axis were 5.4°/11.5 mm and 8.6°/12.8 mm, respectively. Differences between geometry-based axes and EA are larger than differences between fAoR and EA both in orientation (maximum 10.6°).and location (maximum 20.8 mm). Knee joint angle trajectories and the corresponding accelerations for the different knee axes of rotation were estimated using Kalman smoothing. For the joint angles, the maximum RMS

[1]This chapter has been published as a full article in *Journal of Biomechanics*: A. Van Campen, F. De Groote, L. Bosmans, L. Scheys, I. Jonkers, J. De Schutter. Functional knee axis based on isokinetic dynamometry data: comparison of two methods, MRI validation, and effect on knee joint kinematics. 2011, vol. 44, pp. 2595-2600. Only minor changes concerning notational consistency and lay-out have been performed.

difference with the MRI-based equivalent axis, which was used as a reference, was 3°. For the knee joint accelerations, the maximum RMS difference with the equivalent axis was $20°/s^2$. Functional knee axes of rotation describe knee motion better than geometry-based axes. GaL performs better than SARA for calculations based on experimental dynamometry.

4.1 Introduction

To study human motion using musculoskeletal models the knee axes of rotation (AoR) needs to be determined. Substantial research on AoRs has already been reported. AoRs can be determined based on bone geometry. Usually, skin markers placed at the most prominent points of the epicondyles determine the transepicondylar axis (EPI) [35]. However, EPI is susceptible to palpation errors [31]. The geometric center axis (GEO) is another geometry-based axis, defined as the connection of the centers of a shape fitting the epicondyles. GEO can be obtained by imaging a subject's femur [35; 85]. These geometry-based axes are fixed, although it is known that both location and orientation of the AoR vary with knee flexion during motion [53; 92; 109].

In contrast to GEO and EPI, functional axes of rotation (fAoR) are motion-based AoRs. The orientation and location of fAoRs are averaged orientations and locations of the AoRs throughout the motion. This way, an AoR which best explains the recorded joint motion is obtained. Distinction is made between fitting techniques as described by e.g. [41; 44], and transformation techniques as described by e.g. [37; 87]. Fitting techniques optimize an objective function assuming that markers trace out a circle around the fAoR. Transformation techniques find the fAoR by minimizing the variations in distance between markers on each segment and the fAoR. These techniques have been validated in simulation [37; 41; 44], or using a mechanical device [87]. Ehrig et al. [37] quantified the influence of marker errors on the fAoR in simulation by applying Gaussian noise with a standard deviation of 1 mm. MacWilliams [66] compared fAoRs using a mechanical device and added soft tissue artifacts (STA) by attaching a compliant material to the distal tibia part. It has, however, been shown that STA are in the order of centimeters, and are more pronounced for femur markers [3; 57]. Hence, these validation approaches do not model STA correctly. Additionally, they do not evaluate the effect of muscle contraction, including (i) larger STA and (ii) the effect of loading on location and orientation of the AoR [109].

In this study, we aim to find the AoR which best describes the joint motion during isokinetic dynamometry. This knowledge can be used to overcome misalignment and malfixation, problems

inherent to dynamometry [55], and to calculate the knee joint torque more accuratly. To this end, we compare geometry-based axes (GEO and EPI), and fAoRs calculated using the algorithms proposed by Gamage and Lasenby [41] (GaL) and by Ehrig et al. [37] (SARA). GaL is the best performing sphere fitting algorithm according to the simulation study by MacWilliams [66]. SARA is the best performing axis transformation algorithm according to the simulation study by [37]. In contrast to previous simulation studies, we compared both algorithms for experimental 3D motion data of knee flexion/extension obtained during passive and active dynamometry. During passive dynamometry, the effects of muscle contraction on STA and on the pose of the axis are minimized. Comparing the results of passive and active dynamometry therefore allows the study of the influence of active muscle contraction on the estimation of the axis. We validated fAoRs with equivalent axes (EA) obtained from static MR-images [85]. This validation is chosen because the EA describes the relative motion of bones, and thus is not influenced by STA. The setup, combining 3D motion capturing and MRI, allows us to study whether fAoRs or geometry-based axes describe the motion better, and whether the GaL- or the SARA-algorithm performs best.

Additionally, this study includes calculation of knee joint kinematics according to motion-based axes (EA, fAoRs) and geometry-based axes (GEO, EPI) applying Kalman smoothing [28]. This enables us to evaluate whether the application of different AoRs results in statistically relevant differences in joint acceleration from which knee torques are calculated using inverse dynamics.

Summarizing, this study determines whether (i) the fAoRs or geometry-based AoRs are in better agreement with a motion-based EA obtained by MRI,(ii) the GaL- or the SARA-algorithm performs better e.g. under the influence of STA including muscle contraction, and (iii) the kinematics resulting from different AoRs are statistically different.

4.2 Methods

Five healthy subjects (three male, two female; BMI 21 $\pm$ 1.2) seated in a Biodex dynamometer (Biodex Medical Systems) performed isokinetic flexion/ extension of the right knee through its range of motion (ROM), typically between 20° flexion and 100° flexion, at two different speeds (30°/s and 60°/s). Each subject completed three trials actively moving the device and three trials with the device being moved and the leg passively lying on it, to minimize the effect of active muscle contraction. Markers were placed on the femur and tibia as shown in figure 4.1. A Krypton camera (Nikon Metrology) tracked the markers at 100Hz. A static measurement, with the subject

lying down on the left side, knees slightly bent, was performed.

In addition, each subject underwent four MR-scans (T1 weighted SE image series; Trio 3T, Siemens AG) of the right leg at four different knee angles: one while lying on the back with the knees slightly hyperextended (full leg scan), three while lying on the left side with the right knee flexed between 20° and 70° (partial leg scan). Markers were placed as during dynamometry.

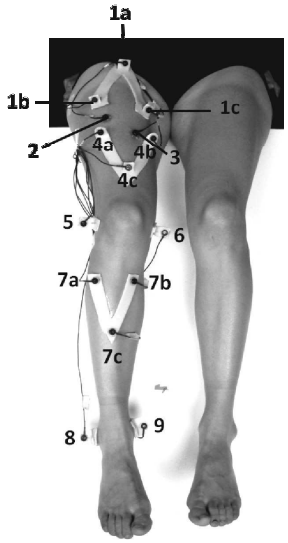

Figure 4.1: Marker protocol applied during dynamometry and MR-imaging. Ten markers were placed on the femur: a marker cluster (markers 1a-1c) at the proximal end of the femur, a marker cluster (markers 4a-4c) at the distal end of the femur, two single markers (markers 2 and 3) between the marker clusters, a marker on the lateral epicondyle (marker 5) and a marker on the medial epicondyle (marker 6). Five markers were placed on the tibia: a marker cluster on the shaft region (markers 7a-7c), a marker on the lateral malleolus (marker 8) and a marker on the medial malleolus (marker 9). All markers were placed on the anterior aspect of the subject, because (i) the subjects were sitting down during dynamometry, and (ii) the markers needed to be visible for the Krypton camera.

Anatomic femur and tibia reference frames were defined according to ISB convention based on the bone geometry extracted from the full leg scan [84]. The femur reference frame had its origin in the hip joint center (HJC), as determined by fitting a sphere to the femur head, y-axis through the midpoint of the transepicondylar connection and the HJC, and x-axis perpendicular to the plane defined by the hip HJC and the transepicondylar connection. The tibia reference frame was defined parallel to the femur reference frame in extended posture, and with its origin at the midpoint of the transepicondylar axis. MR-marker coordinates were expressed in the anatomic

reference frames.

We quantified the combined error on each marker due to (i) differences in STA resulting from different postures during dynamometry and MRI, and (ii) reattaching markers. To this end, we mapped [94] the markers on femur and on tibia from the static measurement during dynamometry and the full leg scan.

Functional axes of rotation were calculated using the algorithms proposed by [41] and [37]. Calculations were based on all 15 markers (figure 4.1). When a marker lost visibility at a certain time instant, the marker was left out of the calculations at that time instant. In contrast to [37], poses of femur and tibia with respect to Krypton camera global frame, which are input to the algorithm, are calculated using Kalman smoothing. Details are given in the supplementary material.

To validate the fAoRs, we calculated equivalent axes and equivalent angles of rotation according to Chasles's theorem based on two MR-images. The equivalent axis exactly describes the rotation of a rigid body, here the tibia, from one position to another with respect to a reference body, here the femur. We selected the two images best representing the subject's ROM during dynamometry (figure 4.2). Femur and tibia were segmented out of both MR-images [86]. We manually selected four reference points on both the femur and the tibia in both images (see figure 4.3). This allowed us to map [94] both femurs onto each other. We applied the corresponding transformation to the tibia segments. We then calculated the transformation (rotation of tibia relative to femur) between tibia segments. Equivalent axis and equivalent angle resulted from the latter transformation.

We quantified the difference in orientation between two axes as the angle between the projection of the axes in the transversal and frontal planes, and the difference in location as the distance between the intersection points of the axes with the sagittal plane. We compared (i) fAoRs calculated using GaL and SARA, (ii) fAoRs and the equivalent axis, (iii) EPI and GEO, and the equivalent axis. We performed a Wilcoxon matched-pair test on the differences in location and orientation between fAoRs resulting from GaL and EA, and between fAoRs resulting from SARA and EA. This test typically obtains whether the mean ranks of the results differ.

fAoRs were calculated based on the entire dataset of three trials for each measurement condition (active vs. passive; 30 vs. 60°/s). We calculated fAoRs for each trial and quantified the consistency of the estimations as the maximal difference in orientation and in location between two trials for each measurement condition.

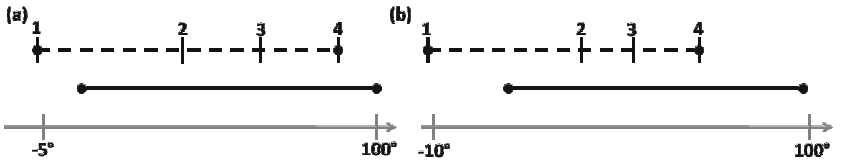

Figure 4.2: Protocol for selection of MR-images to calculate the equivalent axis. The range of motion during dynamometry (solid line between black dots) and MRI (dashed line between black dots) is shown. Knee flexion angles during MRI are indicated (1-4). We selected the two images best representing the subject's ROM during dynamometry without including a part of the range of motion which was not registered during dynamometry or loosing symmetry. For example, in situation (a), we selected images 2 and 3. In situation (b), we selected images 2 and 4.

For all measurement conditions, joint angles and accelerations were estimated by Kalman smoothing using different axes of rotation: fAoRs, EA and geometry-based AoRs. RMS and maximal values of the difference in joint angles and accelerations between AoRs and EA were calculated, both absolute and relative to the kinematics calculated based on the EA. Additionally, we performed a Wilcoxon matched-pair test on the difference in kinematics between all fAoRs resulting from GaL and EA, and the difference between all fAoRs resulting from SARA and EA.

Results were averaged over subjects and standard deviations were calculated.

4.3 Results

The error on each marker position due to different postures during dynamometry and MRI, and due to reattaching the markers is shown in table 4.1.

Comparing fAoRs resulting from SARA and GaL (table 4.2a), maximal differences were 3.8° (transversal) in orientation and 5.1 mm in location for passive measurement conditions, and 5.3° (transversal) in orientation and 12.4 mm in location for active measurement conditions.

Comparing fAoRs and EA (table 4.2b), differences in orientation ranged from 2.4° (GaL) to 5.6° (SARA) in the transversal plane, and from 5.0° (GaL) to 6.3° (SARA) in the frontal plane for passive measurement conditions. Differences in orientation were smaller for fAoRs resulting from GaL than from SARA (transversal 3.2° vs. 5.3°, frontal 4.8° vs. 7.4° respectively) for active measurement conditions. Latero-distal and latero-dorsal inclinations were consistently higher for

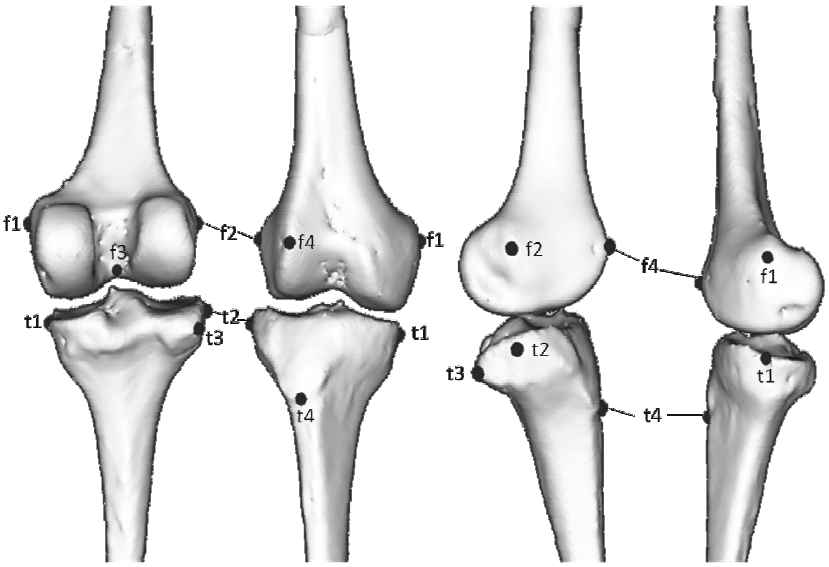

FIGURE 4.3: Reference points on femur (f1: medial epicondyle, f2: lateral epicondyle, f3: most caudal point of fossa intercondylaris, f4: most anterior point on lateral epicondyle) and on tibia (t1: medial condyle, t2: lateral condyle, t3: most proximal and prominent point on facies articularis fibularis, t4: tuberositas tibiae) used for mapping femurs onto each other and for calculating equivalent axis between consecutive images.

TABLE 4.1: Mapping errors [mm].

marker	**1a**	**1b**	**1c**	**2**	**3**
	6.1 (±1)	4.2 (±1.3)	11 (±3.2)	6.5 (±3)	7.8 (±2.9)
marker	**4a**	**4b**	**4c**	**5**	**6**
	4.9 (±2.9)	6.9 (±3)	9.1 (±3.1)	10.8 (±3.2)	10 (±3.1)
marker	**7a**	**7b**	**7c**	**8**	**9**
	5.1 (±2.6)	6 (±2.4)	4.1 (±2.5)	4.3 (±2.2)	5 (±1.9)

Mean errors [mm] between markers expressed in the anatomical reference frame (derived from MRI) and markers expressed in the camera reference (derived from dynamometry) for the calibration positions. Standard deviations are given between brackets. Marker numbers correspond to figure 4.1.

all fAoRs resulting from GaL than for EA. There was no consistency in the inclination of fAoRs resulting from SARA compared to EA. The inter subject variability is smaller for GaL than for SARA, as shown by the standard deviations. Maximal differences in location were 5.1 mm and 12.7 mm for fAoRs resulting from passive and active measurement conditions, respectively. The deviations between fAoRs resulting from GaL and EA, and between SARA and EA were statistically different.

Comparing geometry-based axes, GEO and EPI, and EA (table 4.2c), differences in orientation were respectively 7.8° and 10.6° in the transversal plane, and 8.5° and 9.3° in the frontal plane. Differences in location between geometry-based axes and EA were 20.8 mm (GEO) and 10.6 mm (EPI). The intersubject variability was higher comparing geometry-based AoRs to EA than when comparing fAoRs to EA.

GaL calculates fAoR orientations with a better inter-trial consistency than SARA. SARA calculates fAoR locations with a better inter-trial consistency than GaL for active measurements. GaL and SARA calculate fAoR locations with comparable inter-trial consistency for passive measurement conditions (table 4.3). The overall difference between kinematics resulting from GaL and EA, and the overall difference between kinematics resulting from SARA and EA differed significantly during 90% of the motion cycle for the knee joint angle and during 57% of the motion cycle for knee joint acceleration. Estimates of knee joint angles showed maximal RMS differences with EA smaller than 3.1°. Comparison of knee joint accelerations, however, depended on the measurement condition: passive motion at 30°/s resulted in maximal RMS differences of 5.1°/s^2 and maximal relative differences of 10.6%, whereas active motion at 60°/s^2 resulted in maximal RMS differences of 22.8°/s and maximal relative differences of 44.8% (table 4.4).

4.4 Discussion

We compared geometry-based knee axes, GEO and EPI, and functional axes of rotation based on marker trajectories calculated using two algorithms, GaL and SARA. We evaluated the performance of both algorithms under passive and active measurement conditions. Marker trajectories were obtained during passive and active isokinetic dynamometry, in contrast to previous studies which used simulation data [37; 41; 66]. We validated AoRs by comparing them with EA based on MR-images. Finally, we studied the influence of AoR on knee joint kinematics estimated using Kalman smoothing [28].

TABLE 4.2: Comparison of knee joint axes of rotation.

(a)	***GaL-SARA***		
	Orientation [°]		**Location [mm]**
Measurement condition	*transversal*	*frontal*	*sagittal*
30A	4.7 (±2.3)	3.9 (±2.5)	7.1 (±2.6)
30P	3.8 (±2.2)	2.8 (±1.7)	5.1 (±2.9)
60A	5.3 (±3.1)	3.2 (±1.2)	12.4 (±9.1)
60P	3.2 (±1.9)	2.3 (±1.3)	3.6 (±3.0)

(b)	***GaL-EA***			***SARA-EA***		
	Orientation [°]		**Location [mm]**	**Orientation [°]**		**Location [mm]**
Measurement condition	*transversal*	*frontal*	*sagittal*	*transversal*	*frontal*	*sagittal*
30A	3.2 (±2.4)	4.8 (±2.8)	8.7 (±4.8)	5.0 (±3.2)	5.8 (±2.7)	8.5 (±6.7)
30P	3.1 (±1.3)	5.1 (±2.9)	5.5 (±4.7)	5.2 (±3.6)	6.1 (±4.2)	6.6 (±6.8)
60A	3.5 (±2.1)	5.5 (±2.7)	12.7 (±2.7)	5.3 (±3.3)	7.4 (±3.2)	9.0 (±7.1)
60P	2.4 (±1.5)	5.0 (±3.0)	6.0 (±3.5)	5.6 (±2.6)	6.3 (±3.6)	4.1 (±4.5)

(c)	***EPI-EA***			***GEO-EA***		
	Orientation [°]		**Location [mm]**	**Orientation [°]**		**Location [mm]**
Measurement condition	*transversal*	*frontal*	*sagittal*	*transversal*	*frontal*	*sagittal*
	10.6 (±4.7)	9.3 (±7.2)	10.6 (±3.4)	7.8 (±5.6)	8.5 (±6.9)	20.8 (±6.0)

Comparison of knee joint axes of rotation. Table (a) shows the differences in orientation [°] and location [mm] between axes resulting from GaL and SARA; table (b) shows the differences in orientation [°] and location [mm] between axes resulting from GaL and SARA, respectively, and the EA used as a measure to validate; table (c) shows the differences in orientation [°] and location [mm] between the geometry-based axes GEO and EPI and the EA. The experiments were completed at two velocities, 30°/s and 60°/s, indicated as 30 and 60, both actively (A) and passively (P). Differences in orientation are expressed as the angle between the projection of the axes in the transversal and frontal planes. Differences in location are expressed as the distance between the intersection points of the axes with the sagittal plane. Values are averaged over the subjects. Standard deviations are reported between brackets.

Table 4.3: Inter-trial consistency

	GaL			***SARA***		
	Orientation [°]		**Location [mm]**	**Orientation [°]**		**Location [mm]**
Measurement condition	*transversal*	*frontal*	*sagittal*	*transversal*	*frontal*	*sagittal*
30A	1.3 (±0.6)	2.5 (±2.8)	12.8 (±10.7)	18.4 (±6.1)	18.3 (±5.9)	4.7 (±5.1)
30P	2.4 (±3.7)	2.4 (±3.7)	4.4 (±3.1)	37.4 (±11.1)	36.4 (±11.6)	3.7 (±4.0)
60A	4.1 (±5.0)	3.6 (±3.5)	9.8 (±6.0)	17.3 (±7.4)	17.4 (±7.4)	3.8 (±1.6)
60P	0.7 (±0.4)	1.1 (±1.6)	5.0 (±5.7)	18.2 (±8.0)	17.4 (±7.6)	2.2 (±2.4)

Maximal difference in orientation and location of the fAoR resulting from GaL and SARA between trials for each measurement condition. The experiments were executed at two velocities, 30°/s and 60°/s, indicated as 30 and 60, both actively (A) and passively (P). Differences in orientation are expressed as the angle between the projection of the axes in the transversal and frontal planes. Differences in location are expressed as the distance between the intersection points of the axes with the sagittal plane. Values are averaged over the subjects. Standard deviations are reported between brackets.

Poses of tibia and femur were determined based on local marker positions expressed in the anatomical reference frame. Mapping errors between local marker positions obtained from the MR-images and the marker positions during the static measurement acquired by the Krypton camera are given in table 4.1. The errors are possibly due to (i) reattaching the markers before MR-imaging, (ii) using glycerin markers, to meet nonferrous requirements for MR-imaging, (iii) manually locating the marker centers in the images, and (iv) differences in STA resulting from different postures. Compared to STA induced by motor tasks, these errors are rather small [3]. We also verified that the mapping errors cannot account for the differences in the calculated AoRs (see supplementary material). Moreover, by mapping more than the minimum number of three markers on the femur segment, the influence of the errors on the segment's pose is reduced (if the additional markers move independently). Since the same local marker positions are used for all calculations, these mapping errors do not influence the comparison between fAoRs.

Comparing GaL and SARA for passive measurements, maximal differences in orientation and location were 3.8° (transversal) and 5.1 mm. These differences doubled and quadrupled, respectively, for active measurements. This indicates that both algorithms have different sensitivities to the effect of muscle contraction on the marker trajectories.

TABLE 4.4: Effect of knee joint axis on knee joint kinematics.

(a)	**RMS Angle** [°]									
Meas. condition	*EPI*	*GEO*	*GL30A*	*GL30P*	*GL60A*	*GL60P*	*SARA30A*	*SARA30P*	*SARA60A*	*SARA60P*
30A	3.2 (±1.7)	2.4 (±2.0)	2.0 (±0.8)	1.8 (±0.8)	3.1 (±0.9)	1.6 (±0.8)	2.0 (±1.7)	2.0 (±1.0)	2.0 (±1.6)	1.8 (±1.0)
30P	3.3 (±1.6)	2.5 (±1.9)	1.9 (±0.9)	1.6 (±0.9)	3.0 (±1.0)	1.5 (±0.8)	1.9 (±1.7)	1.7 (±1.1)	2.1 (±1.7)	1.6 (±1.0)
60A	3.2 (±1.6)	2.3 (±1.9)	2.0 (±0.7)	1.9 (±0.8)	3.0 (±1.0)	1.6 (±0.8)	2.1 (±1.6)	2.0 (±1.0)	2.1 (±1.7)	1.8 (±0.9)
60P	3.4 (±1.6)	2.5 (±1.9)	1.9 (±0.8)	1.6 (±0.8)	3.0 (±1.1)	1.4 (±0.7)	2.0 (±1.7)	2.0 (±1.1)	2.0 (±1.7)	1.6 (±1.0)
(b)	**MAX Angle** [%]									
Meas. condition	*EPI*	*GEO*	*GL30A*	*GL30P*	*GL60A*	*GL60P*	*SARA30A*	*SARA30P*	*SARA60A*	*SARA60P*
30A	5.9 (±3.1)	4.5 (±3.5)	3.6 (±1.3)	3.3 (±1.4)	5.6 (±1.8)	2.9 (±1.5)	3.7 (±2.9)	3.8 (±1.7)	3.7 (±2.9)	3.3 (±1.6)
30P	6.1 (±2.9)	4.7 (±3.4)	3.6 (±1.4)	3.1 (±1.6)	5.4 (±1.8)	2.7 (±1.3)	3.6 (±3.1)	3.2 (±2.0)	4.0 (±3.1)	2.9 (±1.9)
60A	5.8 (±3.1)	4.3 (±3.6)	3.7 (±1.2)	3.4 (±1.4)	5.6 (±2.0)	3.0 (±1.4)	3.8 (±2.8)	3.9 (±1.6)	3.9 (±2.8)	3.4 (±1.5)
60P	6.2 (±3.2)	4.6 (±3.6)	3.6 (±1.3)	3.0 (±1.4)	5.5 (±1.8)	2.7 (±1.2)	3.6 (±2.9)	3.2 (±1.8)	3.7 (±2.9)	2.9 (±1.7)
(c)	**RMS Acceleration** [$^\circ/s^2$]									
Meas. condition	*EPI*	*GEO*	*GL30A*	*GL30P*	*GL60A*	*GL60P*	*SARA30A*	*SARA30P*	*SARA60A*	*SARA60P*
30A	8.2 (±4.2)	9.1 (±.5.8)	6.3 (±3.9)	6.9 (±2.6)	9.7 (±8.1)	5.9 (±2.3)	7.9 (±4.6)	8.7 (±4.5)	8.4 (±4.7)	7.5 (±3.9)
30P	5.2 (±2.2)	5.6 (±2.1)	2.6 (±1.3)	3.9 (±0.3)	4.8 (±2.3)	3.4 (±0.9)	3.5 (±2.4)	3.8 (±1.9)	5.1 (±2.9)	3.6 (±1.8)
60A	19.9 (±9.6)	15.9 (±6.1)	16.0 (±9.5)	16.9 (±6.5)	22.8 (±17.3)	14.8 (±7.0)	17.4 (±7.6)	19.9 (±9.2)	17.2 (±6.9)	18.5 (±9.6)
60P	13.5 (±5.6)	11.6 (±4.2)	7.7 (±3.8)	10.1 (±1.7)	14.7 (±6.9)	8.7 (±3.4)	10.3 (±7.5)	10.5 (±5.3)	11.2 (±7.6)	9.5 (±4.9)
(d)	**MAX Acceleration** [%]									
Meas. condition	*EPI*	*GEO*	*GL30A*	*GL30P*	*GL60A*	*GL60P*	*SARA30A*	*SARA30P*	*SARA60A*	*SARA60P*
30A	17.2 (±9.2)	18.5 (±11.6)	13.4 (±8.7)	14.3 (±6.2)	19.7 (±17.0)	12.4 (±5.5)	16.1 (±9.4)	18.2 (±9.5)	17.9 (±10.4)	15.9 (±8.2)
30P	10.5 (±5.0)	12.3 (±4.4)	5.1 (±2.6)	7.9 (±1.0)	9.3(±4.4)	6.7 (±1.8)	7.1 (±5.1)	7.8 (±4.7)	10.6 (±6.1)	7.5 (±4.4)
60A	38.9 (±19.4)	31.1 (±11.3)	31.0 (±20.0)	32.9 (±13.4)	44.8 (±36.6)	28.3 (±13.0)	33.9 (±16.0)	38.5 (±17.1)	34.3 (±14.6)	35.5 (±17.1)
60P	25.7 (±11.1)	23.3 (±10.9)	15.2 (±7.3)	19.6 (±3.6)	28.5 (±12.9)	16.8 (±6.9)	20.3 (±14.5)	21.4 (±11.9)	22.0 (±14.6)	19.0 (±10.9)

Comparison of knee joint axes of rotation. Table (a) shows the differences in orientation $^\circ$ and location [mm] between axes resulting from GaL and SARA; table (b) shows the differences in orientation $^\circ$ and location [mm] between axes resulting from GaL and SARA, respectively, and the EA used as a measure to validate; table (c) shows the differences in orientation $^\circ$ and location [mm] between the geometry-based axes GEO and EPI and the EA. The experiments were completed at two velocities, 30°/s and 60°/s, indicated as 30 and 60, both actively (A) and passively (P). Differences in orientation are expressed as the angle between the projection of the axes in the transversal and frontal planes. Differences in location are expressed as the distance between the intersection points of the axes with the sagittal plane. Values are averaged over the subjects. Standard deviations are reported between brackets.

Comparing fAoRs and EA for passive measurements, differences in orientation in the transversal plane are smaller for GaL (2.4°) than for SARA (5.6°); in the frontal plane, differences are comparable (5.0° for GaL, 6.3° for SARA). Differences in orientation between fAoR and EA for active measurements were smaller for fAoRs resulting from GaL (transversal 3.2°; frontal 4.8°) than for those resulting from SARA (transversal 5.3°, frontal 7.4°). Moreover, the differences between GaL and EA were similar to the ones for passive measurements. This indicates that GaL is less sensitive to the effect of muscle contractions on the marker trajectories for calculations of the orientation. We found a consistent inclination between fAoRs resulting from GaL and EA in the latero-distal and latero-dorsal directions. Maximal difference in location between fAoR and EA for passive measurements was 5.1 mm. Maximal difference in location between fAoRs and EA for active measurements was 12.7 mm. This indicates that both algorithms are sensitive to the effect of muscle contractions on the marker trajectories for calculation of the location. The higher correspondence between fAoRs and EA for passive measurements is as expected, because the images are also taken in passive conditions. The difference between fAoRs and EA might arise from (i) the difference between STA in dynamometry, where the subject is sitting in a chair, and in MR-imaging, where the subject is lying on the side; (ii) the effects of soft tissue motion which are minimized but not completely eliminated in passive dynamometry, and (iii) the different inputs for the calculations of EA and fAoRs: EA results from a transformation between two positions whereas fAoRs are calculated as mean axes describing the recorded ROM. Despite these sources of errors, the fAoRs describe the motion of tibia relative to femur in a good way (as shown by the animation provided in the supplementary material). fAoRs resulting from GaL and SARA showed statistically significant different deviations from EA.

We found larger differences comparing EPI/GEO to EA than comparing fAoRs to EA. This indicates that motion-based axes and geometry-based axes do not concur, nor do geometry-based axes, as reported earlier [35; 71].

The AoR influenced the estimated knee joint angles in a statistically significant, but limited manner (less than 3.1°). The influence on knee joint accelerations however, was more pronounced. We found maximal RMS-differences of 22.4°/s and maximal relative differences of 44.8% when using fAoRs as compared to EA for the active measurement at 60°/s. Differences with EA are larger for geometry-based AoRs than for fAoRs. Differences with EA are larger for faster and active motions. For the active measurement at 60°/s, the maximal knee joint accelerations during the

non-isokinetic part of the measurement are in the order of $200^\circ/s^2$, which is about twenty times smaller than the maximal knee joint accelerations during gait. This finding suggests that the accuracy of the modeled AoR becomes more critical as accelerations increase.

This study has some limitations. Firstly, although our dataset is larger than those evaluated in other studies, e.g. [109], it is still relatively small. Hence, statistical observations should be interpreted carefully. Secondly, our approach only allows a relative quantification of the combined effects of muscle contraction (i.e. larger STA and the direct effect on location and orientation of the AoR) by comparing the results based on passive and active measurement conditions. Thirdly, inaccuracies are introduced during mapping due to the difference in STA during different postures assumed by the subjects. Fourthly, we were restricted by the amount of flexion possible during MRI, which in turn restricted us in calculating EA for the same ROM as during dynamometry. Despite these limitations we found convincingly better agreements between fAoRs and EA than between geometry-based axes and EA. Moreover, the latter limitations account for both algorithms which enables us to distinguish between the performance of the algorithms of GaL and SARA using experimental data.

In summary, we calculated fAoRs based on 3D marker trajectories acquired during passive and active isokinetic dynamometry experiments of the knee, and we validated the fAoRs with EA based on MR-images. We found different fAoRs using GaL and SARA, for both passive and active measurement conditions. In general, GaL showed the best correspondence with EA, mainly for orientation. Moreover, fAoRs resulting from GaL showed a consistent inclination compared to EA both in latero-distal and latero-dorsal direction. fAoRs were in better agreement with EA than geometry-based axes. The AoR had limited influence on the estimated knee joint angles, but did influence the estimated knee joint accelerations, especially at higher velocity. Based on these findings, we suggest using functional knee axes of rotation rather than geometry-based knee axes of rotation, and using the algorithm of [41] to calculate the fAoR.

Acknowledgements

The support of the following projects is gratefully acknowledged: project G.0395.09 of the Research Foundation - Flanders and K.U.Leuven's Interdisciplinary Research Program IDO/07/12.

4.5 Supplementary material

Calculating functional axes

Implementation of algorithms

Gamage and Lasenby [41] (GaL) calculate the orientation n and the location defined by a fixed point m on the axis by minimizing the following objective functions respectively:

$$\text{Cost}(\mathbf{n}, \mathbf{m}^p) = \sum_{p=1}^{P} \sum_{i=1}^{I} \left[(\mathbf{v}_i^p - \mathbf{m}^p) \cdot \mathbf{n} \right]^2, \tag{4.1}$$

and

$$\text{Cost}(r^p, \mathbf{m}) = \sum_{p=1}^{P} \sum_{i=1}^{I} \left[(\mathbf{v}_i^p - \mathbf{m})^2 - (\mathbf{r}^p)^2 \right]^2, \tag{4.2}$$

with $p = 1 \dots P$ indicating the markers on one segment, $i = 1 \dots I$ indicating the time instants, $\mathbf{v}_i^p$ the (measured) position of marker p at time instant i expressed in the reference frame of the other segment, $\mathbf{r}^p$ the distance from the point $\mathbf{m}$ on the line to the circular arc marked out by marker p, $\mathbf{m}^p$ any point on the plane traced out by vector $\mathbf{v}^p$. In our application, we expressed the position of the tibia markers in the femur reference frame, $\mathbf{v}_{tf}$. $P = 5$ is the number of markers on the tibia. i depends on the measurement condition and on the subject.
The orientation $\mathbf{n}$ is obtained by differentiating 4.1 with respect to $\mathbf{m}^p$, and substituting the result in 4.1. The latter expression can be written in matrix form $A\ \mathbf{n} = 0$. The singular value decomposition of A yields $\mathbf{n}$.
The location $\mathbf{m}$ is obtained by differentiating 4.1 with respect to $\mathbf{m}^p$, and substituting the result in 4.2. The latter expression can be written in matrix form $A\ \mathbf{m} = \mathbf{b}$ from which $\mathbf{m}$ can be extracted.

Ehrig et al. [37] (SARA) calculate the orientation n and the location defined by a fixed point m on the axis by minimizing the objective function:

$$\text{Cost}(\mathbf{m}^f, \mathbf{m}^t) = \sum_{i=1}^{I} \left\| R_i^f\ \mathbf{m}^f + t_i^f - \left(R_i^f\ \mathbf{m}^t + t_i^t \right) \right\|^2, \tag{4.3}$$

with $\mathbf{m}^{t/f}$ a fixed point on the axis expressed in the local femur/tibia reference frame and $R_i^{t/f}$ and $t_i^{t/f}$ the rotation and translation, respectively, from the local femur/tibia reference frame to the ground reference frame at time instant i. Expression 4.3 can be written in matrix form

$A\ \mathbf{x} = \mathbf{b}$. The singular value decomposition of A yields $\mathbf{n}$ and $\mathbf{m}$.
The pose of femur and tibia with respect to the ground at every time instant i is described by transformation matrices T_i^{fw} and T_i^{tw}, respectively. These transformation matrices depend on six generalized coordinates (three rotations and three translations) which are obtained by processing marker trajectories with the Kalman smoothing algorithm proposed by [28] (implementation details given below). The positions of the tibia markers measured in the ground reference frame, $\mathbf{v}_{tw}$, are transformed to the femur reference frame to serve as input for equations 4.1 and 4.2:

$$\mathbf{v}_i^{tf} = \left(T_i^{fw}\right)^{-1}\ \mathbf{v}_i^{tw}. \tag{4.4}$$

Rotation matrices $R_i^{f/t}$ and translation vectors $t_i^{f/t}$ used as input for SARA are readily obtained from the transformation matrices from the local femur and tibia reference frames to the ground reference frame, T_i^{fw} and T_i^{tw}, respectively:

$$T_i^{f/t\ w} = \begin{pmatrix} R_i^{f/t} & t_i^{f/t} \\ 0 & 1 \end{pmatrix}. \tag{4.5}$$

Implementation of knee motion model

The knee motion model proposed by Yamaguchi and Zajac [119] is frequently used in musculoskeletal modeling. The model describes the translation of the knee axis of rotation in proximal/distal and anterior/posterior direction as a function of the knee angle θ, $t_{\text{yamaguchi}} = [t_x\ t_y\ 0]'$ while the orientation remains fixed. The rationale behind combining the algorithms described above and the model of [119] is as follows: algorithms for calculating functional knee axes of rotation assume that the location of the axis (all points on the axis) remains fixed. However, it is known that both orientation and location depend on e.g. knee flexion and loading. In order to relax the assumption of a fixed location, we subtracted the scaled translation $t_{\text{yamaguchi}}$ according the model of [119] from the fixed point. Consequently, the optimization algorithms 4.1, 4.2 and 4.3 result in a mean orientation n and a fixed location m at extension. At the end, m is translated to the mean of the recorded range of motion.

The following procedure describes the implementation:

Firstly, the orientation $\mathbf{n}$ of the axis is calculated according to equation 4.1 or 4.3.

Secondly, θ for every time instant i, θ_i, is calculated by aligning the z-axis of a local femur reference frame with n and using inverse XYZ Euler angles to calculate the rotation of tibia with respect to femur around $\mathbf{n}$. θ is the angle between the anatomical z-axis and the orientation of the functional axis:

$$\boldsymbol{\alpha} = \text{acos } (\mathbf{z} \cdot \mathbf{n}). \tag{4.6}$$

To align, $\mathbf{z}$ and $\mathbf{n}$, a rotation around $\mathbf{al}$, the axis perpendicular to $\mathbf{z}$ and $\mathbf{n}$ is needed:

$$\mathbf{al} = \mathbf{z} \times \mathbf{n}. \tag{4.7}$$

The corresponding transformation T_{zn} representing a rotation of $\boldsymbol{\alpha}$ about $\mathbf{a}l$ is:

$$T_{zn} = \begin{pmatrix} R & 0 \\ 0 & 1 \end{pmatrix}. \tag{4.8}$$

R is used to to calculate θ_i:

$$\theta_i = -\text{bgtg } (-R\ R_i^{tf}(1,2), R\ R_i^{tf}(1,1)). \tag{4.9}$$

As θ_i is known, scaling factors $s = [s_x\ s_y\ 0]$ for the unscaled translation $\hat{t}_{\text{yamaguchi}}(\theta_i)$ at each time instant can be obtained by minimizing (based on equation 4.2):

$$\text{Cost} = \sum_{p=1}^{P} \sum_{i=1}^{I} \left[\left(\mathbf{v}_i^p - \left(\mathbf{m} - \mathbf{s}\ \hat{t}_{\text{yamaguchi}} \right) \right)^2 - \left(\mathbf{r}^p \right)^2 \right]^2, \tag{4.10}$$

or (based on equation 4.3)

$$\text{Cost} = \sum_{i=1}^{I} \left\| R_i^f\ \mathbf{m}_f - R_i^t\ \mathbf{m}_t + t_i^f - t_i^t - \mathbf{s}\ \hat{t}_{\text{yamaguchi}} \right\|^2, \tag{4.11}$$

based on GaL and SARA respectively. Cost is minimized with respect to s using the fmincon solver from the Matlab optimization toolbox, with lower bounds [0 0 0] and upper bounds [2 2 0].

$\mathbf{m}$ is than calculated by applying $\mathbf{t}_{\text{yamaguchi}} = \mathbf{s}\ \hat{t}_{\text{yamaguchi}}$ to (equation 4.2):

$$\text{Cost} = \sum_{p=1}^{P} \sum_{i=1}^{I} \left[\left(\mathbf{v}_i^p - \left(\mathbf{m} - t_{\text{yamaguchi}} \right) \right)^2 - \left(\mathbf{r}^p \right)^2 \right]^2, \tag{4.12}$$

TABLE 4.5: Combining GaL and SARA with the model of Yamaguchi.

	GaL-EA		***SARA-EA***	
	Location	**KMY**	textbfLocation	**KMY**
measurement condition	[mm] sagittal	[mm] sagittal	[mm] sagittal	[mm] sagittal
30A	8.7 (±4.8)	16.9 (±12.3)	8.5 (±6.7)	12.2 (±7.8)
30P	5.5 (±4.7)	14.3 (±8.6)	6.6 (±6.8)	13.3 (±11.2)
60A	12.7 (±2.7)	32.4 (±19.6)	9.0 (±7.1)	24.3 (±7.1)
60P	6.0 (±3.5)	31.7 (±23.5)	5.1 (±4.5)	21.2 (±8.7)

Differences [mm] between marker position before and after the transformation ((a) according to Gamage and Lasenby [41] based on passive measurements at 30°/s (GL30P); (b) according to Ehrig et al. [37] based on passive measurements at 30°/s (SARA30P)) and mapping errors (c) for one subject. Directional differences (x, y, z) and total distances are shown. Markers are according figure 1 in the paper.

and to (equation 4.3):

$$\text{Cost} = \sum_{i=1}^{I} \left\| R_i^f \ \mathbf{m}_f - R_i^t \ \mathbf{m}_t + t_i^f - t_i^t - t_{\text{yamaguchi}} \right\|^2 . \tag{4.13}$$

Relaxing the assumption of a fixed location of the functional axis by combining GaL and SARA with the knee motion model of [119], results in a worse location of the functional axis in comparison to the location of the equivalent axis (see table 4.5).

Kalman smoothing

The Kalman smoother combines prior knowledge, described by a process and measurement model, with the measured marker trajectories to produce an estimate of the joint kinematics while minimising the estimation error statistically. In contrast to e.g. [94], Kalman smoothing takes into account that the joint kinematics at a certain time instant depend on the joint kinematics at the previous and next time instants.

Process model

The process model predicts the expected time evolution of the generalized coordinates. To guarantee a smooth motion, it is assumed that the fourth derivative of the generalized co-ordinates is constant. A noise term takes into account the model errors introduced by this assumption.

Measurement model

The measurement model is based on a biomechanical model. Segments were modeled by relating local marker positions in the segment's anatomical reference frame to the marker positions in the camera reference frame by six generalized coordinates. As an input for the algorithm of [41], generalized coordinates were based on a femur model. As an input for the algorithm of [37], generalized coordinated were based on a femur model and on a tibia model. As for the calculation of joint kinematics, generalized coordinates were based on a model of femur and tibia with 7 DOFs: the femur has 6 DOFs with respect to the world, the tibia is connected to the femur by a 1 DOF joint defined by the geometry-based axes and the motion-based axes (nine calculations).

Transformation matrices between the segment's anatomical reference frame and the ground at each time instants are derived from the generalized coordinates. Each marker in the model is weighted to indicate its reliability, e.g. markers on the epicondyles were given lower weights (higher uncertainty) as they suffer from large STA. The higher the weights, the more the estimate will be based on the measurement model.

Influence of mapping errors

The magnitude of the mapping errors as presented in table 1 of the paper suggest that the differences between equivalent axes (EA) and functional axes (fAoR) might arise from these errors. To qualify the effect of the mapping errors on the reported differences between the axes, we transformed the fAoR to the EA, we applied this transformation to the femur markers (these markers showed the largest mapping errors), and calculated the difference between markers before and after the transformation. This allows us to verify whether the differences in marker positions before and after the transformation are explained by mapping errors.

The following procedure explains how we retrieved differences in femur marker positions when the fAoR's pose is transformed to the EA's pose:

1. Define a frame with origin in the intersection point (m0) of the equivalent axis with the sagittal plane. Each marker position is originally expressed in the anatomic reference frame (as defined in the paper) with origin in the hip joint center. To express the marker positions in the new frame, each marker is translated over -m0 (expressed in the anatomic reference frame).

TABLE 4.6: Marker differences and mapping errors [mm].

(a) GL30P										
Marker	1a	1b	1c	2	3	4a	4b	5	6	
X	9.1	9.2	3.8	5.4	6.4	8.0	2.5	3.8	5.8	-2.2
Y	-4.5	-1.7	-12.3	-8.8	-6.5	-2.9	-13.5	-9.6	-3.7	-18.5
Z	-42.9	-27.8	-32.1	-28.7	-26.2	-22.1	-25.1	-15.6	-3.5	-3.4
Distance	44.1	29.3	34.6	30.5	27.7	23.7	28.7	18.7	7.8	18.9
(a) GL30P										
Marker	1a	1b	1c	2	3	4a	4b	5	6	
X	12.6	12.6	7.1	8.7	9.8	11.3	5.7	7.0	9.0	0.8
Y	1.8	4.7	-6.5	-2.8	-0.4	3.4	-7.8	-3.6	2.5	-13.0
Z	-44.1	-28.2	-32.7	-29.2	-26.5	-22.3	-25.4	-15.4	-2.8	-2.7
Distance	45.9	31.3	34.1	30.6	28.3	25.2	27.2	17.3	9.7	13.3
(a) GL30P										
Marker	1a	1b	1c	2	3	4a	4b	5	6	
X	3.5	1.3	8.2	-4.9	0.8	-9.7	-6.6	6.2	5.8	-4.6
Y	-1.0	-0.9	-8.5	-0.1	-0.6	-4.5	0.2	6.2	5.2	3.9
Z	-4.1	3.8	5.2	-1.3	1.3	-0.7	0.2	-3.3	-0.7	-0.5
Distance	5.5	4.2	12.9	5.1	1.6	10.7	6.6	9.4	7.8	6.1

Differences [mm] between marker position before and after the transformation ((a) according to Gamage and Lasenby [41] based on passive measurements at 30°/s (GL30P); (b) according to Ehrig et al. [37] based on passive measurements at 30°/s (SARA30P)) and mapping errors (c) for one subject. Directional differences (x, y, z) and total distances are shown. Markers are according figure 1 in the paper.

2. To align the EA and fAoR, a rotation around the axis perpendicular to both EA and fAoR is needed (cfr. eq. 4.7). This results in a transformation representing the rotation from the functional axis to the equivalent axis (cfr. eq. 4.8).

3. To make the EA and fAoR coincide, a translation between the intersection points of the axes with the sagittal plane is added to the transformation.

4. The transformation matrix resulting from 2. and 3. is then applied to the marker positions calculated in 1. Differences between marker positions before and after the transformation can now be calculated.

5. To qualify the influence of the mapping errors on the comparison of EA and fAoRs, the calculated differences between marker positions before and after the transformation are compared to the mapping errors (see Table 4.6 for one subject).

From table 4.6, we conclude that:

(i) the differences between marker positions corresponding to EA and fAoR are systematic in contrast to the mapping errors. E.g.: 1) from inspection of the signs of the differences in X-, Y-, and Z-directions, and 2) the larger the distance between the AoR and the marker, the larger the difference between markers corresponding to EA and fAoR ;

(ii) the average difference between marker positions corresponding to EA and fAoR is much larger compared to the mapping errors.

In summary, the described differences between equivalent axis and functional axes cannot be attributed to the mapping errors only.

Chapter 5

An extended dynamometer set-up to improve the accuracy of knee joint moment assessment

Abstract[1]

This paper analyses an extended dynamometry setup that aims at obtaining accurate knee joint moments. The main problem of the standard setup is the misalignment of the joint and the dynamometer axes of rotation due to non-rigid fixation, and the determination of the joint axis of rotation by palpation. The proposed approach (i) combines 6D registration of the contact forces with 3D motion capturing (which is a contribution to the design of the setup), (ii) includes a functional axis of rotation in the model to describe the knee joint (which is a contribution to the modelling), and (iii) calculates joint moments by a model-based 3D inverse dynamic analysis. Through a sensitivity analysis, the influence of the accuracy of all model parameters is evaluated. Dynamics resulting from the extended setup are quantified, and are compared to those provided by the dynamometer. Maximal differences between the 3D joint moment resulting from the inverse dynamics and measured by the dynamometer were 16.4Nm (16.9%) isokinetically and 18.3Nm (21.6%) isometrically. The calculated moment is most sensitive to the orientation and location of the axis of rotation.

In conclusion, more accurate experimental joint moments are obtained using a model-based 3D inverse dynamic approach that includes a good estimate of the pose of the joint axis.

[1]This chapter has been published as a full article in *IEEE Transactions on Biomedical Engineering*: A. Van Campen, F. De Groote, I. Jonkers, J. De Schutter. An extended dynamometer set-up to improve the accuracy of knee joint moment assessment. 2013, vol. 60, pp. 1202-1208. Only minor changes concerning notational consistency and lay-out have been performed.

5.1 Introduction

Dynamometry is the process of obtaining selective subject-specific strength profiles by measuring joint moments in controlled conditions: isometric at selected joint angles or isokinetic at selected angular velocities. However, the standard setup does not result in accurate control of the joint's motion [103] and measurements of the joint's moment (see e.g. [97]). The dominant factor causing dynamometer measurement inaccuracy is the misalignement between machine axis and joint axis of rotation (AoR). In case of the knee joint, the cause of this misalignment is twofold. First, the fixation between the body segments and the dynamometer is not rigid. This results in a motion of the segments relative to the dynamometer and an absolute displacement of the AoR. Second, the AoR's location is not accurately known as the alignment is based on palpation of the lateral epicondyle. The alignment errors will be minimized if the joint angle and the joint load are the same during the measurement and the alignment procedure. In practice however, alignment under active conditions is mostly not feasible as discussed further in this paper. Also, the AoR's pose depends on the joint angle and the joint load [103; 109].

One way to improve the measurement accuracy, is to track the motion of the body segments. Herzog [46] and Arampatzis et al. [5] collected 3D kinematic data based on skin markers. The disadvantage of using skin markers is that they do not represent the true bone motion. Kaufman et al. [55] collected 3D kinematic data with tri-axial goniometry. However, this device is known to be inaccurate. Tsaopoulos et al. [101] collected 2D kinematic data with X-ray fluoroscopy to obtain true bone motion, and hence to overcome the errors introduced by soft tissue. But, as the knee motion is a 3D motion, out-of-plane motion corrupts the kinematic data [93]. Joint moments can be calculated by inverse dynamics based on a model. Herzog [46], Arampatzis et al. [5] and Tsaopoulos et al. [101] analysed this 3D problem with a 2D model, and did not measure reaction forces and moments. This necessitates them to make assumptions concerning moment arms, reaction moment, and orientation of the force transmitted between limb segment and dynamometer. Kaufman et al. [55] were able to analyze a 3D lower limb model, because they mounted a load cell between lower leg and device. A common limitation of these studies is that they model the knee's AoR as a geometry-based AoR whereas Van Campen et al. [103] recently showed that a functional axis of rotation better describes the actual joint kinematics during dynamometry, and hence, results in more reliable joint dynamics.

The aim of this paper is twofold. First, we describe an experimental setup that extends a standard

Biodex Pro3 System to obtain 3D knee joint dynamics. The setup combines 3D motion capturing of foot, tibia, femur and crank, and registration of the reaction forces and moments by a 6D load cell. Data processing consists of inverse kinematics and inverse dynamics based on a model including a functional AoR instead of a geometry-based AoR. A functional AoR is a one degree of freedom joint axis model. It does however not represent a pure flexion/extension axis (according to the ISB convention), but it describes the coupled rotations in the knee joint as well. The sensitivity of the calculated joint moment to all model parameters is evaluated. Second, we compare the knee joint moment obtained by the proposed approach with dynamometer results and with the knee joint moment obtained by the approach proposed by Herzog [46] to quantify the of influence the assumptions which had to be made by [5; 46; 101].

5.2 Methods

5.2.1 Dynamometry

Two international athletes (19y female, BMI 21; 20y male, BMI 18) performed isometric and isokinetic contractions at five angles (30 ° to 90 ° with 15 ° increment) and three velocities (30, 60, 120 °/s, the range of motion was between 20 ° and 100 °). Three contractions were performed for each of these conditions in both directions. The direction of motion is referred to as flexion/extension although there are small coupled rotations in the other directions as well. The subject could relax for 10s between contractions. The procedure was approved by the ethical committee, and an informed consent was signed.

Subjects were seated in a Biodex Pro3 dynamometer at 60 ° hip flexion, attached with the regular belts. The hip joint center was determined by palpation. 90 ° knee flexion was defined as the line connecting lateral epicondyle and maleolus being perpendicular to the line connecting the epicondyle and the hip center of rotation. Alignment of the knee joint axis with the dynamometer axis of rotation was performed at 60 ° knee flexion in passive conditions assuming that the lateral epicondyle defined the transepicondylar axis. Active markers were placed on foot (3), tibia (5), femur (7) and crank (3) (see fig. 5.1a), and were tracked by a Krypton camera (K600, Nikon) which was placed in front of the subject at a distance of 2.5 to 3m. A 6D force sensor (JR3 inc.) was mounted in the crank of the dynamometer, without changing its regular setup (fig. 5.1 c). Data acquisition was synchronized at 200Hz. Analog signals of the dynamometer where collected through a NI SCB-68 I/O connector (National Instruments). Krypton data where transferred by a

regular ethernet cable. Load cell data where received by a 1-channel PCI. Software was customized (orocos.org) to trigger the logging of all data streams simultaneously.

5.2.2 Model

The system was modelled with four segments and nine degrees of freedom (DOF) (see fig. 5.1 a-b): the crank has one rotational DOF about the dynamometer AoR, the femur has six DOFs, the tibia has one DOF relative to the femur, and the foot has one DOF relative to the tibia. The knee joint was described by a one DOF functional AoR which 3D pose was calculated from the 3D positions of the active markers on tibia and femur [41; 103]. Scaled musculoskeletal models of the subjects were available. To this end a generic model [32] was scaled based on 62 markers as is described by [52]. Mass and inertia parameters resulted from the scaled model (see also table 1B). Inertial parameters of the crank were obtained from experimental identification. MR-images of each subject with non-ferrous markers were obtained in order to define local marker positions in the anatomic reference frames according to ISB conventions for each segment. For details about the imaging procedure and the location of the anatomic reference frames, we refer to [103].

5.2.3 Analysis

For inverse kinematics of the lower limb, a Kalman smoothing algorithm [28] was used. Van Campen et al. [103] provide details on inverse kinematics and determination of functional AoRs. In addition, the ankle kinematics are calculated by modelling the foot's rotation relative to the tibia by the dorsi/plantarflexion axis adopted from the scaled model. From inverse dynamics, the knee moment generated about the functional AoR (M3D, see Appendix for details on equations of motion) and the interaction forces between tibia and crank ($\mathbf{F}_{tc}$) were obtained. For comparison, knee moments according to the 2D analysis [46] were calculated. Dynamometer voltage signals representing joint angle and moment were converted according to the manufacturer's specifications. Dynamometer moments (Mdyn) were corrected for gravitation.

Dynamics resulting from the dynamometer's processed voltage signals are compared to the results of the 3D dynamic analysis. Absolute differences and relative differences with respect to the peak moments in flexion and extension are reported. Mean differences between M3D and Mdyn based on all data samples are calculated, as well as corresponding 95% limits of agreement. Differences between 2D and 3D analysis are quantified. The orientation of the interaction force between tibia and crank was calculated to verify the perpendicularity to the crank, an assumption underly-

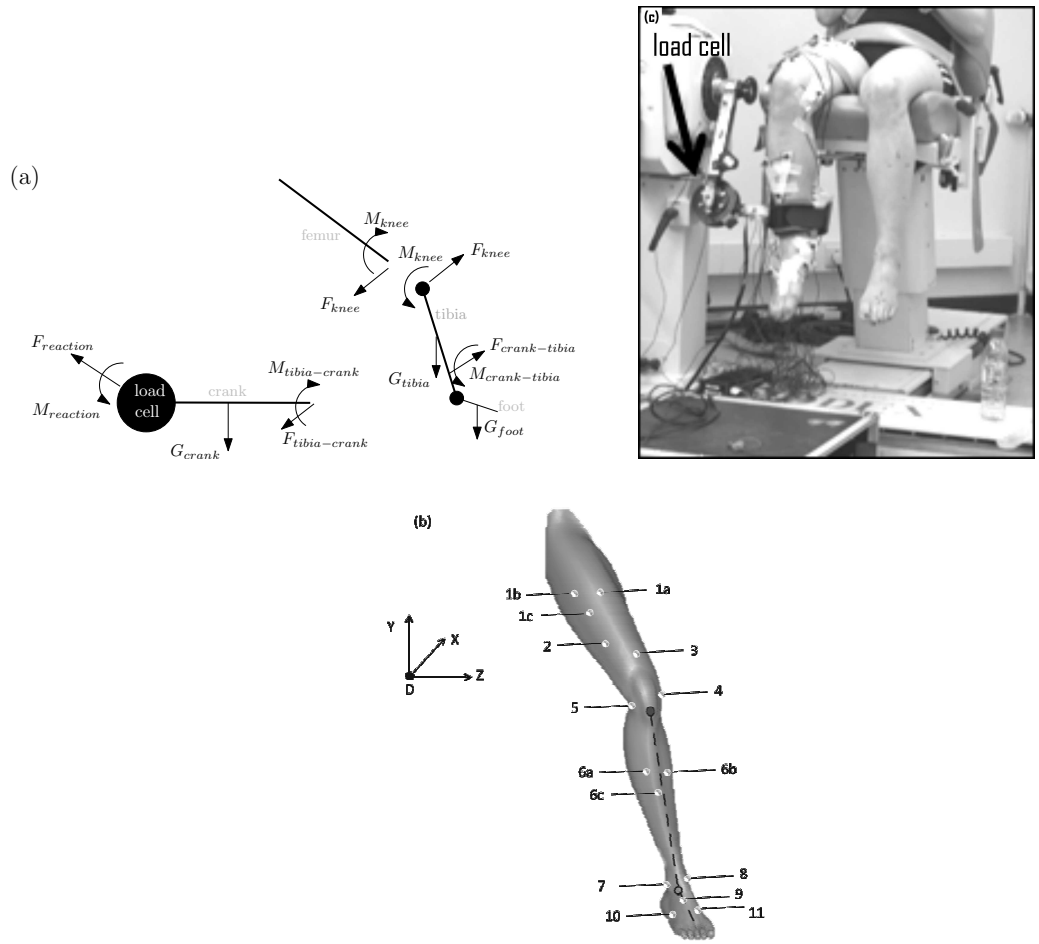

FIGURE 5.1: (a) Free body diagram of the foot-tibia-crank-system. The knee and ankle joint are indicated with •. $\mathbf{F}_{knee}$ and $\mathbf{M}_{knee}$ are the reaction forces and moments at the knee joint. $\mathbf{F}_r$ and $\mathbf{M}_r$ are the reaction forces and moments at the load cell. $\mathbf{G}_{knee}$, $\mathbf{G}_{foot}$ and $\mathbf{G}_{crank}$ are the gravitational forces of knee, foot and crank, respectively. $\mathbf{F}_{reaction}$ and $\mathbf{M}_{reaction}$ are the reaction forces and moments at the load cell. $\mathbf{F}_{tibia-crank}$ and $\mathbf{M}_{tibia-crank}$ are the reaction forces and moments exerted by the tibia on the crank. All vectors used to derive the equations of motion are expressed relative to D in the XYZ reference frame. D is the reference point on the dynamometer axis of rotation. (b) Markerprotocol as applied during dynamometry. Markers are indicated: seven markers on femur (1-5; 4 and 5 are placed on the femoral epicondyles), five on tibia (6-10; 9 and 10 are placed on the maleoli), and three on foot (11-13; 12 and 13 are placed on the lateral and medial side of the midfoot, 11 is placed on the midfoot). Clusters are indicated with a-b-c. All markers were placed on the anteriori aspect of the subject. (c) The picture of the experimental setup illustrates the mounting of the load cell.

ing the 2D analysis as described in literature. Finally, the sensitivity to all model parameters was examined by quantifying the effect of parameter perturbations on the calculated joint moment. Segment's centres of mass and AoR's position are perturbed in anterior and proximal direction (X,Y). AoR's orientation is perturbed about X- and Y-axis. Perturbations of the functional AoR are based on the differences between geometry-based and functional AoR as reported by [103]. Perturbations of the centre of mass were based on [72].

5.3 Results

Alignment

The location of the functional AoR was never constant with respect to the dynamometer AoR during the experiments. Figure 5.2 illustrates the motion of $\mathbf{r}_{knee}$ (intersection of the functional AoR with the sagittal plane) in a plane perpendicular to the dynamometer AoR during isokinetic and isometric conditions. The displacement of the functional AoR depends on the measurement condition and on the direction of motion (flexion versus extension). During isokinetic measurements, the average displacements with respect to the dynamometer AoR were 40.6mm (±2.4: S1) and 65.5 mm (±31.6: S2) during flexion and 18.4mm (±9.3: S1) and 36.0mm (±22.2: S2) during extension. During isometric measurements, average displacements were 50.1mm (±16.5: S1) and 71.4mm (±16.5: S2) during flexion, and 10.9mm (±2.8: S1) and 8.7mm (±1.2: S2) during extension. The motion of the functional axis relative to its initial position during isometric conditions results from the subject's muscle contraction (axis moves away from initial position), and relaxation (axis moves again towards the initial position).

Dynamics

The three dimensional knee joint moment M3D differs from the dynamometer moment Mdyn during isokinetic and isometric conditions. The differences are subject-dependent. The differences are larger at higher velocities (isokinetic) and at positions near the middle of the rom (isometric). Mean differences between M3D and Mdyn for both subjects during all measurement conditions indicate a systematic difference between M3D and Mdyn (table 5.2).

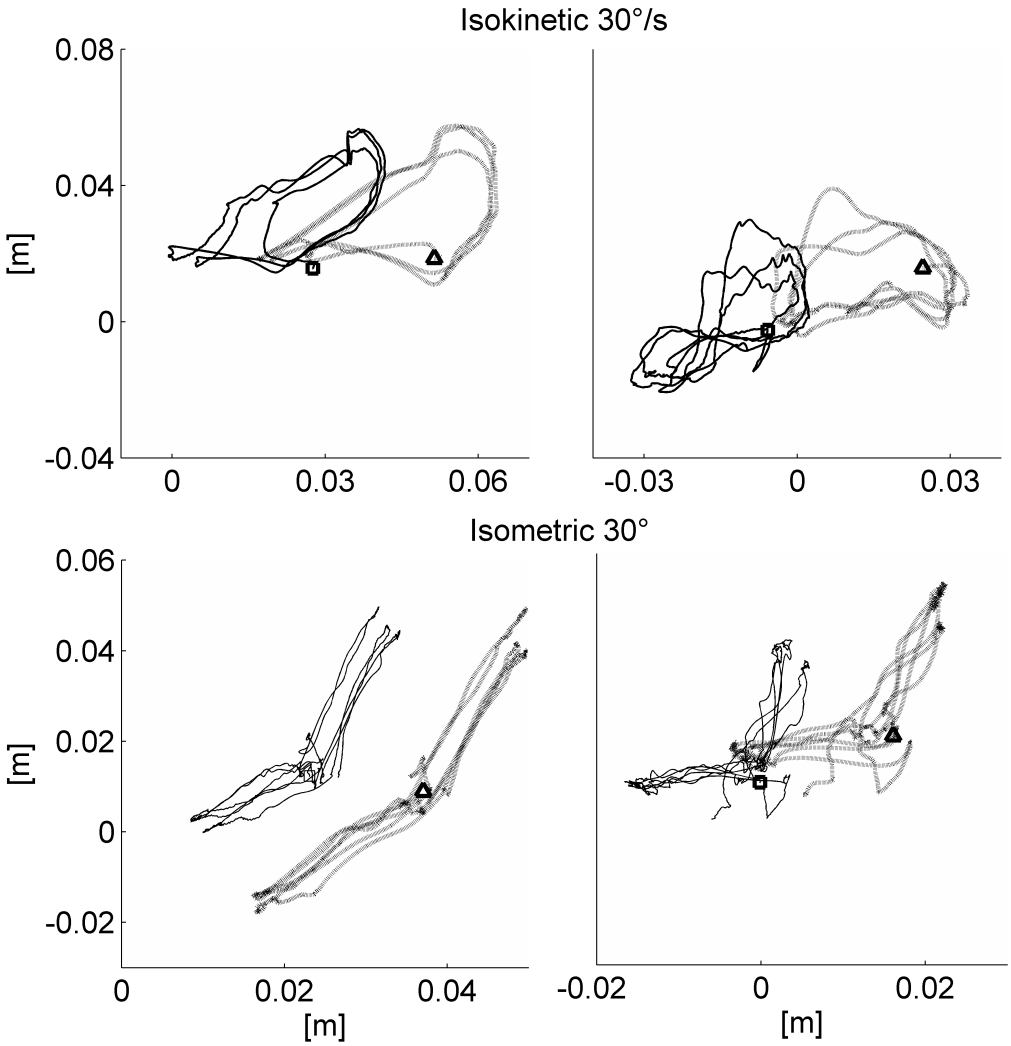

FIGURE 5.2: Motion of the functional AoR (black dots) and the lateral epicondyle (black full) in the sagittal plane for both test subjects (S1: left column; S2: right column) for two measurement conditions. The position of the biodex axis of rotation is located at (0,0). The location of the functional AoR and the lateral epicondyle at the beginning of the measurement are indicated (Epicondyle:square; functional AoR: triangle).

Table 5.1: Sensitivity analysis:
perturbations and resulting effect on moment.

		S1		**S2**	
A.	Δp	*isok*	*isom*	*isok*	*isom*
n_{knee}	10 °	4.0 (0.7)	4.3 (2.7)	4.8 (0.7)	5.0 (2.7)
r_{knee}	2cm	3.9 (0.4)	4.1 (0.7)	3.2 (0.4)	3.8 (0.5)
mass °	0.25kg	1.0 (0.1)	0.7 (0.2)	1.1 (0.1)	0.7 (0.3)
com*	2cm	0.7 (0.1)	0.5 (0.1)	0.7 (0.04)	0.3 (0.2)
B.		**S1**		**S2**	
$mass_{foot}$		0.91kg		0.92kg	
$mass_{tibia}$		2.69kg		2.74kg	
com_{foot}		[0.053 -0.012 0.008] m		[0.055 -0.013 0.009] m	
com_{tibia}		[0 -0.1875 0] m		[0 -0.2017 0] m	

A. Overview of changes in joint moment (given in [Nm]) due to perturbations in model parameters (Δ p). Maximal changes averaged over the conditions are shown for both subjects (S1-S2) during isokinetic and isometric contractions (standard deviations are given between brackets). For mass, centre of mass, and inertia tensor only the maximal changes for either foot or tibia (° indicates foot, $*$ indicates tibia) are shown. For orientation and location of the functional AoR the maximal changes are shown for perturbations about the anatomical X-axis and along the Y-axis respectively.
B. Overview of the most important inertia parameters of the limb segments as used in the model. Centre of mass of the tibia is expressed in the tibia reference frame (according to ISB convention), centre of mass of the foot is expressed in the foot reference frame (origin at midpoint of malleoli, axes parallel with tibia frame in anatomic position).

TABLE 5.2: 95% Limits of Agreement

	Flexion				**Extension**			
	|Δmean| [Nm]		**LOA [Nm]**		**|Δmean| [Nm]**		**LOA [Nm]**	
condition	**S1**	**S2**	**S1**	**S2**	**S1**	**S2**	**S1**	**S2**
30 °/s	3.5	11.7	11.5	21.9	0.2	5.3	9.1	21.9
60 °/s	6.6	9.3	11.4	18.6	2.4	4.1	10.6	10.1
120 °/s	2.5	4.4	14.1	16.7	2.6	1.1	14.5	17.4
30 °	11.1	14.0	7.4	8.0	7.7	14.5	6.7	6.7
45 °	10.6	19.4	6.3	10.0	7.7	17.8	6.8	9.8
60 °	10.4	20.7	6.6	13.3	6.2	16.5	5.6	10.9
75 °	6.6	19.7	5.3	14.8	3.9	13.1	8.3	10.2
90 °	10.9	17.6	6.5	13.8	1.9	5.2	13.3	7.9

Mean differences between M3D and Mdyn (absolute values) for all measurement conditions and for subject 1 (S1) and subject 2 (S2). 95% limits of agreement (LOA) are indicated as 2 x 1.96 x standard deviation of the differences. The mean difference indicates the averaged difference between M3D and Mdyn during the experiment. The limits of agreement indicate the interval (around the mean difference) which contains 95% of the measurment points.

The moments resulting from a 2D analysis [46] (M2D) differ from M3D during isokinetic and isometric conditions as presented in table 5.3 and fig. 5.3. The differences during isometric conditions are similar in magnitude as those between Mdyn and M3D, although there are small changes; e.g. for S1, the mean difference during flexion was larger (6.4Nm). The differences during isokinetic conditions are almost double compared to those between Mdyn and M3D; during extension M2D underestimates the joint moment whereas during flexion M2D overestimates the joint moment.

The interaction force vector was considered to be perpendicular to the crank if its angle with the normal to the crank was less than 15 °. During isokinetic conditions the perpendicularity condition was satisfied during 8.1% (S1) and 70.1% (S2) of the experimental time. The higher the velocity, the less the orientation of the force was perpendicular to the crank throughout the range of motion. During isometric conditions the perpendicularity condition was satisfied during 0.8% (S1) and 95.6% (S2) of the contraction time. Overall, the orientation of the interaction force is highly subject-dependent.

Sensitivity analysis

Table 5.1 shows maximal changes in calculated knee joint moments averaged over the isokinetic and isometric conditions. When perturbing the pose of the functional AoR, the changes in joint moment were slightly larger for isometric conditions (S1/S2: 4.0/4.8Nm isokinetically versus 4.3/5.0Nm isometrically, and 3.9/3.2Nm isokinetically versus 4.1/3.8Nm isometrically for respectively orientation and location). For isometric conditions, changes in joint moment perturbing the orientation became larger at higher knee flexion. Perturbing the centre of mass of the tibia of tibia and foot in proximal direction resulted in ΔM between 0.7Nm and 1.1Nm. Pertubing the ankle AoR or $\mathbf{I}$ resulted in changes smaller than 0.6Nm.

5.4 Discussion

The main problems to obtain an accurate knee moment by standard dynamometry are due to misalignment between the dynamometer's AoR and the joint's AoR. In this paper, first, a full 3D analysis for isokinetic and isometric dynamometry at the knee joint is presented. In contrast to previous studies, marker-based 3D motion capture is combined with 6D load cell data. Second, the joint AoR is modelled as a functional AoR. Functional AoRs better explain the joint's motion than geometry-based AoRs (e.g. the transepicondylar axis), and hence result in more accurate dynamics. Third, Kalman smoothing, which has been shown to give good estimates of the joint kinematics [28], is used for inverse kinematics. Kinematics obtained using Kalman smoothing and a functional AoR differ from dynamometer kinematics confirming results reported in literature [5; 46; 55; 101]. A sensitivity analysis revealed that the accuracy of the estimation of the knee joint axis' pose is much more important than the accuracy of other model parameters. Applications which rely on joint moments e.g. to obtain information about the joint's actuators [42] will benefit from experimental data with improved accuracy [29].

Isokinetic

Inverse dynamics showed that M3D and Mdyn differ during isokinetic conditions. The differences were at most 15.2Nm/12.6Nm (31.8%/12.7%) (S1) and 21.5Nm/16.4Nm (58.3%/16.9%) (S2) during flexion/extension. The lower the velocity, the smaller the difference became, and M3D was typically smaller than Mdyn.

In literature, there are two studies, Herzog [46] and Kaufman et al. [55], that reflected on the accuracy of isokinetic dynamometry albeit using other measuring and modelling techniques. Her-

TABLE 5.3: Comparison of M3D with Mdyn and M2D

	Flexion				**Extension**			
	S1	**S2**	**S1**	**S2**	**S1**	**S2**	**S1**	**S2**
A	**Δmax**		**Δmean**		**Δmax**		**Δmean**	
Isok	15.2	21.5	4.5	8.6	12.6	16.4	2.8	4.3
[Nm]	(5.8)	(0.9)	(1.8)	(3.7)	(6.8)	(2.9)	(0.9)	(1.1)
Isok	35.7	58.3	10.4	21.1	18.0	16.9	4.0	4.4
[%]	(16.7)	(20.9)	(3.9)	(4.3)	(11.8)	(3.4)	(2.4)	(1.1)
Isok-2D	27.5	35.7	14.6	20.4	34.3	35.7	16.3	16.6
[Nm]	(5.7)	(13.6)	(4.5)	(4.1)	(5.2)	(13.7)	(4.6)	(1.4)
Isom	18.7	25	9.9	18.3	13.9	21.5	5.7	13.4
[Nm]	(3.9)	(3.3)	(1.9)	(2.6)	(2.1)	(4.2)	(2.2)	(4.9)
Isom	27.8	29.6	14.6	21.6	12.5	15.2	5.4	9.7
[%]	(5.6)	(5.8)	(2.0)	(3.9)	(6.9)	(5.2)	(3.8)	(4.8)
Isom-2D	18.9	26.8	10.8	19.9	12.5	18.0	4.6	9.5
[Nm]	(3.9)	(3.5)	(1.8)	(2.8)	(2.6)	(2.9)	(2.0)	(4.8)
B [Nm]	**max**		**mean**		**max**		**mean**	
30 °/s	56.1	33.1	55.4	34.8	84.2	48.7	103.7	69.2
60 °/s	55.6	32.7	37.1	21.9	109.6	65.2	86.3	49.2
120 °/s	40.9	24.9	27.9	10.1	100.3	57.9	103.5	36.2
30 °	85.4	92.8			71.9	98.3		
45 °	77.5	93.1			99.9	129.2		
60 °	64.6	87.6			128.3	169.2		
75 °	50.8	80.6			161.2	186.6		
90 °	63.0	72.9			184.9	171.8		

A. Maximal and averaged (absolute) differences between moments calculated by 3D inverse dynamics and moments registered by the dynamometer (*Isok/Isom*). Maximal and averaged (absolute) differences between moments calculated by 3D and 2D inverse dynamics (*Isok-2D/Isom-2D*) are reported. Relative differences to the peak moment ([%]) between moments resulting from 3D inverse dynamics and moments resulting from the dynamometer are reported. For all isokinetic and isometric measurement conditions respectively, absolute values are averaged over the measurement conditions. Standard deviations are given between brackets.

B. Maximal moments calculated by 3D inverse dynamics per measurement conidition. For isokinetic measurements, the averaged moments over the flexion and extension part of the motion are reported additionaly.

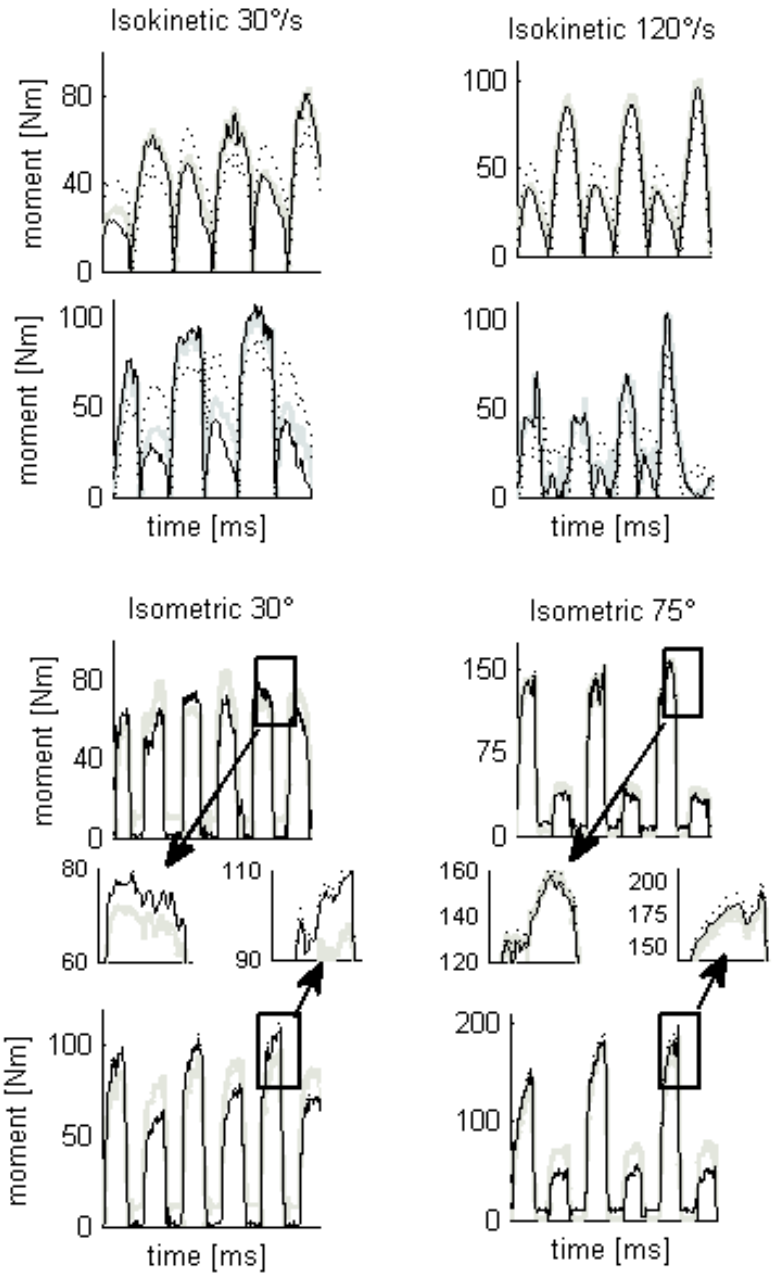

FIGURE 5.3: M3D (grey), Mdyn (dashed black), and M2D (black) for subject 1 (upper row) and subject 2 (lower row). Four measurement conditions are given: isokinetic 30 °/s and 120 °/s, and isometric 30 ° and 75 °.

zog obtained joint positions by videotaping four markers on crank and tibia segment. Kaufman et al. obtained joint positions with a tri-axial electro-goniometer. Basically, the presented inverse kinematics differs in two ways: the joint's AoR is described as a functional AoR, and kinematic data is collected by a 3D motion capture system and post processed by Kalman smoothing [28]. When comparing the resulting dynamics, the magnitude of the averaged differences between the calculated joint moment and Mdyn obtained in this study is higher than reported by Herzog, and comparable to those reported by Kaufman et al. In agreement with Kaufman et al., the contribution of the inertia to the joint moment was limited. However, Kaufman et al. found smaller differences at higher velocities, and both studies reported that the calculated moments were larger than Mdyn. Likely causes for these opposing observations are: (i) Herzog performs a 2D analysis whithout measuring reaction forces, and therefore has to make assumptions concerning the application point of the interaction force $\mathbf{F}_{tc}$ between tibia and crank and concerning the orientation of $\mathbf{F}_{tc}$, (ii) kinematic data is more accurate in the present study, and (iii) the description of the joint's AoR is different. (ii) and (iii) will both influence inverse dynamics. From a theoretical point of view, the approach proposed here will deliver the most accurate results. Moreover, according to the sensitivity analysis, the pose of the joint's AoR has the largest influence on the inverse dynamics results.

Kaufman et al. [55] reported the orientation of the interaction force between tibia and crank. Some 2D studies ([5] and [101]) rely on these findings to justify the assumptions concerning the interaction force between crank and tibia. Kaufman et al. reported long periods during which $\mathbf{F}_{tc}$ was perpendicular to the crank. However, in this study, the interaction force was not perpendicular to the crank throughout the isokinetic measurement. These different findings might result from the setup or different modelling approach. Kaufman et al. attached the crank anteriorly to the tibia whereas in this paper, the crank was attached posteriorly.

In general, the subject-dependency of the results might be explained by the overall difference in strength between the subjects. Additionally, differences in muscle and soft tissue volumes can explain the different amounts of motion between the segments and the dynamometer. Although the setup was standardized, the subject's comfort was a priority. Figure 5.2 illustrates that the motion of the joint's AoR relative to the dynamometer AoR was larger for S2 than for S1.

Performing the 2D analysis similar to Herzog [46], the averaged differences between M3D and M2D were 14.6Nm/20.4Nm (S1/S2) during flexion and 16.3Nm/16.6Nm (S1/S2) during extension. These findings demonstrate the effect of the assumptions in a 2D analysis, which boil down to

accounting only for an offset of the lever arm in the direction of the crank. In this study the lever arm was based on the pose of the functional AoR and the application of $\mathbf{F}_{tc}$ resulted from the 3D analysis.

Isometric

M3D and Mdyn do differ during isometric conditions as well. Averaged differences were 9.9Nm/18.3Nm (14.6%/23.0%) (S1/S2) during flexion and 5.7Nm/13.4Nm (5.4%/6.1%) (S1/S2) during extension.

In literature, there are two studies, Arampatzis et al. [5] and Tsaopoulos et al. [101], that reflected on the accuracy of isometric dynamometry, again using other measuring and modelling techniques. Arampatzis et al. [5] and Tsaopoulos et al. [101] studied isometric conditions by a 2D approach. Arampatzis et al. obtained kinematic data by 3D motion capturing, Tsaopoulos et al. by fluoroscopy. The absolute and relative differences between calculated joint moment and Mdyn are larger than those reported by Arampatzis et al. and Tsaopoulos et al. In contrast to both studies, here, the joint moment during extension was larger than Mdyn, which was more pronounced at lower knee flexion, and vice versa during flexion. The opposite findings result from the different approaches: 3D versus 2D inverse dynamics. For the 2D approach, not based on interaction forces, following assumptions have to be made: (i) the application point of $\mathbf{F}_{tc}$ is known, and (ii) the orientation of $\mathbf{F}_{tc}$ is known. The latter assumption is based on the findings of Kaufman et al. [55] which were reported for isokinetic conditions and for a non-regular setup: the contact was located at the anterior part of the tibia. Here, the contact is located at the posterior part of the tibia where soft tissue volumes are larger. The coefficient of friction depends on the soft tissue volume, and hence on the subject. Following this reasoning we expect that the range of possible angles between $\mathbf{F}_{tc}$ and the perpendicular orientation would be higher for a person with a higher BMI. Our experimental findings (only two subjects) are in line with this expectation. Moreover, estimating or measuring the application point of $\mathbf{F}_{tc}$ is inaccurate as there is no precise point contact, and defining the application point of $\mathbf{F}_{knee}$ based on a transepicondylar axis is inaccurate as well, because the AoR does not correspond to the transepicondylar axis [103]. In fact, the sensitivity analysis shows that the AoR's pose is the most important parameter to obtain accurate results. These assumptions will affect the calculations of the reaction forces in the knee and hence also the joint moment.

Performing the 2D analysis similar to Herzog [46], the averaged differences between M3D and M2D were 10.8Nm/19.9Nm (S1/S2) during flexion and 4.6Nm/9.5Nm (S1/S2) during extension.

Sensitivity analysis

A sensitivity analysis was performed and revealed that (i) orientation and location of the functional knee joint axis are the most crucial model parameters for both isokinetic and isometric conditions, and (ii) that the accuracy of model parameters adopted from the scaled Opensim model suffices.

Limitations

The limitations of this study are the following. (i) Inverse kinematics (and hence the pose of the functional AoR [103]) is based on motion capturing of skin mounted markers. As a consequence the moments resulting from the inverse dynamic analysis are influenced by soft tissue artefacts. However, the described methodology takes advantage of the Kalman smoothing for inverse kinematics, which has been shown to improve the accuracy of the estimated joint kinematics over previously used methods [28]. Anatomical landmark displacements are minimized by linking the skin markers to the underlying bone segements [103]. (ii) The alignement of the AoR's was passively performed at one position. For a fair comparison between studies, the alignement should be performed under the same conditions (knee angle, passive or active). In general, the alignement should preferably be done under conditions as close as possible to the experimental conditions. Tsaopoulos et al. [101] performed the alignment both passively and actively as during experimental conditions, but the difference between M2D and Mdyn were larger using the latter approach. In the end, it would be unfeasible to repeat the alignment procedure for each measurement condition given the number of experiments, and because isokinetic experiments result in motion of the joint axis relative to the dynamometer axis (see fig. 5.2). (iii) The dataset was too limited to link the differences between the subjects to the subject's characteristics.

5.5 Conclusion

A 3D model-based analysis of knee joint dynamics showed that the difference between the results as given by a dynamometer (Biodex 3Pro) and by a 3D analysis can grow up to 21.5Nm during isokinetic conditions and 25Nm during isometric conditions. Differences depend on the measurement condition and on the subject. Whether these differences are important depends on the application: for some applications repeatibility might be needed (which was not part of this study) whereas whenever accurate measurements are needed, for validation purposes or to extract actuator information from the joint-angle relationships, these differences are considerable. Another interesting finding of the study is the sensitivity of the joint dynamics to the axis of rotation's pose.

Although the dataset for this study was rather limited, this study demonstrated the large differences between 3D and 2D inverse dynamic analysis of knee joint dynamometry. In contrast to the 2D analyses reported in literature, our 3D analysis relies less on assumptions and more on experimental data provided by the extended setup measuring 3D reaction forces and moments. This leads to a better description of the joint's behavior. Moreover, the sensitivity analysis showed the importance of the definition of the knee joint axis' pose. Altogether, it can be concluded that a 3D inverse dynamic analysis with a good estimate of the joint axis' pose is needed to obtain accurate results. Further studies including more subjects might give insight in the correlation between the subject's physical activity and antropometry, and the differences between the joint moment and the moment resulting from the dynamometer.

Acknowledgment

The support of the following projects is gratefully acknowledged: project G.0395.09 of the Research Foundation - Flanders and KU Leuven's Interdisciplinary Research Program IDO/07/12.

5.6 Appendices

3D calculation of the knee joint moment

To calculate forces and moments at the knee joint we applied conservation of linear (eq. 5.1) and angular momentum (eq. 5.2) (fig. 5.1):

$$\sum_{s=1}^{S} \mathbf{F}_s = \sum_{s=1}^{S} m_s \left(\ddot{\mathbf{q}}_s + \mathbf{g} \right) , \tag{5.1}$$

with $\mathbf{F}_s$ the external non-gravitational forces acting on segment $s = 1 \ldots \mathrm{S}$, m_s the segment's mass, $\ddot{\mathbf{q}}_s$ the linear acceleration of the segment's center of mass and $\mathbf{g}$ the gravitational acceleration, all expressed in the same reference frame. Vectors are written in bold.

$$\begin{aligned} \sum_{s=1}^{S} \mathbf{M}_s^P &= \sum_{s=1}^{S} \underbrace{\left(\mathbf{I}_s \alpha_s + \left(\omega_s \times \mathbf{I}_s \omega_s \right) \right)}_{a} \\ &+ \sum_{s=1}^{n} \underbrace{\left(\mathbf{s^{com}} \times \mathbf{m_s} \ddot{\mathbf{q}}_\mathbf{s} \right)}_{b}, \end{aligned} \tag{5.2}$$

with $\mathbf{M}_s^P$ the sum of the external moments and the moments of the external forces on segments about any point P, and the right hand side equalling the change in angular momentum $\mathbf{L}_s$ consisting of (a) the change in angular momentum about the segment's com; (b) the change in $\mathbf{L}_s$ caused by the moment of the linear momentum of the segment's com about P.
To obtain reaction forces and moments at the knee joint, we solve the equations about a point D on the crank and to express all components in the reference frame XYZ with its origin in D. XYZ was defined by the dynamometer AoR (Z) and the perpendicular plane (XY) derived from the circular motion of the markers on the crank. Eq. 5.1 and 5.2 can then be written as:

$$\mathbf{F}_r + \mathbf{F}_{knee}^{XYZ} = \sum_{s=1}^{3} m_s \left(\ddot{\mathbf{q}}_\mathbf{s} + \mathbf{g} \right) , \tag{5.3}$$

with $\mathbf{F}_r$ the reaction forces as registered by the load cell, $\mathbf{F}_{knee}^{XYZ}$ the reaction force in the knee joint expressed in XYZ, for s = crank, tibia and foot, and:

$$\begin{aligned}\mathbf{M}_{knee}^{XYZ} &= \sum_{s=1}^{3} \frac{d\mathbf{L}_s}{dt} \\ &- \left(\mathbf{M}_r + (\mathbf{r}_r \times \mathbf{F}_r) + \left(\mathbf{r}_{knee} \times \mathbf{F}_{knee}^{XYZ}\right)\right) \\ &+ \sum_{s=1}^{3} \left(\mathbf{r}_s^{com} \times m_s \mathbf{g}\right), \end{aligned} \tag{5.4}$$

with $\mathbf{M}_{knee}^{XYZ}$ the reaction moment in the knee joint expressed in XYZ, $\mathbf{M}_r$ the moments as registered by the load cell, $\mathbf{r}_r$ and $\mathbf{r}_{knee}$ the position vectors of the application points of the external forces at the sensor and the knee joint expressed in XYZ with respect to D. $\mathbf{r}_{knee}$ results from the calculation of the functional AoR. The application point is the point on the functional AoR with anatomical z-component equal to zero, so the intersection point with the sagittal plane.

To obtain the knee moment $M3D$ generated about the functional AoR, $\mathbf{M}_{knee}^{XYZ}$ was projected onto the functional AoR:

$$M3D = \frac{\mathbf{M}_{knee}^{XYZ} \cdot \mathbf{n}}{\|\mathbf{n}\|}, \tag{5.5}$$

with $\mathbf{n}$ the vector representing the orientation of the functional AoR.

Internal forces between tibia and crank $\mathbf{F}_{tc}$ were calculated by applying eq. 5.1 to the crank (fig. 5.1 b):

$$\mathbf{F}_r + \mathbf{F}_{tc} = \sum_{s=1}^{1} m_s \left(\ddot{\mathbf{q}}_s + \mathbf{g}\right) \tag{5.6}$$

2D calculation of the knee joint moment

To obtain the knee moment $M2D$ according to Herzog [46], we calculated

$$\begin{aligned} M2D &= \frac{d_k}{d_c} M_{dyn} \\ &+ G_c \; m_c d_c \frac{d_k}{d_c} + G_{tf} \; m_{tf} d_{tf} \\ &+ \mathbf{I}_c \alpha_c \frac{d_k}{d_c} + \mathbf{I}_{tf} \alpha_t, \end{aligned} \tag{5.7}$$

with d_k the distance between the application point of $\mathbf{F}_{tc}$ and $\mathbf{r}_{knee}$ projected in XY, d_d the distance between $\mathbf{F}_{tc}$ and the dynamometer AoR (projected in XY and assuming that M_{tc} equals zero; an assumption which resulted in a feasible point given the contact area), d_c the distance between the com of the crank and the AoR of the dynamometer, and d_{tf} the distance between the com of the tibia-foot segment and the AoR of the dynamometer. m_c and m_{tf}, I_c and I_s, and α_c and α_t are respectively the mass, the inertia tensor and angular acceleration of the crank and the tibia-foot segment (tibia for α). For isometric conditions, only the first term remains.

Chapter 6

A new method for estimating subject-specific muscle-tendon parameters of the knee joint actuators: a simulation study

Abstract[1]

A new method for the estimation of subject-specific muscle-tendon parameters of the knee actuators based on dynamometry experiments is presented. The algorithm aims at estimating the tendon slack length and the optimal muscle fiber length by minimizing the difference between synthetically reproduced and model-based joint moments. The key innovative features are (i) the inclusion of *a priori* physiological knowledge to define a physiologically feasible set, the hot start for the optimization, and constraints for the optimization, and (ii) the introduction of a new (affine) transformation of the muscle-tendon parameters which greatly improves the numerical condition of the optimization.

The influence of the initial guess and of measurement noise was studied in a simulation environment, and the performance was compared to the method presented earlier by Garner and Pandy for the upper limb. The tendon slack length was estimated for 97.5/63% (extensors/flexors) of all initial guesses within 2% of the ground truth. The optimal fiber length was estimated for 89/90% (extensors/flexors) of all initial guesses within 2% of the ground truth. When 10Nm measurement noise was added, the mean value of the estimated tendon slack length deviated at most 1.9/1.6% (extensors/flexors) from the ground truth whereas the standard deviations were at most 5.1/3.9%. The mean value of the estimated optimal fiber length deviated at most 4.3/3.0% (extensors/flexors) from the ground truth whereas the standard deviations were at most 10.2/15.5%. In comparison,

[1]This chapter has been submitted for review as a full article in *Numerical methods in Biomedical Engineering*: A. Van Campen, G. Pipeleers, F. De Groote, I. Jonkers, J. De Schutter.

mean values resulting from the method of Garner and Pandy deviated up to 181% (± 123%) and 119% (± 30%) from the ground truth for, respectively, optimal fiber length and tendon slack length of rectus femoris.

We concluded that the presented method had a low dependency on the initial guess, and outperformed the method of Garner and Pandy in terms of accuracy by at least one order of magnitude when parameters were estimated from noisy data. The improvements open new perspectives for subject-specific modelling of muscles and tendons, which is beneficial for the accuracy of human motion simulations.

6.1 Introduction

Biomechanical analyses of human motion often rely on computer simulations based on musculoskeletal (MS) models. MS-models contain: (i) the skeletal and muscle geometry, and (ii) the muscle-tendon (MT) dynamics which are represented by Hill-type models [120]. A Hill-type model is described by four MT-parameters: the maximum isometric force $F_{\mathrm{m}}^{\mathrm{max}}$, the optimal fiber length $L_{\mathrm{m}}^{\mathrm{opt}}$, the tendon slack length $L_{\mathrm{t}}^{\mathrm{s}}$, and the optimal pennation angle α_{opt}. Whereas imaging techniques allow us to extract subject-specific geometric features such as MT-lengths and moment arms (e.g. [85]), it is hard to extract values for the MT-parameters *in vivo*. As a result, the MT-parameters are often collected from cadaver studies [7; 32; 56]. However, the MT-parameters are subject-specific and reported values vary widely [91]. Moreover, the sensitivity of dynamic motion analyses to these parameters differs (e.g. [2; 29; 81]). All studies rank $L_{\mathrm{t}}^{\mathrm{s}}$ as the most important parameter, followed by $L_{\mathrm{m}}^{\mathrm{opt}}$. Lower sensitivities are reported for $F_{\mathrm{m}}^{\mathrm{max}}$, negligible sensitivities are reported for α_{opt}. Yet, these sensitivity analyses are not indicative of whether a set of experiments contains the information necessary to identify the MT-parameters of importance in order to enhance the accuracy of motion analyses.

Winby et al. [115] compared different techniques to anthropometrically scale $L_{\mathrm{m}}^{\mathrm{opt}}$ and $L_{\mathrm{t}}^{\mathrm{s}}$ as a first step to make these parameters subject-specific. They conclude that it is essential to preserve the muscle's operating range, i.e. the part of the joints' range of motion in which the muscle contributes to the joint moment. This finding is supported by studies of [26], and more recently by [8], which show that the physiological operating range is muscle-specific. However, these scaling methods do not reflect subject-specific muscle strength or moment-angle relationships.

Ten years ago, Garner and Pandy [42] and Lloyd and Besier [63] presented the only functional scaling methods to date. The former method was applied to the upper limb actuators. The latter

method was applied to the lower limb and focussed on the estimation of $L_{\mathrm{t}}^{\mathrm{s}}$ in combination with scaling factors for maximal muscle force and the level of activation.
The algorithm of Garner and Pandy [42] minimizes the difference between the joint moments experimentally obtained by isometric dynamometry at different joint angles and the corresponding model-based joint moments. The optimization variables are transformations of $L_{\mathrm{m}}^{\mathrm{opt}}$ and $L_{\mathrm{t}}^{\mathrm{s}}$ of all muscles: per muscle, two transformed parameters are estimated. It was however not verified whether this procedure was feasible: did the experiments contain sufficient information? Nor were the results validated: does the initial guess influence the solution of this non-linear optimization problem? And how is the optimization affected by measurement errors which are inherent to dynamometry as e.g. [104] illustrated? In the mean time the demand for subject-specific MT-parameters, and hence MT-parameter estimation methods, only increased [38].

The contributions of the work presented in this paper are twofold:

- The development of **a new method for estimation of subject-specific MT-parameters of the knee actuators** using a (i) **new transformation of MT-parameters** that increases the numerical efficiency, and (ii) physiological *a priori* knowledge to reduce the feasible set.
- The validation of the proposed method in a simulation environment based on synthetically generated isometric dynamometry data, including the benchmarking of the method against the only functional scaling method available to date [42] when applied to knee actuators

6.2 Methods

6.2.1 Data simulation

For this simulation study, synthetic experimental dynamometer moments (further referred to as 'synthetic moments') were generated using the generic model in OpenSim [33]. To model experimental noise, noise is added to the synthetic moments when explicitly indicated. Muscles included in the estimation procedure were the knee extensors (RF: rectus femoris, VI: vastus intermedius, VL: vastus lateralis, VM: vastus medialis) and the knee flexors (BFL: biceps femors long head, GL: gastrocnemius lateralis, GM: gastrocnemius medialis, SM: semimembranosus) because they showed the highest sensitivity for optimal muscle fiber lenghts and tendon slack lengths according to [29]. The activation level for all muscles was set to 0.8 for the dynamometer data, as it has been reported that no maximum activation is reached during isometric dynamometry (e.g. [10]).

The generic MT-parameter values according to [32] that were used to generate the synthetic moments will be referred to as the ground truth values.

Our protocol consisted of isometric dynamometry of the knee joint at five equidistant knee angles ($-90\,^\circ$ to $-30\,^\circ$; full extension is zero degrees) at a fixed hip flexion of $80\,^\circ$ from which the moment-angle relationship was obtained. Aditionally, the estimation protocol makes ues of muscle fiber length data at rest (hip and knee fully extended, without ankle dorsi/plantar flexion). For this study, joint moments and muscle fiber lengths were synthetically reproduced. In this study, fiber length data was synthetically generated. When applying the method to experimental data, we suggest to use the values as presented by [112].

Two additional sets of isometric dynamometer experiments were generated for ten and twenty equidistant knee angles ($-100\,^\circ$ to $-10\,^\circ$) at the same hip flexion angle. These additional sets allowed us to (i) verify whether augmenting the experimental cost resulted in an equivalent rise in information on the MT-parameters, and (ii) to properly evaluate the method of [42]. The latter method needed a larger set of dynamometer data.

6.2.2 Hill-type model

The muscle dynamics were described by a Hill-type model as shown in figure 2.2.3. In isometric conditions, the force generating capacity of the muscle depends on (i) $L_{\mathrm{m}}^{\mathrm{opt}}$, the muscle-specific optimal fiber length at which the muscle produces (ii) the maximum isometric force $F_{\mathrm{m}}^{\mathrm{max}}$. The force transfer by the tendon depends on $L_{\mathrm{t}}^{\mathrm{s}}$, the tendon slack length at which the tendon starts to transfer force. The equilibrium between F_{m}, the force produced by the muscle, and F_{t}, the force transferred by the tendon, is governed by α_{opt}, the pennation angle of the muscle at $L_{\mathrm{m}}^{\mathrm{opt}}$. The model equations (assuming isometric conditions) are:

$$F_{\mathrm{m}} = F_{\mathrm{act}}\left(\frac{L_{\mathrm{m}}}{L_{\mathrm{m}}^{\mathrm{opt}}}, a\right) + F_{\mathrm{pas}}\left(\frac{L_{\mathrm{m}}}{L_{\mathrm{m}}^{\mathrm{opt}}}\right), \tag{6.1}$$

$$F_{\mathrm{t}} = F_{\mathrm{mt}} = f\left(\epsilon = \frac{L_{\mathrm{t}} - L_{\mathrm{t}}^{\mathrm{s}}}{L_{\mathrm{t}}^{\mathrm{s}}}\right), \tag{6.2}$$

$$F_{\mathrm{t}} = F_{\mathrm{m}}\ \cos\ \alpha, \tag{6.3}$$

$$L_{\mathrm{mt}} = L_{\mathrm{t}} + L_{\mathrm{m}} \cos\ \alpha, \tag{6.4}$$

$$\cos\ \alpha = \sqrt{1 - \left(\frac{L_{\mathrm{m}}^{\mathrm{opt}} \sin\ \alpha_{\mathrm{opt}}}{L_{\mathrm{m}}} \right)^2}, \tag{6.5}$$

$$F_{\mathrm{m}},\ F_{\mathrm{t}},\ \alpha = f(L_{\mathrm{m}}, L_{\mathrm{mt}}),, \tag{6.6}$$

with $F_{\mathrm{act/pas}}$ the active/passive muscle force, $f(.)$ indicates a dependency on $(.)$, a the muscle activation, $L_{\mathrm{m/t}}$ the muscle/tendon length, and α the pennation angle at the current MT-length L_{mt}. Force-length-velocity characteristics were implemented according to [68].

The MT-lengths L_{mt} and muscle activations a were assumed to be known inputs to the optimizations. L_{mt} follows directly from the kinematics during the (synthetically reproduced) experiments. The estimation method developed in this paper benefits from restricting the search space to the physiological operating range of the muscle. According to the Hill-type model, each muscle can actively generate force throughout the range $\widetilde{L}_{\mathrm{m},jk} = 0.4$ to 1.6, for muscle $j = 1 \dots J$, and experimental condition $k = 1 \dots K$. $\tilde{L}_{\mathrm{m},jk}$ is the normalized muscle fiber length (i.e. the muscle fiber length $L_{\mathrm{m},jk}$ divided by the muscle's $L_{\mathrm{m},j}^{\mathrm{opt}}$) [120]. States $L_{\mathrm{m},jk}$ and parameters $L_{\mathrm{m},j}^{\mathrm{opt}}$ and $L_{\mathrm{t},j}^{\mathrm{s}}$define at which part of the force-length curve the muscle is operating. Each muscle contributes to the joint moment within its specific operating range [8; 26].

6.2.3 Estimation

The parameter estimation procedure comprised the solution of a non-linear constrained optimization problem (NLP) preceded by a heuristic phase which provided the physiologically feasible set and the hot start for the NLP. The motivation to introduce the heuristics was to put as much as possible physiological knowledge into the problem to prevent the solver to get stuck at points which were numerically feasible, yet not physiologically sound.

In this section the derivation of the physiological constraints (first subsection), and the hot start (second subsection) is discussed. Furthermore, the transformation of parameters (third subsection) and the formulation of the NLP are described.

Physiological constraints

The physiological constraints are constraints which exclude the combinations of MT-parameters $[L_{\mathrm{m},j}^{\mathrm{opt}}\ L_{\mathrm{t},j}^{\mathrm{s}}]$ resulting in normalized fiber lengths outside the operating range, and in muscle fiber lengths outside an interval around the reference fiber length values (here, reference lengths equal

ground truth lengths, however, in an experimental environment reference lengths can be based on the cadaver study of [112]). Hence, the physiological constraints result in the physiologically feasible set in two steps.

In the first step, two extreme knee joint angles were considered within the muscle's operating range. Extreme angles were selected at the ends of the range of motion where a muscle still contributed to the joint moment. The extreme angles were set to knee flexion angles of $-105\,^\circ$ ($-90\,^\circ$ for gastrocnemii) and $-30\,^\circ$ (which is a conservative choice). Given an initial guess of parameters $\left[L^{\text{opt}}_{\text{m},j}\ L^{\text{s}}_{\text{t},j}\right]$ for a muscle, discrete combinations in a chosen area around these parameters were evaluated at the considered extreme joint angles for a specific muscle j and a condition k:

$$\min_{\widetilde{L}_{\text{m},jk},s} \quad s, \tag{6.7}$$

$$\text{subject to} \quad -s \leq \widetilde{F}_{\text{t},jk}(\widetilde{L}_{\text{m},jk}) - \widetilde{F}_{\text{m},jk}(\widetilde{L}_{\text{m},jk})\ \cos\ \alpha_{jk} \leq s, \tag{6.8}$$

$$0.4 \leq \widetilde{L}_{\text{m},jk} \leq 1.6, \tag{6.9}$$

with $\widetilde{L}_{\text{m},jk}$ the normalize muscle fiber length $\dfrac{L_{\text{m},jk}}{L^{\text{opt}}_{\text{m},j}}$, and s a slack variable which bounded constraint (6.8).

Here, the area around the parameters was set to $\pm 50\%$ of the initial values, while the discrete values were chosen at increments of 10%:

for $\quad 0.5\ L^{\text{s}}_{\text{t},j}\ :\ 0.1\ L^{\text{s}}_{\text{t},j}\ :\ 1.5\ L^{\text{s}}_{\text{t},j}$,
  for $\quad 0.5\ L^{\text{opt}}_{\text{m},j}\ :\ 0.1\ L^{\text{opt}}_{\text{m},j}\ :\ 1.5\ L^{\text{opt}}_{\text{t},j}$,
    solve optimization (equations (6.7) to (6.9)) for both extreme angles,
      if $\quad s\ ==\ 0$ & constraints fullfilled,
        solution physiologically feasible,

else,

solution not physiologically feasible or infeasible,

end

end,

end.

All discrete parameter combinations $[L^{\mathrm{opt}}_{\mathrm{m},j}\ L^{\mathrm{s}}_{\mathrm{t},j}]$ resulting in physiologically feasible $\tilde{L}_{\mathrm{m},jk}$ at both extreme knee angles, were selected. A feasible solution fullfiled the constraints. A physiologically feasible solution implied that additionally s equalled 0, and hence $\tilde{L}_{\mathrm{m},jk}$ solves the Hill-model equations.

In the second step, we evaluated the muscle fiber lengths $L^{0}_{\mathrm{m},j}$ for the body in the anatomical position at rest, resulting from the feasible combinations $[L^{\mathrm{opt}}_{\mathrm{m},j}\ L^{\mathrm{s}}_{\mathrm{t},j}]$ for each muscle j in the first step. For this simulation study, the reference muscle fiber lengths $L^{\mathrm{ref},0}_{\mathrm{m},j}$ were synthetically reproduced. However, in an experimental environment, $L^{\mathrm{ref},0}_{\mathrm{m},j}$ are not known. Therefore, we imposed a soft constraint on $L^{\mathrm{ref},0}_{\mathrm{m},j}$ demanding that $L^{0}_{\mathrm{m},j}$ did not deviate more than $\Delta_{\mathrm{fl},j}$ from $L^{\mathrm{ref},0}_{\mathrm{m},j}$. This variability, hence uncertainty on $L^{\mathrm{ref},0}_{\mathrm{m},j}$, was modelled as the sum of the inter-subject and intra-muscle variabilities on $L^{0}_{\mathrm{m},j}$ as observed in cadavers [112]:

$$\min_{\widetilde{L}^{0}_{\mathrm{m},j},s} \quad s, \tag{6.10}$$

$$\text{subject to} \quad -s \leq \widetilde{F}^{0}_{\mathrm{t},j}(\widetilde{L}^{0}_{\mathrm{m},j}) - \widetilde{F}^{0}_{\mathrm{m},j}(\widetilde{L}^{0}_{\mathrm{m},j})\ \cos\ \alpha^{0}_{j} \leq s, \tag{6.11}$$

$$L^{\mathrm{ref},0}_{\mathrm{m},j} - \Delta_{\mathrm{fl},j} \leq L^{0}_{\mathrm{m},j} \leq L^{\mathrm{ref},0}_{\mathrm{m},j} + \Delta_{\mathrm{fl},j}, \tag{6.12}$$

where ^{0} indicates that the body was in the anatomical position at rest. Again, only the discrete combinations resulting in physiologically feasible $\tilde{L}_{\mathrm{m},jk}$ were selected.

Figure 6.1 illustrates the procedure to select the physiologically feasible MT-parameter combinations.

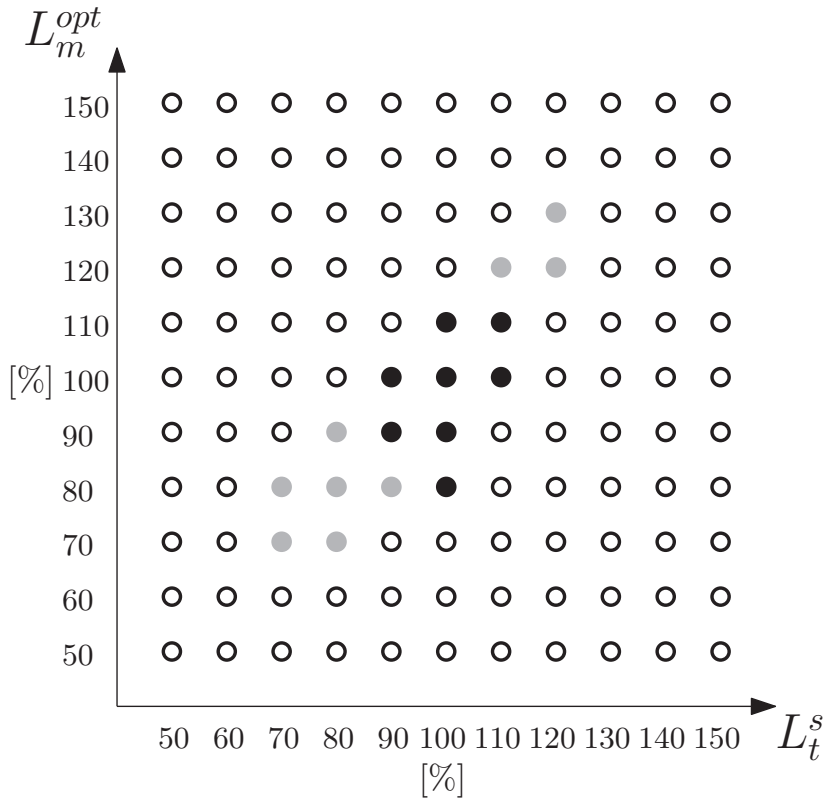

Figure 6.1: Representation of a physiologically feasible set of parameter combinations for a muscle. The grid represents the area in which discrete combinations of $L_{\mathrm{m}}^{\mathrm{opt}}$ and $L_{\mathrm{t}}^{\mathrm{s}}$ have been evaluated. The circles represent the rejected combinations i.e. combinations which result in $\tilde{L}_{\mathrm{m}}$ outside the operating range, The grey and black bullets represent the combinations which result in $\tilde{L}_{\mathrm{m}}$ inside the operating range. The black bullets represent the parameter combinations resulting in a muscle length L_{m} within a certain range of the ground truth lengths.

Hot start

To obtain the hot start for the optimization, $\widetilde{L}_{\mathrm{m},jk}$ were calculated for all experimental isometric dynamometer conditions according to equations (6.7) to (6.9). An extra constraint was added to make sure that the fiber length at a more flexed position was shorter/longer for the flexors/extensors.

Assuming that the moment arms were known (from the geometry), applying equations (6.1) to (6.6), for each physiological MT-parameter combination, model-based muscle forces, and hence model-based joint moments were calculated as the product of the muscle forces and the respective moment arms. These joint moments are further referred to as 'model-based moments'. The hot start was chosen as the physiological MT-parameter combination $[L^{\mathrm{opt}}_{\mathrm{m},j}\ L^{\mathrm{s}}_{\mathrm{t},j}]$ for $j = 14$ which resulted in the smallest difference between simulated moments and synthetic moments (see section 6.2.1).

Transformation of MT-parameters

From the Hill-type model (equations (6.1) to (6.6)), we noticed that there is an implicit correlation between $L^{\mathrm{opt}}_{\mathrm{m},j}$ and $L^{\mathrm{s}}_{\mathrm{t},i}$. Furthermore, we found that this correlation was approximately linear when representing the physiologically feasible parameter combinations as $\dfrac{1}{L^{\mathrm{opt}}_{\mathrm{m},j}}$ as a function of $\dfrac{L^{\mathrm{s}}_{\mathrm{t},j}}{L^{\mathrm{opt}}_{\mathrm{m},j}}$. This linear relation can be described by fitting a line through the physiologically feasible combinations per muscle using least squares regression:

$$c_{1,j}\ \frac{L^{\mathrm{s}}_{\mathrm{t},j}}{L^{\mathrm{opt}}_{\mathrm{m},j}} + c_{2,j} \approx \frac{1}{L^{\mathrm{opt}}_{\mathrm{m},j}}, \tag{6.13}$$

with $c_{1/2,j}$ the regression coefficients for muscle j. The parameter δ_j is introduced to quantify the deviation of a (MT-) parameter combination from the regression line. $\delta_{j,\max}$ was the maximum value of δ_j:

$$\delta_j = \frac{1}{L^{\mathrm{opt}}_{\mathrm{m},j}} - c_{1,j}\ \frac{L^{\mathrm{s}}_{\mathrm{t},j}}{L^{\mathrm{opt}}_{\mathrm{m},j}} - c_{j,2}. \tag{6.14}$$

This relationship allows us to introduce δ_j and $\dfrac{L^{\mathrm{s}}_{\mathrm{t},j}}{L^{\mathrm{opt}}_{\mathrm{m},j}}$ as optimization variables in the optimiza-

tion problem instead of $\frac{1}{L^{\text{opt}}_{\text{m},j}}$ and $\frac{L^{\text{s}}_{\text{t},j}}{L^{\text{opt}}_{\text{m},j}}$. The advantages of this change of variables are following: (i) δ_j is small for MT-parameter combinations in the feasible set and can easily be bounded in contrast to $\frac{1}{L^{\text{opt}}_{\text{m},j}}$ (as illustrated in figure 6.2); and (ii) when $\delta_j = 0$, equations (6.13) and (6.14) are equivalent. Then, equation (6.13) can be used to eliminate $\frac{1}{L^{\text{opt}}_{\text{m},j}}$ from the force equilibrium (equation (6.3)). Hence, the force imbalance only depends on $\frac{L^{\text{s}}_{\text{t},j}}{L^{\text{opt}}_{\text{m},j}}$ and $\widetilde{L}_{\text{m}}$. With δ_j we allow for a small deviation between $1/L^{\text{opt}}_{\text{m},j}$ and the linear regression.

Optimization

Instead of the Hill MT-parameters $\left[L^{\text{opt}}_{\text{m},j}\ L^{\text{s}}_{\text{t},j}\right]$, we adopted the transformation introduced in section 6.2.3 as optimization variables. The vector $\mathbf{x}$ of optimization variables was therefore:

$$\mathbf{x} = \left[\widetilde{L}_{\text{m},jk} \quad \frac{L^{\text{s}}_{\text{t},j}}{L^{\text{opt}}_{\text{m},j}} \quad \delta_j \quad s\right], \tag{6.15}$$

with $j = 1 \ldots 4$, $k = 1 \ldots 5$, $\widetilde{L}_{\text{m},jk}$ the state of muscle j at condition k, and s a slack variable.

The goal criterium was formulated as a bi-objective goal criterium:

$$\min_{\mathbf{x}} \quad \underbrace{s}_{a} + \underbrace{\|M_{k,\text{mod}} - M_{k,\text{synt}}\|^2_{\infty}}_{b}, \tag{6.16}$$

where (a) and constraint (6.17) imposed the equilibrium between muscle and tendon force for each muscle j at each condition k by minimizing the maximum difference given by s, whereas (b) minimized the maximum error between the model-based ($M_{k,\text{mod}}$) and the synthethically reproduced experimental moments ($M_{k,\text{synt}}$) over all experimental conditions j.

The NLP was constrained by:

$$-s \leq \tilde{F}_{\mathrm{m},jk}(\tilde{L}_{\mathrm{m},jk}) \cos \alpha_{jk} - \tilde{F}_{\mathrm{t},jk}(\tilde{L}_{\mathrm{m},jk}) \leq s, \tag{6.17}$$

$$(\epsilon)^{\min} \leq \epsilon_{jk} \leq (\epsilon)^{\max}, \tag{6.18}$$

$$0.4 \leq \tilde{L}_{\mathrm{m},jk} \leq 1.6, \tag{6.19}$$

$$\tilde{L}_{\mathrm{m},jk} - \tilde{L}_{\mathrm{m},j(k+1)} > 0.005, \tag{6.20}$$

$$\left(\frac{L^{s}_{\mathrm{t},j}}{L^{\mathrm{opt}}_{\mathrm{m},j}}\right)^{\min} \leq \frac{L^{\mathrm{s}}_{\mathrm{t},j}}{L^{\mathrm{opt}}_{\mathrm{m},j}} \leq \left(\frac{L^{\mathrm{s}}_{\mathrm{t},j}}{L^{\mathrm{opt}}_{\mathrm{m},j}}\right)^{\max}, \tag{6.21}$$

$$-\delta_{\max,j} \leq \delta_j \leq \delta_{\max,j}. \tag{6.22}$$

Constraint (6.18) ensured that the tendon length was minimum the slack length without becoming excessively long, by constraining the tendon strain ϵ. Constraint (6.19) imposed $\tilde{L}_{\mathrm{m},jk}$ to be within its physiological operating range. Constraint (6.20) is an additional condition on $\tilde{L}_{\mathrm{m},jk}$ which imposed that the state in the current experiment k cannot be equal to the state in the next experiment $k+1$. For the knee extensors $\tilde{L}_{\mathrm{m},jk}$ at higher knee flexion j should be larger than $\tilde{L}_{\mathrm{m},j(k+1)}$ at the next knee flexion $k+1$. For the knee flexors the constraint imposed the opposite. Constraints (6.21) and (6.22) represented physiological bounds on the respective optimization variables.

Whenever the experimental set could not guarantee good estimations for certain parameters due to a lack of information (e.g. different parameters had the same influence on the joint moments), extra relationships between specific muscle parameters were added as a constraint to the NLP. E.g. from an anatomical point of view it makes sense to assume that the $L^{\mathrm{opt}}_{\mathrm{m},j}$ of all three vasti and both gastrocnemii are in the same range. Following extra contraints were therefore respectively added to the optimization:

$$0.9 \leq \frac{L^{\mathrm{opt}}_{\mathrm{m,vi}}}{L^{\mathrm{opt}}_{\mathrm{m,vl}}}, \frac{L^{\mathrm{opt}}_{\mathrm{m,vi}}}{L^{\mathrm{opt}}_{\mathrm{m,vm}}}, \frac{L^{\mathrm{opt}}_{\mathrm{m,vl}}}{L^{\mathrm{opt}}_{\mathrm{m,vm}}} \leq 1.1, \tag{6.23}$$

$$0.9 \leq \frac{L^{\mathrm{opt}}_{\mathrm{m,gm}}}{L^{\mathrm{opt}}_{\mathrm{m,gl}}} \leq 1.1. \tag{6.24}$$

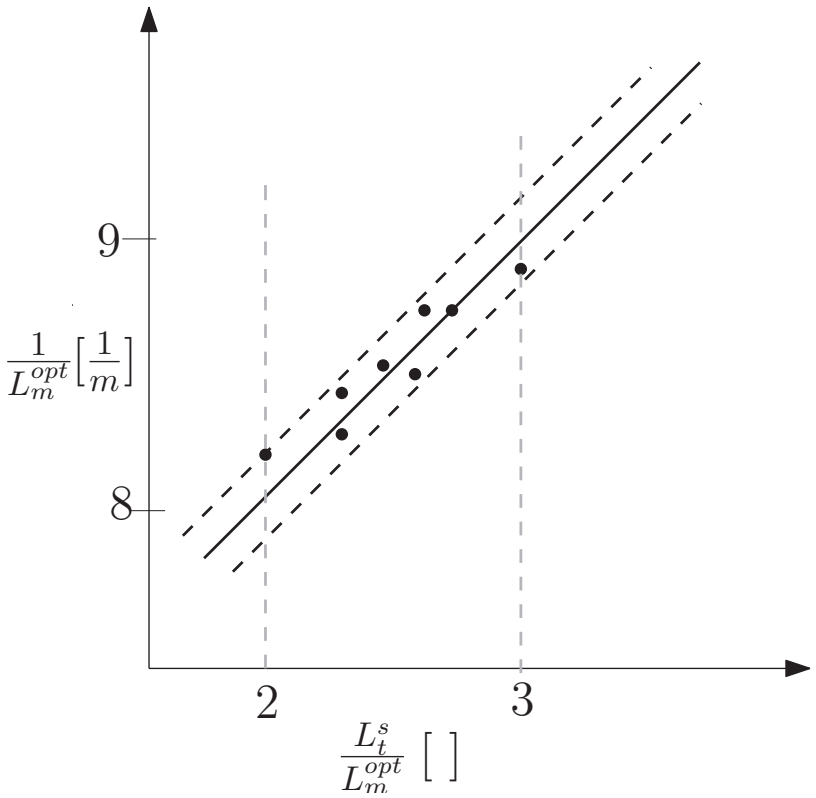

Figure 6.2: The graph represents the correlation between the physiologically feasible parameter combinations. The black line is obtained by linear regression, the black dashed lines represent the maximum deviation from the line, the grey dashed lines represent the bounds on the parameters. The intersection of the four dashed lines defines the physiologically feasible set for the parameters.

The optimization was solved with the local solver KNITRO [20].

Calculations were performed on a Core2, 2.4GHz processor with 4GB RAM.

6.2.4 Analysis

Influence of muscle fiber lengths

The definition of the physiologically feasible set relied on data of muscle fiber lengths (which can be obtained from cadaver data [112] for adults). Although the inter-cadaver variabilities and intra-muscle variabilities were taken into account when defining the physiologically feasible set, the available reference might deviate from the actual ground truth. To investigate the influence of the reference fiber lengths, the physiologically feasible sets were redefined: the reference values were perturbed (positive and negative) with the inter-cadaver variabilities [112] to generate *new reference fiber lengths* for all initial guesses. Means and standard deviations of the lines' slope, maximum deviations $\delta_{\max,j}$ from the lines, and minimum and maximum values for $\frac{L^{\mathrm{s}}_{\mathrm{t},j}}{L^{\mathrm{opt}}_{\mathrm{m},j}}$ were calculated.

Influence of initial guess

For each muscle j that was part of a specific muscle group (here knee extensors and knee flexors, with $j = 1...4$), three initial guesses of $L^{\mathrm{opt}}_{\mathrm{m},j}$ and $L^{\mathrm{s}}_{\mathrm{t},j}$ were generated. The generic values as reported by [32] were chosen as ground truth value. The first initial guess was the ground truth combination of the MT-parameters. The two other initial guesses were $[75\ 125; 125\ 75]\%$ of the ground truth values. Hence, it was assumed that whenever either $L^{\mathrm{opt}}_{\mathrm{m},j}$ or $L^{\mathrm{s}}_{\mathrm{t},j}$ decreased, the other parameter had to increase in order to guarantee a physiological operating range. To each of the intial guesses a uniformily distributed noise was added (mean 0%, maximum magnitude 5%) to avoid that discrete parameter combinations would equal the ground truth parameter combination when applying the procedure as described in 6.2.3 to 6.2.3.

The estimation procedure (sections 6.2.3 to 6.2.3) was performed for all 3^4 combinations of initial guesses. Resulting absolute and relative deviations from the ground truth values for $L^{\mathrm{opt}}_{\mathrm{m},j}$ and $L^{\mathrm{s}}_{\mathrm{t},j}$, and the maximum fitting error between synthetic and simulated joint moments were calculated. To study the influence of the initial guesses the simulated moments were noise-free.

Table 6.1: Parameter sets for OED.

	$[\boldsymbol{L}^{\text{opt}}_{\text{m},\boldsymbol{j}}\ \boldsymbol{L}^{\text{s}}_{\text{t},\boldsymbol{j}}]$	$[\frac{\boldsymbol{L}^{\text{s}}_{\text{t},\boldsymbol{j}}}{\boldsymbol{L}^{\text{opt}}_{\text{m},\boldsymbol{j}}}\ \boldsymbol{\delta_j}]$	$[\tilde{\boldsymbol{L}}^{\text{min}}_{\text{m},\boldsymbol{j}}\ \tilde{\boldsymbol{L}}^{\text{max}}_{\text{m},\boldsymbol{j}}]^{\dagger}$
$\mathbf{SET}_5^{+\text{Fl}}$	yes	yes	no
$\mathbf{SET}_{10}^{\text{-Fl}}$	yes	yes	yes
$\mathbf{SET}_{10}^{+\text{Fl}}$	yes	yes	no
$\mathbf{SET}_{20}^{\text{-Fl}}$	yes	yes	yes

Experimental sets and parameter transformations are shown. OED has been performed for experimental sets of five (set_5), ten (set_{10}), and twenty (set_{20}) isometric dynamometer measurements. $^{\pm\text{Fl}}$ indicates whether the muscle fiber lengths as obtained in the anatomical position at rest, have been included. † is the transformation of parameters introduced by [42]. δ_i is a parameter which reflects the correlation between $L^{\text{opt}}_{\text{m},j}$ and $L^{\text{s}}_{\text{t},j}$ for a specific muscle i. *Yes* or *no* indicates whether the parameters have been evaluated or not.

Influence of measurement noise

All measurement errors were modelled as noise on the joint moments. As MT-geometric features can be extracted from MR-images, they were assumed to be quite accurate and their uncertainty was therefore neglected. A common technique to obtain the mean and covariance of a set of parameters identified based on measurements suffering from uncertainties is Monte Carlo simulation. However, this technique is highly time expensive. Therefore, sigma points were used here. The theory of the sigma points was originally developed in the field of unscented Kalman filtering [54]. Schenkendorf et al. [83] illustrated the determination of the mean and the confidence region of a set of identified parameters $\boldsymbol{x}$ based on sigma points. The main idea is to deterministically choose a set of weighted points so that certain properties of the distribution of $\boldsymbol{x}$ are captured. Hence, given a vector of measurements, and assuming a (symmetrical) Gaussian distribution $\boldsymbol{z}$, a second order approximation of $\boldsymbol{z}$ captures the mean and covariance. Here, we used a fourth order approximation of $\boldsymbol{z}$ which additionally captured the kurtosis. The sigma points and corresponding weights were chosen as proposed by [54] by solving an optimization problem constrained by the mean, covariance, and kurtosis, a constraint to ensure that the weights summed up to one, and a goal function which minimized the errors in higher order moments. The optimization was needed to solve the underdetermined set of equations. Furthermore, the sigma points were forced to be within two standard deviations of the mean. Mathematical details are provided in Appendix A.

For this paper, the mean values and covariances of the estimated parameters resulting from simulated moments subject to two different sets of noise were calculated. Standard deviations on the simulated moments were set to 5 and 10Nm. Results from the estimation procedure described in section 6.2.3 and from the procedure proposed by Garner and Pandy (2003) [42] were evaluated and compared. In comparison to Garner and Pandy (2003) [42] we were able to estimate a higher number of parameters thanks to the description of the inter-dependency between $L_{\mathrm{m}}^{\mathrm{opt}}$ and $L_{\mathrm{t}}^{\mathrm{s}}$. Hence, for a fair comparison between the methods, the analysis was performed for the same experimental set (being the set of five isometric dynamometer experiments). This way, the same sigma points and covariances can be used. Therefore, only four parameters (of two muscles, here RF and VI) were estimated using the method of Garner and Pandy (2003) [42] whereas the other four parameters of the remaining muscles VL and VM were kept constant at their ground truth values during the optimization. The initial guesses for both algorithms were the optimization variables resulting from the ground truth Hill MT-parameter values.

Optimal Experimental Design (OED)

The aim of OED is to compare the identifiability of specific sets of parameters (either the MT-parameters themselves, or a transformation of the MT-parameters) based on the information contained in a specific set of experiments. Hence, OED examines the choice of the experimental set, and the choice of the parameter transformations. Additionally, OED allows to verify to which extent noise affects the identifiability.

The experimental sets evaluated in this study were listed in section 6.2.1. This paper focused on the identification of the two most sensitive MT-parameters being $L_{\mathrm{m},j}^{\mathrm{opt}}$, and $L_{\mathrm{t},j}^{\mathrm{s}}$, while $F_{\mathrm{m},j}^{\mathrm{max}}$ and $\alpha_{\mathrm{opt},j}$ were kept constant [32]. Three parameter transformations (per muscle j) were evaluated:

1. the Hill MT-parameters $[L_{\mathrm{m},j}^{\mathrm{opt}}\ L_{\mathrm{t},j}^{\mathrm{s}}]$ themselves;
2. the transformation proposed by [42]: $[\tilde{L}_{\mathrm{m},j}^{\mathrm{min}}\ \tilde{L}_{\mathrm{m},j}^{\mathrm{max}}]$ being the minimum and maximum normalized muscle fiber lengths, respectively;
3. the new transformation $[\frac{L_{\mathrm{t},j}^{\mathrm{s}}}{L_{\mathrm{m},j}^{\mathrm{opt}}}\ \delta_{\mathrm{max},j}]$, introduced in section 6.2.3.

To compare the informativeness of the experimental sets and the parameter transformations, two scalarizations of the Fisher information matrix FIM were evaluated: D-optimal design and E-optimal design criteria [15]. FIM is a matrix which contains the sensitivities, i.e. the partial

Table 6.2: Influence of L_{m} on physiologically feasible set.

	lb [ ]	**ub** [ ]	**a**	$\delta_{\max}$
RF	2.42 (±0.28)	3.23 (±0.29)	0.40 (±0.15)	3.04 (±0.28)
VI	1.17 (±0.11)	2.01 (±0.23)	0.97 (±0.17)	4.60 (±0.59)
VL	1.41 (±0.22)	2.38 (±0.19)	0.91 (±0.25)	4.64 (±0.76)
VM	1.06 (±0.08)	1.91 (±0.30)	1.01 (±0.13)	5.02 (±0.67)
BFL	2.35 (±0.25)	3.55 (±0.36)	0.51 (±0.17)	2.48 (±0.43)
GL	4.81 (±0.84)	9.44 (±0.77)	0.37 (±0.11)	2.55 (±0.14)
GM	6.27 (±1.78)	9.27 (±3.33)	0.30 (±0.0)	2.57 (±0.09)
SM	3.90 (±0.56)	6.94 (±0.79)	0.55 (±0.19)	2.38 (±0.25)

The mean and standard deviations of the slope a of the line, the deviation $\delta_{\max}$ from the line and the lower and the upper bounds (lb, ub) on $\frac{L_{\mathrm{t}}^{\mathrm{s}}}{L_{\mathrm{m}}^{\mathrm{opt}}}$ are given per muscle over all physiologically feasible sets (see figure 6.2).

derivatives of the simulated data (moments and fiber length) to the parameters. D-optimality maximizes the determinant of FIM, and hence minimizes the total error in all parameters. E-optimality maximizes the minimum eigenvalue of FIM, and hence minimizes the maximum error over all parameters. For the evaluation, scaling was applied and noise was taken into account according to [110].

D-optimality and E-optimality were compared for different sets of experiments and parameters (see also table 6.1).

For simplicity, subscript j is omitted in the next sections.

6.3 Results

Influence of the muscle fiber length at rest on the physiologically feasible set

The influence of the reference muscle fiber lengths on the definition of the physiologically feasible set is shown in table 6.2. The general observations were that the physiologically feasible sets in all cases comprised the MT-parameter ground truth values.

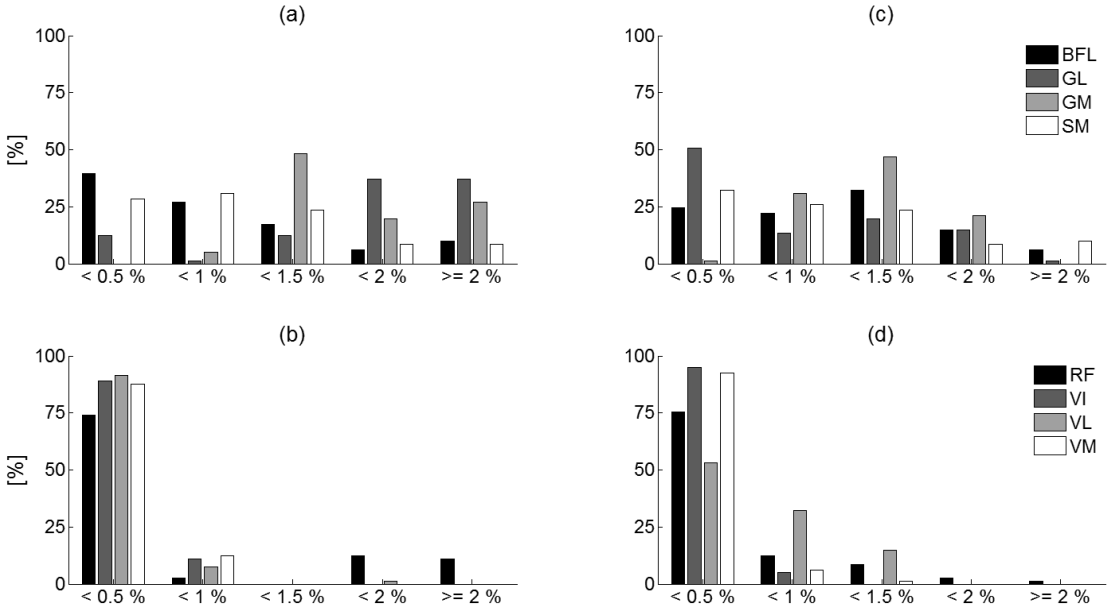

FIGURE 6.3: Estimated parameters resulting from all initial guesses are divided into five subgroups based on the remaining relative difference with the ground truth parameter value: smaller than 0.5%, between 0.5% and 1% (< 1%), between 1% and 1.5% (< 1.5%), between 1.5% and 2% (< 2%), and larger than 2% (>= 2%). (a) for flexors and (b) for extensors show the relative number of estimates contained in each group for $L_{\mathrm{m}}^{\mathrm{opt}}$, while (c) for flexors and (d) for extensors show the relative number of estimates contained in each group for $L_{\mathrm{t}}^{\mathrm{s}}$.

Influence of initial guess

The influence of the initial guess on the estimated parameters is shown in figure 6.3. All initial guesses of the flexor parameters, and 97.5% of the initial guesses of the extensor parameters resulted in feasible estimates. Whenever a solution was infeasible, this was indicated by the solver's exitflag. For flexors, 63% of the estimated $L_{\mathrm{m}}^{\mathrm{opt}}$ and 90% of the estimated $L_{\mathrm{t}}^{\mathrm{s}}$ were within 2% of the ground truth value. For extensors, 89% of the mean values for the estimated $L_{\mathrm{m}}^{\mathrm{opt}}$ and 97.5% of the mean values for the estimated $L_{\mathrm{t}}^{\mathrm{s}}$ were within 2% of the ground truth value.

Influence of measurement noise

The influence of measurement noise on the estimated means and covariances is given in table 6.3 for noise levels 5Nm and 10Nm. The mean values for the estimated $L_{\mathrm{t}}^{\mathrm{s}}$ were overall closer to the ground truth value than the mean value for the estimated $L_{\mathrm{m}}^{\mathrm{opt}}$. For noise level 5Nm, the maximum absolute and relative standard deviations on the estimation of $L_{\mathrm{m}}^{\mathrm{opt}}$ were 1.0/0.77cm (BFL/VL) and 15.3/9.2% (GM/VL). The maximum absolute and relative standard deviations on the estimation of $L_{\mathrm{t}}^{\mathrm{s}}$ were 1.6/0.76cm (BFL/VL) and 4.8/5.4% (BFL/VI). For noise level 10Nm, the maximum absolute and relative standard deviations on the estimation of $L_{\mathrm{m}}^{\mathrm{opt}}$ were 0.94/0.85cm (BFL/VL) and 15.5/10.2% (GM/VL). The maximum absolute and relative standard deviations on the estimation of $L_{\mathrm{t}}^{\mathrm{s}}$ (for flexors/extensors) were 1.3/0.69cm (BFL/VI) and 3.9/5.1% (GM/VL,VI).

The influence of measurement noise on the mean value and standard deviations of the estimated parameters of RF and VI resulting from the algorithm proposed by [42] was different compared to the influence on the estimated parameters from the method presented in this paper. The mean of the estimated $L_{\mathrm{m}}^{\mathrm{opt}}$ differed up to 9cm (181%) (RF). The mean of the estimated $L_{\mathrm{t}}^{\mathrm{s}}$ differed up to 5cm (119%) (RF). Standard deviations on the estimated parameters were large (123% and 30% for $L_{\mathrm{m}}^{\mathrm{opt}}$ and $L_{\mathrm{t}}^{\mathrm{s}}$ respectively for RF).

Optimal Experimental Design

Results of the identifiability study are summarized in table 6.4. Overall, the identifiability for extensors and flexors was comparable. The Hill MT-parameters $[L_{\mathrm{m}}^{\mathrm{opt}}\ L_{\mathrm{t}}^{\mathrm{s}}]$ clearly showed low identifiability. $[\frac{L_{\mathrm{t}}^{\mathrm{s}}}{L_{\mathrm{m}}^{\mathrm{opt}}}\ \delta]$ showed higher identifiability than $[\tilde{L}_{\mathrm{m}}^{\mathrm{min}}\ \tilde{L}_{\mathrm{m}}^{\mathrm{max}}]$. Identifiability benefitted more from a transformation of the parameters, and from including data of the muscle fiber lenghts, than from including more isometric dynamometer experiments.

TABLE 6.3: Influence of measurement noise.

	$L_{\mathbf{m}}^{\mathbf{opt},1}$		$L_{\mathbf{m}}^{\mathbf{opt},2}$		$L_{\mathbf{t}}^{\mathbf{s},1}$		$L_{\mathbf{t}}^{\mathbf{s},2}$	
	mean ± std [cm]	mean ± std [%]	mean ± std [cm]	mean ± std [%]	mean ± std [cm]	mean ± std [%]	mean ± std [cm]	mean ± std [%]
BFL	10.7 ± **1.0**	98.4 ± 9.2	10.9 ± **0.94**	99.9 ± 8.6	33.6 ± **1.6**	102.9 ± **4.8**	33.1 ± 1.3	101.6 ± **3.9**
GL	6.4 ± 0.95	100.4 ± 14.8	6.3 ± 0.85	98.7 ± 13.2	37.9 ± 0.38	99.7 ± 1.0	38.0 ± 0.5	99.9 ± 1.4
GM	6.2 ± 0.92	102.6 ± **15.3**	5.9 ± 0.93	99.4 ± **15.5**	39.1 ± 0.51	100.1 ± 1.3	39.1 ± 0.6	100.3± 1.6
SM	7.8 ± 0.76	97.6 ± 9.5	7.8 ± 0.92	97.0 ± 11.6	36.1 ± 0.93	100.6 ± 2.6	36.2 ± 1.2	100.9 ± 3.5
RF	11.3 ± 0.64	99.4 ± 5.6	11.2 ± 0.57	98.6 ± 5.0	31.0 ± 0.41	100.0 ± 1.3	31.0 ± 0.51	100.1 ± 1.6
VI	8.9 ± 0.62	102.8 ± 7.2	8.9 ± 0.84	102.9 ± 9.7	13.2 ± 0.74	97.3 ± **5.4**	13.4 ± 0.69	98.3 ± **5.1**
VL	8.8 ± **0.77**	104.7 ± **9.2**	8.8 ± **0.85**	104.3 ± **10.2**	15.4 ± **0.76**	98.2 ± 4.9	15.4 ± 0.8	98.1 ± **5.1**
VM	9.1 ± 0.66	101.9 ± 7.4	9.1 ± 0.75	101.9 ± 8.5	12.4 ± 0.56	98.6 ± 4.5	12.4± 0.55	98.7 ± 4.3

Absolute mean values and standard deviations (std) and relative (to ground truth value) values and standard deviations for the parameters $L_{\mathrm{m}}^{\mathrm{opt}}$ and $L_{\mathrm{t}}^{\mathrm{s}}$ per noise level (5Nm [1] and 10Nm [2]) are shown. The largest standard deviations in each muscle set (flexors/extensors) per parameter are indicated in **bold**.

Table 6.4: Summary of the results of the OED

	Extensors		**Flexors**	
	Dcrit	Ecrit	Dcrit	Ecrit
$\mathbf{SET}_5^{+\mathrm{Fl}}$				
$[L_\mathrm{m}^\mathrm{opt}\ L_\mathrm{t}^\mathrm{s}]$	$2.1e^{-8}$	$2.2e^{-5}$	$1.8e^{-6}$	$4.1e^{-6}$
$[\frac{L_\mathrm{t}^\mathrm{s}}{L_\mathrm{m}^\mathrm{opt}}\ \delta]$	$3.0e^{14}$	$3.9e^{-2}$	$3.9e^{19}$	$7.1e^{-2}$
$\mathbf{SET}_{10}^{-\mathrm{Fl}}$				
$[L_\mathrm{m}^\mathrm{opt}\ L_\mathrm{t}^\mathrm{s}]$	$1.2e^{-9}$	$2.4e^{-6}$	$4.6e^{-11}$	$3.2e^{-6}$
$[\frac{L_\mathrm{t}^\mathrm{s}}{L_\mathrm{m}^\mathrm{opt}}\ \delta]$	$1.7e^{14}$	$5.0e^{-3}$	$1.9e^{20}$	$2.9e^{-1}$
$[\tilde{L}_\mathrm{m}^\mathrm{min}\ \tilde{L}_\mathrm{m}^\mathrm{max}]$	$8.8e^{3}$	$4.1e^{-4}$	$1.7e^{2}$	$1.6e^{-4}$
$\mathbf{SET}_{10}^{+\mathrm{Fl}}$				
$[L_\mathrm{m}^\mathrm{opt}\ L_\mathrm{t}^\mathrm{s}]$	$2.2e^{-4}$	$2.1e^{-4}$	$2.1e^{-3}$	$4e^{-5}$
$[\frac{L_\mathrm{t}^\mathrm{s}}{L_\mathrm{m}^\mathrm{opt}}\ \delta]$	$3.5e^{-18}$	$2.1e^{-1}$	$1.5e^{25}$	$6.7e^{-1}$
$\mathbf{SET}_{20}^{-\mathrm{Fl}}$				
$[L_\mathrm{m}^\mathrm{opt}\ L_\mathrm{t}^\mathrm{s}]$	$3.5e^{-6}$	$1.0e^{-4}$	$5.6e^{-8}$	$2.1e^{-5}$
$[\frac{L_\mathrm{t}^\mathrm{s}}{L_\mathrm{m}^\mathrm{opt}}\ \delta]$	$6.3e^{19}$	$1.7e^{1}$	$2.7e^{22}$	$5.7e^{-1}$
$[\tilde{L}_\mathrm{m}^\mathrm{min}\ \tilde{L}_\mathrm{m}^\mathrm{max}]$	$2.1e^{6}$	$1.0e^{-3}$	$3.6e^{4}$	$4.6e^{-4}$

The determinant (D-criterium), and the minimum eigenvalue (E-criterium) of the Fisher-information matrix are shown per experimental set and per parameter transformation. Higher values are an indication for a better identifiability of the parameters from the respective experiments. Results are shown for experimental sets of five (set_5), ten (set_{10}), and twenty (set_{20}) isometric dynamometer measurements. $^{\pm Fl}$ indicates whether the information on the muscle fiber lengths has been included.

6.4 Discussion

Influence of the muscle fiber length on the physiologically feasible set

The influence of the fiber length at rest on the physiologically feasible set was limited i.e. little changes were observed in the slope of the regression line, the maximum deviation of the line, and the bounds on $\frac{L^{\mathrm{s}}_{\mathrm{t},i}}{L^{\mathrm{opt}}_{\mathrm{m},i}}$, and the real solution remained within the physiologically feasible set. However, the fiber lengths as obtained from literature [112] are representative for healthy adults. Caution is required when subjects who are part of a different sub-population (e.g. children) are studied. Either the reference values should be adapted and/or the uncertainties should be increased.

Influence of initial guess

Per muscle, three sets of initial guesses of the parameters have been evaluated. Combining the initial guesses of all muscle groups, 81 resulting combinations have been evaluated. For the flexors, most $L^{\mathrm{s}}_{\mathrm{t}}$ are estimated witin 0.8cm of the ground truth value, and most $L^{\mathrm{opt}}_{\mathrm{m}}$ are estimated within 0.25cm of the ground truth value. For the extensors, all $L^{\mathrm{s}}_{\mathrm{t}}$ are estimated within 0.5cm of the ground truth value, and all $L^{\mathrm{opt}}_{\mathrm{m}}$ are estimated within 0.25cm of the ground truth value. Differences between the ground truth and the estimated $L^{\mathrm{s}}_{\mathrm{t}}$ are six to 50 times smaller than the differences between values for $L^{\mathrm{s}}_{\mathrm{t}}$ reported for three frequently used MS-models [7; 32; 69] (see table 6.5). Differences between the ground truth and the estimated $L^{\mathrm{opt}}_{\mathrm{m}}$ are four to twelve times smaller than the *natural variability* on $L^{\mathrm{opt}}_{\mathrm{m}}$ as reported by [112] (see table 6.5).
De Groote et al. [29] showed in their sensitivity analysis of isometric experiments that perturbations in $L^{\mathrm{s}}_{\mathrm{t}}$ can lead to moment sensitivities of about 20Nm for gait and about 150Nm for isometric dynamometry. These sensitivities are defined as the ratio between the change in the muscle moment and the relative change in a parameter. Similarly, perturbations in $L^{\mathrm{opt}}_{\mathrm{m}}$ can lead to moment sensitivities of about 7.5Nm for gait and about 50Nm for isometric dynamometry. Hence, for the considered moment sensitivities reported in [29] in the muscle moment of 0.4Nm for gait and 3Nm for dynamometry are obtained for (i) 97.5% (extensors) and 63% (flexors) of the initial guesses of $L^{\mathrm{s}}_{\mathrm{t}}$, and for (ii) 89% (extensors) 90% (flexors) of the initial guesses of $L^{\mathrm{opt}}_{\mathrm{m}}$.

The maximum fitting errors, reflecting the remaining discrepancy between the synthetic moments and the simulated moments, are for more than 50% of the initial guesses smaller than 0.1Nm for the extensors, and smaller than 1Nm for the flexors.

Table 6.5: Parameter values from literature

	$\mathbf{L}_{\mathrm{m}}^{\mathrm{opt}}$			$\mathbf{L}_{\mathrm{t}}^{\mathrm{s}}$	
	min [cm]	max [cm]	Δ [cm]	min [cm]	max [cm]
BFL	8.5	10.9	3.0	13.0	32.9
GL	5.7	6.4	1.0	23.4	38.5
GM	5.1^{D}	6.0^{KH}	0.95	21.2	40.1^{A}
SM	6.9^{A}	8.1^{KH}	1.9	15.7	37.8^{A}
RF	7.6^{A}	11.4	1.4	9.6	34.6^{A}
VI	7.7	9.9^{A}	2.2	10.6^{A}	13.6
VL	8.4^{D}	9.9^{A}	2.5	9.6	15.7
VM	7.6	9.7^{A}	2.8	9.6	12.6

Minimum and maximum values for $L_{\mathrm{m}}^{\mathrm{opt}}$ and $L_{\mathrm{t}}^{\mathrm{s}}$ as obtained from models available via OpenSim [33]: the London lower limb model [69] relies on the cadaver study of [56], the lower limb model of Delp et al. [32] relies on the cadaver studies of [39; 113], the lower limb model of Arnold et al. [7] relies on the cadaver studie of [112]. Minimum and maximum values are according to [56] and [32] respectively, unless otherwise indicated ($^{\mathrm{A}}$ value adopted from Arnold et al. [7], $^{\mathrm{D}}$ value adopted from Delp et al. [32], $^{\mathrm{KH}}$ value adopted from Klein-Horsman et al. [56]). For $L_{\mathrm{m}}^{\mathrm{opt}}$ a natural variability Δ is given based on [112]. Therefore, the reported variabilities in muscle fiber lengths are multiplied by a ratio of the optimal sarcomere length (2.7m) and the reported sarcomere lengths cfr. [32].

Evaluating the results, it appears that there are many suboptimal solutions of the optimization. Based on the goal criterion values it is possible that the number of local optima is limited, however that the neigbourhood of these few local optima is valley-like shaped. As a results the local solver might fullfil the stopping criteria before the optimum is reached.

Influence of measurement noise

When adding measurement noise, the mean values of the estimated parameter are within 5% of the ground truth value. The standard deviations are higher for $L_{\mathrm{m}}^{\mathrm{opt}}$ (up to 15.3%) than for $L_{\mathrm{t}}^{\mathrm{s}}$ (up to 5.4%). Means and standard deviations resulting from both levels of measurement noise, are comparable. Comparing the standard deviations for the estimation of $L_{\mathrm{m}}^{\mathrm{opt}}$ to the natural variabilities reported by [112] (see table 6.5), it appears that the natural variabilities are two to four times larger than the standard deviations, except for GL and GM where they are similar. This shows that it is beneficial to estimate the value for $L_{\mathrm{m}}^{\mathrm{opt}}$ using the proposed procedure rather than to adopt a value from literature. Comparing the standard deviations for the estimation of $L_{\mathrm{t}}^{\mathrm{s}}$ to the differences between parameter values in literature (see table 6.5), it is even more obvious that using the estimation procedure is beneficial as the variabilities are 6.6/2 (BFL/VI) to 16.4/25 (GM/RF) times larger than the two standard deviations (representing 95% of the estimates) from the mean values.

Again, these results can be interpreted in light of the sensitivity analysis of [29]. $L_{\mathrm{t}}^{\mathrm{s}}$ is the most crucial parameter. From the results in this paper, it can be seen that the identifiability of $L_{\mathrm{t}}^{\mathrm{s}}$ is also better as the estimated means are closer to the ground truth than the estimated means for $L_{\mathrm{m}}^{\mathrm{opt}}$. 95% of the estimations are within two times the standard deviation of the mean value. Hence, assuming the same moment sensitivities as earlier, 95% of the estimated $L_{\mathrm{t}}^{\mathrm{s}}$ result in an error in muscle moment smaller than 2Nm (gait)/15Nm (dynamometry). The standard deviation for the estimation of $L_{\mathrm{m}}^{\mathrm{opt}}$ is three times larger than for $L_{\mathrm{t}}^{\mathrm{s}}$, about 15%. Hence, 95% of the estimations are within 30% of the mean values. As the moment sensitivities are reported to be two to three times smaller for $L_{\mathrm{m}}^{\mathrm{opt}}$ than for $L_{\mathrm{t}}^{\mathrm{s}}$, 95% of the estimated $L_{\mathrm{m}}^{\mathrm{opt}}$ also result in an error in muscle moment smaller than 2Nm (gait)/15Nm (dynamometry). For a maximum offset (defined as the maximum deviation between the mean of the estimates and the ground truth) of 2.9% in the estimated $L_{\mathrm{t}}^{\mathrm{s}}$, the additional error in muscle moment is smaller than 0.4Nm/3Nm (gait/dynamometry). For a maximum offset of 4.7% in the estimated $L_{\mathrm{m}}^{\mathrm{opt}}$, the additional error in muscle moment is smaller than 0.4Nm/2.5Nm (gait/dynamometry).

Studying the effect of measurement noise on the estimation algorithm presented by [42], $L_{\mathrm{t}}^{\mathrm{s}}$ also appears to be best identifiable. There are some remarkable differences in performance of this algorithm compared to the algorithm presented in this paper. The mean value of the parameters estimated by [42] deviates much from the ground truth value, and the standard deviation is higher. This can be explained as follows: the transformation of the parameters determines the shape of the objective function. Clearly, the objective function contains local optima which do not lie close to the global optimum. In addition, the introduction of the physiologically feasible set is beneficial in the new algorithm.

When interpreting the effect of the measurement noise, following limitations should be kept in mind: (i) the method of the sigma points adds noise to one or two experiments at a time. This alternative approach to the more commonly used Monte Carlo analysis bears the huge advantage that it is less time expensive (as only a limited set of evaluations have to be performed); (ii) the *a priori* assumption that the transformation (here the parameter estimation) of a limited set of points (here the vector of experiments including noise) are a symmetric Gaussian with a certain mean and covariance might not hold for the evaluated non-linear problems; (iii) the sigma points are chosen in a deterministic manner. Nevertheless, these limitations do not affect the comparison between both methods and hence, we can conclude that our method is more robust against measurement errors than the algorithm of [42] when using it for the estimation of $L_{\mathrm{m}}^{\mathrm{opt}}$ and $L_{\mathrm{t}}^{\mathrm{s}}$ of the knee actuators.

For our analyses, the implementation of the algorithm of [42] is according to the information provided by the authors, i.e., the same goal function, constraints, MT-model and transformation of parameters are used for the optimization. However in this paper, the hot starts were set to their ground truth values as the hot starts suggested by [42] never lie close to the ground truth value, and the implementation of the muscle characteristics is as described by [68]. The solver used is KNITRO [20], a local solver.

Our approach is a local optimization incorporating as much knowledge as possible. Alternatively, a global optimization procedure, such as genetic algorithms or simulated annealing, can be used. However, these global optimization approaches do neither guarantee convergence to the global optimal solution, and moreover they are very numerically expensive.

In this study the maximum isometric forces $F_{\mathrm{m}}^{\mathrm{max}}$ were assumed to be known, because the sen-

sitivity study of dynamic simulations to this MT-parameter is low [29]. However, the maximum isometric forces might differ significantly between subjects. In these cases, it is possible to derive a value of the maximum isometric forces based on imaging techniques (e.g. [100]).

A general limitation of this study is that only one ground truth model has been evaluated, being the model described by [32]. Considering other ground truth values might influence the results. However, the motivation for our approach is that the sensitivity analyses of [29] showed similar results for several (five) models, and these senstivities are used to define the Hessian (and hence the Fisher information matrix), which in turn is similar for the different models.

Optimal Experimental Design

The basic idea of optimal experimental design is extracting maximum information from a minimum set of experiments. Here, we mainly adopted OED to illustrate that the optimization numerically benefitted from the newly introduced parameter transformation, and that thanks to the interdependency between $L_{\mathrm{t}}^{\mathrm{s}}$ and $L_{\mathrm{m}}^{\mathrm{opt}}$ for the knee actuators, and the *a priori* physiological knowledge, we only need a limited set of experiments. Limiting the experimental set lowers the experimental load for subjects.
The parameter transformation most influenced the results: the identifiability clearly benefitted from the transformation as introduced in this paper $\left[\frac{L_{\mathrm{t}}^{\mathrm{s}}}{L_{\mathrm{m}}^{\mathrm{opt}}},\ \delta\right]$, and from the inclusion of information on muscle fiber lengths. Also a rise in the number of isometric experiments is beneficial, albeit to a lesser extent. However, as joint kinematics cannot accurately be imposed during dynamometry (e.g. [55]), it is not straightforward to obtain measurements at a high number of preselected joint angles. Garner and Pandy [42] interpolated a limited set of experiments. Yet, care should be taken when following this approach as there is no guarantee that the activation levels are the same at all measurements [10].

Taking noise into account, resulted in a proportional decay of the criteria. For those cases where only isometric dynamometer experiments were taken into account, the effect of the noise was straightforward. As the noise term was equal for all synthetic moments, the criteria downscaled equivalent to the noise level.

Some issues have to be taken into account concerning this identifiability study. (i) The information on the muscle fiber lengths is used as *a priori* knowledge to define the physiologically

feasible set, and hence is not directly used in the optimization. (ii) This study includes isometric dynamometer experiments. It is however possible that the identifiability benefits from the inclusion of isokinetic experiments. Although the noise on isokinetic measurements is larger [104], and the numerical cost for the optimization rises, it is definitely an item for further research.

6.5 Conclusion

We presented and validated a new method for subject-specific estimation of the optimal muscle fiber length and the tendon slack length based on local optimization techniques. The method was applied to four flexors and four extensors of the knee in a simulation environment. The key innovative features in the method are: (i) the inclusion of *a priori* physiological knowledge to define a physiologically feasible set of solutions and to provide a good hot start for the non-linear constrained optimization, and (ii) the introduction of a new transformation of the MT-parameters which was beneficial for the numerical condition of the optimization. These two features, together with the inter-dependency between the optimal muscle fiber length and the tendon slack length we described, also made that the method required a smaller experimental set (isometric dynamometry).

We found that the method showed a low dependency on the initial parameter guess, and that it outperformed the method of Garner and Pandy (2003) [42] in terms of accuracy by at least one order of magnitude when parameters were estimated from noisy data.

Notwithstanding the progress we made concerning the demanding issue of subject-specific MT-parameters identification, some aspects are open for future research. The additional value of isokinetic experiments for the identification should be evaluated. Furthermore, although the method showed a good robustness to measurement noise compared to the method of Garner and Pandy (2003) [42], for application of the method to experimental data, the success will still rely on the quality of the data acquisition and processing. Also, verifying the validity of the method for the estimation of subject-specific MT-parameters of actuators of the hip and the ankle joint is a subject for further research, together with the design of an experimental setup comparable to [104] which allows (i) to obtain reliable measurement data, and (ii) to obtain measurement data for all degrees of freedom. A last item of research might focus on the more accurate determination of the individual muscle operating ranges, as the method clearly benefits from this information.

Acknowledgment

The support of the following projects is gratefully acknowledged: project G.0395.09 of the Research Foundation - Flanders, KU Leuven's Interdisciplinary Research Program IDO/07/12n and KU Leuven-BOF PFV/10/002 Center-of-Excellence Optimization in Engineering (OPTEC).

6.6 Appendix A

Julier and Uhlmann [54] provide details on the optimization and constraints to obtain the position of the sigma points and the corresponding weights. The number of sigma points required is $2n^2+1$ with n the dimension of the problem, here $n = 5$ (the number of experiments).
The normalized sigma points are:

$$\psi_0 = s_0, \tag{6.25}$$

$$\psi_1 = (\pm\ s_1)\ \ (I_n)_{\mathrm{sp1}}\,, \tag{6.26}$$

$$sp1 = 1...n, \tag{6.27}$$

$$\psi_2 = \pm\ s_2\ \ (I_n)_{\mathrm{sp2}}\ \pm\ \ s_2\ \ (I_n)_{\mathrm{sp3}}\,, \tag{6.28}$$

$$\mathrm{sp2} = 1...n-1, \tag{6.29}$$

$$\mathrm{sp3} = (\ sp2+1)\,...n, \tag{6.30}$$

with one point ψ_0 at distance $s_0 = 0$, ten points ψ_1 at distance $\pm s_1$, and 40 points ψ_2 at distance $\sqrt{s_2^2+s_2^2}$ from the ground truth value. I_n is the identity matrix from which the $(\mathrm{sp1,2,3})^{\mathrm{th}}$ column is taken. Hence, the noise on the measurements ν is:

$$\nu_0 = \left(\sqrt{\boldsymbol{C}_y}\right)\ \psi_0^T, \tag{6.31}$$

$$\nu_1 = \left(\sqrt{\boldsymbol{C}_y}\right)\ \psi_1^T, \tag{6.32}$$

$$\nu_2 = \left(\sqrt{\boldsymbol{C}_y}\right)\ \psi_2^T, \tag{6.33}$$

$$\tag{6.34}$$

and is assumed to be additive to $\boldsymbol{y}$ (which are the synthetic moments). $\boldsymbol{C}_y$ is assumed to be a diagonal matrix with equal diagonal entries.

Now, the mean value of the estimated $\bar{\boldsymbol{x}}$ (which are $L_{\mathrm{m}}^{\mathrm{opt}}$ and $L_{\mathrm{t}}^{\mathrm{s}}$) and the covariance $\boldsymbol{C}_x$ of the

identified parameters $\hat{\boldsymbol{x}}$ are:

$$\bar{\boldsymbol{x}} = w_0\ \hat{\boldsymbol{x}}_0 + \sum_{sp=1}^{2n} w_1\ \hat{\boldsymbol{x}}_{\mathrm{sp1}} + \sum_{\mathrm{sp}=2n+1}^{2n^2+1} w_2\ \hat{\boldsymbol{x}}_{\mathrm{sp2}}, \tag{6.35}$$

$$\boldsymbol{C}_x = w_0\ (\hat{\boldsymbol{x}}_0 - \bar{\boldsymbol{x}})\ (\hat{\boldsymbol{x}}_0 - \bar{\boldsymbol{x}})^T \tag{6.36}$$

$$+ \sum_{\mathrm{sp}=1}^{2n} w_1\ (\hat{\boldsymbol{x}}_{\mathrm{sp1}} - \bar{\boldsymbol{x}})\ (\hat{\boldsymbol{x}}_{\mathrm{sp1}} - \bar{\boldsymbol{x}})^T \tag{6.37}$$

$$+ \sum_{\mathrm{sp}=2n+1}^{2n^2+1} w_2\ (\hat{\boldsymbol{x}}_{\mathrm{sp2}} - \bar{\boldsymbol{x}})\ (\hat{\boldsymbol{x}}_{\mathrm{sp2}} - \bar{\boldsymbol{x}})^T\ . \tag{6.38}$$

with w_0 w_1, and w_2 the weights resulting from the optimization.

Chapter 7

The added value of the estimation of subject-specific muscle-tendon parameters of the knee joint actuators in musculoskeletal modeling: two case studies

Abstract[1]

In this study we applied a recently developed method for functional scaling (i.e. subject-specific estimation) of the most sensitive Hill muscle-tendon parameters being the optimal muscle fiber length and the tendon slack length of the knee joint actuators. The method, which has been validated in a simulation environment, was applied to isokinetic dynamometry, treadmill walking and countermovement jumping for two healthy power athletes. It was the first time that functional scaling was applied to evaluate dynamic simulations. The performance of four musculoskeletal models was compared. The four models were: two models including linearly scaled muscle-tendon parameters in combination with respectively linearly scaled and image-based geometry, and two models including functionally scaled muscle-tendon parameters for the knee joint actuators in combination with respectively linearly scaled and image-based geometry. An EMG-driven forward simulation was performed for isokinetic dynamometry. We found differences (averaged over the subjects) between the moments resulting from inverse dynamics and the predicted moments expressed as root mean square values as low as 38.3 ($\pm$27.6) /29.1 ($\pm$0.4) Nm (flexion/extension, models including functionally scaled muscle-tendon parameters for the knee joint actuators), and as high as 54.1 ($\pm$24.6) /59.6 ($\pm$12.4) Nm (flexion/extension, models including linearly scaled muscle-tendon parameters). An inverse analysis was performed for all movements. Predicted activations for all

[1]This chapter is edited for submission as a full paper in *Journal of Biomechanics*.

models were compared with experimentally obtained activations. In general, better correlations were found for the musculoskeletal models including functionally scaled muscle-tendon parameters of the knee joint actuators.
Altogether, we showed the potential of our functional scaling method, and we showed how musculoskeletal modeling benefits from functionally scaled muscle-tendon parameters of the knee joint actuators.

7.1 Introduction

Dynamic simulations of human motion have the potential to support biomechanical analyses e.g. to plan intervention in pathologic gait, to design prostheses, and to enhance sport performance. Currently, dynamic simulations are widely used in research. Typically, the dynamic simulations rely on a musculoskeletal (MS-) model. The MS-model presented by Delp et al. [32] is often used. This MS-model represents an average male, and its actuators, muscles and tendons, are modeled as Hill-type actuators [120] for which the characteristics are mainly based on data obtained from cadaver studies. Muscle-tendon (MT-) parameters are scaled linearly, in accordance to the segment's length. In order to personalize the analyses and to gain accuracy, a common objective of many biomechanical researchers is to develop subject-specific MS-models. Such models include the subject-specific information concerning (i) MS-geometry as moment arm lengths, origin and insertion points of tendons, and (ii) MT-parameters which describe the muscle and tendon force-length-velocity characteristics. Much progress has already been made when it comes to extracting subject-specific geometric information because of the development of imaging techniques (e.g. [85; 100]). Scheys et al. [85] showed that image-based models estimate more accurate moment arm lengths for children with bone deformities causing pathologic gait patterns. Tsai et al. [100] reported that their image-based MS-geometry better predicts the knee joint moment than the generic model and the linearly scaled (geometry and MT-parameters) generic model. However, linear scaling is not a valid procedure to adapt MT-parameters subject-specifically, as shown by [115]. The study revealed that scaling methods which preserve the muscles' operating range outperform linear scaling. Yet, no subject-specific information on muscle strength is taken into account in these methods. In fact, subject-specific MT-parameter estimation is a challenging task as it relies typically on experimental data and non-linear optimization techniques. The MT-parameter estimation is based on the experimentally obtained moment-angle relationship, hence the joint moments are obtained at predefined joint angles. Further this type of scaling is referred to as functional scaling. It is very likely that it is not possible to estimate the MT-parameters

for all actuators, because the experimental data do not contain sufficient information on all MT-parameters and/or the identifiability of the MT-parameters is poor. The former can be investigated by a sensitivity analysis (e.g. [29]), the latter can be investigated by an identifiability analysis (e.g. as presented in chapter 6). De Groote et al. [29] showed that dynamometer experiments mainly contain information on the tendon slack length and to a lesser extent on the optimal fiber length of a limited set of specific knee joint actuators. Van Campen et al. [105] showed that the respective MT-parameters can be identified from a minimum set of isometric dynamometer experiments.

Lloyd and Besier [63] described a calibration method to obtain the $L_{\mathrm{t}}^{\mathrm{s}}$ of 13 knee actuators together with three activation-related parameters and two scaling factors to enforce a relative strength distribution between flexors and extensors. The parameter set was obtained through a non-linear least-square fit resulting in the best agreement between the joint moments as measurend during five experimental trials and the respective joint moments obtained via inverse dynamics. $L_{\mathrm{m}}^{\mathrm{opt}}$ varied linear with the level of activation. The method was validated. However, to evaluate the performance, some of the calibration trials were also used as validation trials.

Garner and Pandy [42] described a method for subject-specific scaling of MT-parameters ($L_{\mathrm{t}}^{\mathrm{s}}$ and $L_{\mathrm{m}}^{\mathrm{opt}}$, $F\mathrm{m}^{\mathrm{max}}$). A transformation of variables was introduced. The parameter set was obtained through a non-linear least-square fit resulting in the best agreement between experimental isometric dynamometer data and the respective model-based joint moments.

We [105] recently proposed an alternative estimation procedure for subject-specific scaling of MT-parameters (of a Hill-type muscle model). The procedure relies on subject-specific strength measurements obtained by isometric dynamometry [104] while it aims at preserving the muscle's operating range. In a simulation environment, the robustness of the estimation procedure to the initial guess and to measurement noise was found to be better compared to the algorithm proposed by [42]. However, our functional scaling method has not yet been validated on experimental data.

The aim of this study is to evaluate the recently presented functional scaling method [105] by the evaluation of the predictions by MS-models with increasing subject-specificity: (i) an MS-model with linearly scaled geometry, and linearly scaled MT-parameters, (ii) an MS-model with linearly scaled geometry, and functionally scaled MT-parameters of the knee joint, (iii) an MS-model with image-based geometry, and linearly scaled MT-parameters, and (iv) an MS-model with image-based geometry, and functionally scaled MT-parameters of the knee joint actuators. To our knowledge, no studies are available which compare the performance of functional scaling to linear scaling. Three motion conditions are used to validate the different models: isokinetic dynamom-

etry at 30°/s, treadmill walking at 4km/h, and countermovement jumping. The correspondence between simulated and experimental quantities is assessed.
The evaluation is via (i) a forward simulation (dynamometry) which forces to make an assumption concerning maximum muscle activation rates and (ii) inverse simulations (dynamometry, walking, jumping) which forces to make an assumption on how muscles are recruited, hence on the performance criterion to be optimized.

We hypothesize that the higher the subject-specificity of the MS-model, the better it predicts the experiments.

7.2 Methods

Subjects

Two subjects participated in this study. Both subjects (S1: 22y male, BMI 19; S2: 19y female, BMI) were elite power athletes. A written informed consent was provided to all subjects before participation. The experimental procedure was approved by the Ethical Committee.

Musculoskeletal modeling

The generic MS-model [32] consisted of eight segments (trunk, pelvis, left and right thigh, lower leg, and foot) and 19 degrees of freedom. Each leg was actuated by 43 muscles. Contraction dynamics were described by a Hill-type model [120]. Force-length-velocity characteristics were according to [68].

Four subject-specific MS-models were constructed for both subjects. The geometry of the MS-models was either linearly scaled to the segment lengths, further referred to as GEO-linear, or the geometry was image-based, referred to as GEO-image. The MT-parameters were either all linearly scaled to the segment lengths, further referred to as MT-linear, or the MT-parameters of the knee joint actuators were obtained by functional scaling (see Supplementary Material for details), further referred to as MT-specific. Hence the four models were: GEO-linear/MT-linear, GEO-linear/MT-specific, GEO-image/MT-linear, GEO-image/MT-specific.

The optimal muscle fiber length and tendon slack length of the knee joint actuators were as given in table 7.1 for all models. Maximum isometric force and optimum pennation angle for all muscles

and the optimal muscle fiber length and tendon slack length for hip and ankle joint actuators were adopted from [32]. These MT-parameters were linearly scaled to the segment's lengths.

To extract subject-specific geometry, MR-images were obtained for each subject lying supinely with knees extended [85]. Local marker positions were obtained from the MR-image, and were expressed relative to the bones in anatomical reference frames as described by [103].

Data acquisition

The experimental setup and data acquisition for treadmill walking (4km/h) and countermovement jump were described by [52]. Data contained three-dimensional (3D) marker trajectories, ground reaction forces (GRF), and surface electromyography (EMG) of gastrocnemius (GAS), vastus lateralis (VL), rectus femoris (RF), lateral hamstrings (HamLat), and medial hamstrings (HamMed). The experimental setup and data acquisition for isometric and isokinetic dynamometry (30°/s) was as described by [104]. Data contained 3D kinematics, registration of 3D reaction forces and moments, and EMG of RF, VL, GAS, HamLat, and HamMed.
The raw EMG signals were collected at 1000Hz (walking, jump) and 500Hz (dynamometry).

Data processing

The raw EMG signals were band-passed filtered, rectified and peak dynamic normalized [19]. For dynamometry, the peak signal was set to 0.9 instead of 1 as it has been reported that during isokinetic dynamometry, no maximal activation is reached [10]. Because only five EMG signals were measured during dynamometry, we made following assumptions: all three vasti were driven by the signal of VL, lateral hamstrings were driven by the signal of HamLat, medial hamstrings were driven by the signal of HamMed, and gastrocnemii were driven by the signal of GAS.

Inverse kinematics (IK) were calculated with a Kalman smoothing algorithm [28]. Inverse dynamics (ID) were obtained via OpenSim [33] for walking and jumping, and as described by [104] for dynamometry. Forward (dynamometry) and inverse (all motion conditions) simulations were performed as schematically represented in figure 7.1. The forward simulations were EMG-driven and calculated the joint moment M_{joint} of the knee which was actuated by 13 muscles. The actuator lengths L_{mt} resulted from the joint kinematics and the MS-model. The inverse simulations calculated the muscle activations underlying the motion using a physiological inverse approach [30]. The goal criterion was altered to the minimization of the maximal activation according to [1].

Table 7.1: MT-parameter values for different musculo-skeletal models

	S1				**S2**			
	1	*2*	*3*	*4*	*1*	*2*	*3*	*4*
$\mathbf{L}^{\mathrm{m}}_{\mathrm{opt}}$	[cm]	[cm]	[cm]	[cm]	[cm]	[cm]	[cm]	[cm]
RF	12.39	11.75	12.31	**8.81**	11.06	10.84	12.02	**10.43**
VI	9.5	10.32	9.69	9.43	8.49	**11.03**	8.89	**11.52**
VL	9.17	**10.61**	9.87	9.86	8.21	**10.52**	9.33	**12.21**
VM	9.72	9.86	10.8	10.11	8.69	**10.72**	9.89	**11.85**
BFL	11.93	**16.84**	11.32	**13.74**	10.77	**7.71**	10.81	**14.4**
GL	6.92	7.41	6.85	**5.02**	6.43	**8.68**	6.18	**5.42**
GM	6.48	**8.23**	6.31	**5.42**	6.03	**7.89**	5.81	5.32
SM	12.39	11.22	8.3	**11.58**	7.9	**8.77**	7.79	8.05
$\mathbf{L}^{\mathrm{s}}_{\mathrm{t}}$	[cm]	[cm]	[cm]	[cm]	[cm]	[cm]	[cm]	[cm]
RF	33.69	**35.77**	33.49	**36.76**	30.08	**32.56**	32.69	**36.05**
VI	14.86	15.17	15.15	**20.55**	13.26	**11.33**	13.91	13.88
VL	17.14	**13.92**	18.44	**15.64**	15.34	**15.98**	17.45	**15.62**
VM	13.76	**16.94**	15.28	**14.51**	12.3	**10.73**	13.99	13.99
BFL	35.67	**27.54**	33.85	**32.81**	32.2	**35.45**	32.33	**28.21**
GL	41.07	41.67	40.67	**41.52**	38.18	38.8	36.71	37.23
GM	42.15	42.84	41.01	41.66	39.18	**40.24**	37.79	**38.74**
SM	39.29	**36.18**	37.23	**31.26**	35.44	**31.62**	34.97	**31.90**

Values for optimal fiber length ($L^{\mathrm{m}}_{\mathrm{opt}}$) and tendon slack length ($L^{\mathrm{t}}_{\mathrm{s}}$) are given for both subjects and four models: Model 1 is the GEO-linear/MT-linear model, model 2 is the GEO-linear/MT-specific model, model 3 is the GEO-image/MT-linear model, model 4 is the GEO-image/MT-specific model. Muscles included are according to the findings of [29]. The changes in the MT-parameter values due to functional scaling relative to the linearly scaled MT-parameter values (models 1 and 3) for all bold values (models 2 and 4) were larger than the standard deviations on the estimated means based on noisy experimental data as reported by [105].

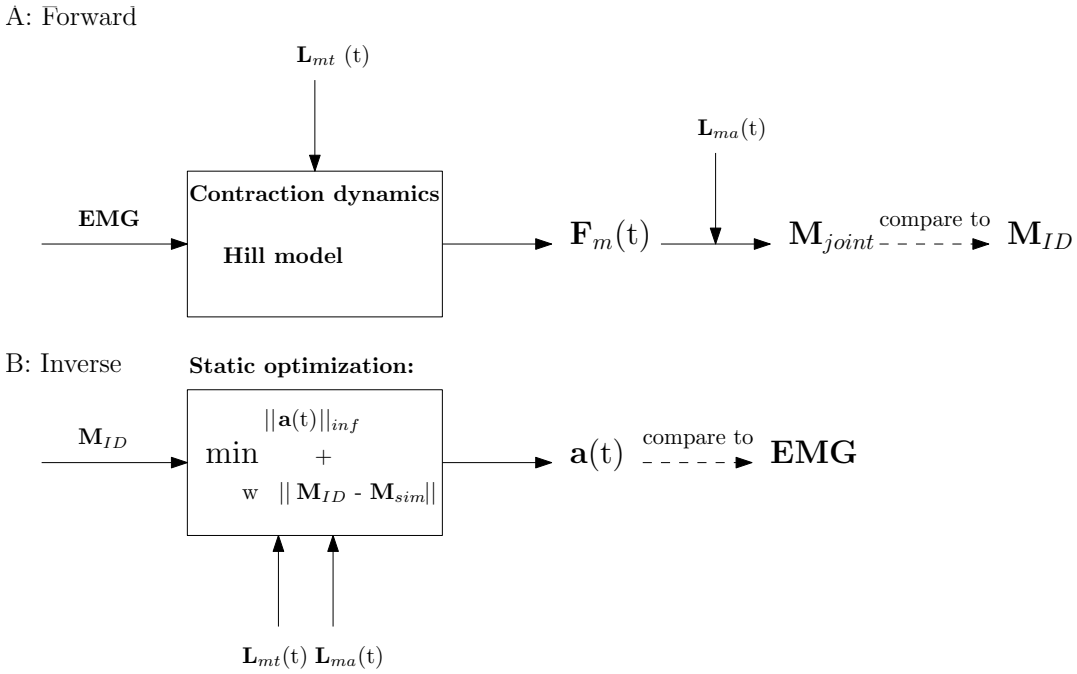

FIGURE 7.1: Schematic representation of the forward (A) and inverse simulations (B). Forward simulations are driven by activations a(t) obtained by EMG. By integration of a Hill-type MT-model MT-forces $\mathbf{F}_{\mathrm{mt}}$ are obtained. The Hill-type MT-model is described by active ($\mathbf{F}_{\mathrm{act}}$) and passive ($\mathbf{F}_{\mathrm{pas}}$) force-length characteristics and the tendon ($\mathbf{F}_{\mathrm{t}}$) force strain characteristic. Muscle-tendon length $\mathbf{L}_{\mathrm{mt}}$, are input to the model. Simulated joint moments $\mathbf{M}_{\mathrm{joint}}$ result from the multiplication of the muscle moment arms $\mathbf{L}_{\mathrm{ma}}$ with $\mathbf{F}_{\mathrm{m}}$. $\mathbf{M}_{\mathrm{joint}}$ is compared to $\mathbf{M}_{\mathrm{ID}}$ the joint moment according to an inverse dynamic analysis. Inverse simulations estimate a(t) by solving a goal criterion which minimizes the maximum activation while fitting $\mathbf{M}_{\mathrm{ID}}$ to M_{joint}. The estimated activations are than compared to the experimentally obtained activation by EMG.

Data analysis

To evaluate the performance of the models, (i) we calculated the root mean squared differences between the predicted moments for the isokinetic dynamometry (isokinetic parts of the motion) resulting from the forward simulation and the results from inverse dynamics, and (ii) we compared predicted activation patterns resulting from inverse simulations with EMG recordings quantitatively (activation pattern) by cross-correlations. Also, the fitting errors between muscle moments corresponding to the estimated activations (hip flexion, knee flexion, ankle plantar flexion) and the inverse dynamics were reported as RMS values. Since the inverse dynamics were imposed via a penalty term, a value of the fitting error within modeling uncertainty rather than an exact fit was required.

7.3 Results

Table 7.1 shows how the linear scaling changes the MT-parameter values. Relevant changes in light of the uncertainty on the estimated means due to measurement noise are indicated in bold.

Forward simulation

Dynamometry

The differences at the isokinetic parts of the motion between the moments resulting from inverse dynamics, and the predicted moments based on the MS-models are given as RMS values in table 7.2. Forward simulations of the knee joint moment showed that GEO-linear/MT-specific and GEO-image/MT-specific models drastically improved the predicted extensor moment, whereas for the predicted flexor moments the improvement was more explicit for the GEO-image/MT-linear (S1) ./MT-specific (S2) models. Overall the GEO-image/MT-specific models predicted the joint moment best. The model predictions are visualized in figure 7.2.

Inverse simulation

Dynamometry

Inverse simulations showed in general that, the predicted activation patterns by the MS-models which were MT-specific show higher correlations with the EMG recordings. Overall, muscles were differently recruited depending on the MS-model type.

Correlations are presented in table 7.3c. The most relevant activation signals are shown in figure 7.3, an overview of all signals is provided in figure 7.4 of the Supplementary Material.

TABLE 7.2: Experimental versus predicted knee joint moments.

	S1				**S2**			
	1	*2*	*3*	*4*	*1*	*2*	*3*	*4*
	[Nm]	[Nm]	[Nm]	[Nm]	[Nm]	[Nm]	[Nm]	[Nm]
Ext	66.9	28.8	68.4	33.9	42.6	29.4	50.8	29.2
Flex	36.8	28.3	16.3	18.7	71.4	57.8	62.6	57.8

Root mean square (RMS) differences in [Nm] between the isokinetic moment resulting from inverse dynamics and the predicted moment based on four MS-models: Model 1 is the GEO-linear/MT-linear model, model 2 is the GEO-linear/MT-specific model, model 3 is the GEO-image/MT-linear model, model 4 is the GEO-image/MT-specific model. RMS-values are calculated for the isokinetic parts of the motion.

Treadmill walking

Inverse simulations showed in general comparable correlations between the pattern of the EMG recordings and the GEO-linear models at one side, and the GEO-image models at the other side. The predicted activation levels for VL and HamLat are low compared to the EMG recordings.
Correlations for the MS-models which were MT-specific were mostly higher, except for VL. Correlations are presented in table 7.3a. An overview of the activation patterns as measured and predicted during gait are provided in Supplementary figure 7.6.
The fitting errors between muscle moments corresponding to the estimated activations and inverse dynamics were within modeling uncertainty (RMS smaller than 6Nm)

Countermovement jumping

Inverse simulations showed in general the highest correlations between EMG recordings and the GEO-linear/MT-specific models for GL, SOL, and RF, and the GEO-image/MT-specific models for the hamstrings. The predicted activation levels were in general lowest for the GEO-linear/MT-specific models. The predicted activation levels by the GEO-image models of subject 2 were maximum, i.e. saturated, for VL and the hamstrings.
Correlations are presented in table 7.3b. Most relevant patterns are shown in figure 7.4b; an overview of all measured and predicted patterns is provided in Supplementary figure 7.7.
The fitting errors between muscle moments and inverse dynamics were within modeling uncertainty.

Table 7.3: EMG versus predicted activations: Cross-correlations

	S1				S2			
	1	*2*	*3*	*4*	*1*	*2*	*3*	*4*
A. Treadmill								
GL	**.95**	**.95**	.91	.91	.73	.80	.66	**.81**
SOL	.69	**.72**	.58	.57	.23	.34	.44	**.49**
RF	.41	**.42**	.34	.34	.23	.31	.58	**.69**
VL	.55	.71	**.75**	.66	**.47**	.32	.28	.20
HamLat	.73	.69	.73	**.74**	.18	**.30**	.18	.23
HamMed	.48	.49	**.85**	.83	**.42**	**.42**	.39	.39
B. Jump								
GL	.87	**.91**	.82	.82	.90	**.92**	.63	.66
SOL	**.93**	**.93**	.90	.91	.89	**.95**	.93	**.95**
RF	.88	**.93**	.82	.83	**.91**	.80	.72	.64
VL	**.93**	.88	.89	.91	.93	.93	**.95**	.90
HamLat	**.95**	.94	**.95**	**.95**	.83	.86	.83	**.90**
HamMed	**.92**	.90	.91	.89	.82	.85	.86	**.88**
C. Isokinetic								
GAS	.69	.71	.89	**.91**	.84	.90	.85	**.92**
RF	**.93**	.89	.92	.87	**.76**	.56	.62	.55
VL	.97	**.98**	.94	**.98**	.92	**.98**	.89	.91
HamMed	.95	**.96**	**.96**	**.96**	.95	.92	.89	**.96**
HamLat	.87	.87	**.94**	**.94**	.95	.92	.89	**.96**

Cross-correlations between predicted activations and EMG recordings for subject 1 (S1) and subject 2 (S2) per model. Model 1 is the GEO-linear/MT-linear model, model 2 is the GEO-linear/MT-specific model, model 3 is the GEO-image/MT-linear model, model 4 is the GEO-image/MT-specific model.

7.4 Discussion

In this study, the capability of MS-models with a different level of subject-specificity to predict experimental motion data is evaluated. The four MS-models contained either linearly scaled geometry or image-based geometry combined with linearly scaled MT-parameters or functionally scaled MT-parameters of the knee joint actuators. The evaluated motions were isokinetic dynamometry, treadmill walking, and countermovement jumping. The functional scaling of the optimal muscle fiber lengths and the tendon slack lengths of the knee joint actuators relies on mono-articular isometric dynamometry (see chapter 6).
This study allowed analyzing the effect of subject-specific MS-geometry versus the effect subject-specific MT-parameters. Two simulation approaches are applied: (i) A forward simulation which uses recorded EMG signals as input to simulate the knee joint moment. This forward simulation was used to simulate isokinetic dynamometry. This simulation approach is equivalent to the simulation approach underlying the estimation method. (ii) An inverse approach which calculates muscle activations underlying a given motion based on a performance criterion. Inverse approaches are frequently applied in motion analysis since they require no EMG recordings. However, because of the optimization involved in the prediction of the muscle activations, the model uncertainties increase when using inverse approaches.

Functional scaling mostly adapted the MT-parameter values significantly: the changes in de values were mostly larger than the uncertainty on the estimated mean value due to measurement noise as reported by [105]. Otherwise, whenever the changes of the MT-parameter values after functional scaling were whithin the uncertainty on the estimated mean value e.g. L_t^s of GL, this can be linked to a lower sensitivity of the MT-parameters to isometric dynamometry [29; 102].

Forward simulation

Dynamometry
The forward simulations showed large improvements of the predicted joint moment when functionally scaled MT-parameters are included in the MS-model. Surprisingly, the GEO-image/MT-specific models, the most subject-specific models, did not outperform the GEO-linear/MT-specific models. In our case studies, the improvement of the simulations resulting from subject-specific MT-parameters was larger than the improvement resulting from subject-specific MS-geometry. This is probably a consequence of the test-subjects being power athletes.
Systematic differences in shape between predicted moments and measurement-based moments are

present for both subjects. This likely demonstrates the presence of modelling errors e.g. the simplified description of the joints, the representation of the muscles as line segments, and the phenomenological Hill-model especially the force-velocity characteristic. However, adapting the model was not into the scope of this paper.

From our perspective, two main reasons for the remaining discrepancy between experimental and simulated moments, and hence limitations to this study, can be put forward: (i) the maximum isometric force $F^{\mathrm{m}}_{\mathrm{max}}$, which is adopted from the generic model [32] for all muscles, and (ii) the EMG acquisition and processing. Concerning the former, Tsai et al. [100] derived $F^{\mathrm{m}}_{\mathrm{max}}$ from the muscle volume as observed in the images. Whereas for the knee extensors the image-based values are in reasonably good agreement with the generic values, the flexor values reported by [100] were up to 30% smaller than the generic values. According to the Hill-model equations [120], an overestimation of $F^{\mathrm{m}}_{\mathrm{max}}$ results in an overestimation of the muscle forces and hence, in an overestimation of the joint moment as observed in our results. Including $F^{\mathrm{m}}_{\mathrm{max}}$ in the estimation procedure however is not feasible as the dynamometer experiments show in general lower sensitivities to this MT-parameter [29].
Concerning the latter, we were limited by the number of EMG signals, which forced us to make some assumptions. We also opted for peak moment scaling of the EMG signals which is typically adopted for gait analysis too. However, there is no such thing as 'a golden rule' when it comes to scaling of processed EMG signals [43].

In literature, either the influence of image-based MS-geometry [100] or the influence of the functionally scaled MT-parameters [63] has been studied.

Tsai et al. [100] performed an EMG-driven forward simulation of knee extensor isokinetic dynamometry. An unscaled model, a linearly scaled model (MT-parameters and geometry), and an image-based model (MT-parameters linearly scaled) were evaluated. In contrast to their results, we found that our MS-models overestimated the dynamometer result. A possible explanation is that the measurement errors in the experimental data of [100] were higher, because the experimental data were as recorded by the dynamometer, whereas we relied on results from a full 3D analysis which has been shown to result in more accurate measurements [104]. We also found lower differences between the MS-models with image-based geometry and MS-models with linearly scaled geometry (both with linearly-scaled MT-parameters). A possible explanation for this difference is that the value of $F^{\mathrm{max}}_{\mathrm{m}}$ in our study was equal for both models, whereas in theirs the value was

image-based (MS-model equivalent to GEO-image/MT-linear) or the value was derived from the subject's strength (MS-model equivalent to GEO-linear/MT-linear).

Lloyd and Besier [63] also performed an EMG-driven forward simulation. The studied MS-model includes linearly scaled geometry. Values for $F_{\mathrm{m}}^{\mathrm{max}}$, α_{opt} and $L_{\mathrm{m}}^{\mathrm{opt}}$ were adopted from literature. In their model, $L_{\mathrm{m}}^{\mathrm{opt}}$ was a linear function of activation. Two parameters enforced the relative force distribution between flexors and extensors. Three parameters regulated the amount of activation. These five adjustable parameters, together with 13 adjustable $L_{\mathrm{t}}^{\mathrm{s}}$ values (one per knee joint actuator), were calibrated so that the forward dynamics results best matched the respective five experimental trials. Considering the results, the predicted knee joint moment at its maxima deviated up to 40Nm (extension) and 20Nm (flexion) from the experimental data which was comparable to the performance of our model with linearly scaled MS-geometry and functionally scaled MT-parameters. However, the experimental velocities were different (120°/s versus 30°/s). Moreover, the concentric isokinetic dynamometry trial as presentd by Lloyd and Besier was part of the calibration pool of experiments. When evaluating their model against an experiment which was not part of the calibration trials, the performance level of their model reduced. In general, it is hard to say which method performs best, the calibration method of Lloyd and Besier or our functional scaling method. A huge advantage of our estimation method in contrast to the approach of Lloyd and Besier, is the need for only a limited set of experiments which results from the numerically efficient formulation. However, in contrast to Lloyd and Besier our method allows to vary $L_{\mathrm{m}}^{\mathrm{opt}}$. We also assumed that the relative strength between flexors and extensors can be deduced from imaging technique [40]. Additionnaly, (i) it is not reported whether the amount of parameters is identifiable from the proposed set of calibration experiments, and (ii) $L_{\mathrm{t}}^{\mathrm{s}}$ of some muscles are estimated although [29] showed that al least three of the calibration experiments do not contain information on these parameters. Although Lloyd and Besier rely on dynamometer data too, which have been shown to be noisy (e.g. [104]), the influence of measurement noise is not studied nor is the influence of the initial guesses.

Inverse simulation

For the inverse analyses, cross-correlations were consistently higher for jumping and isokinetic dynamometry than for gait. This can be attributed to how muscles were recruited during these different tasks. During the jump and the dynamometry, muscles are recruited at full strength, whereas during gait muscles are recruited at lower activation levels according to the performance criterion.

Dynamometry

Considering dynamometry, the inverse simulation seemed to support the results of the forward simulation: patterns resulting from MS-models which were MT-specific showed better correspondence to the EMG recordings. For the quadriceps, this held specifically for VL. The weaker correspondence between the predicted activation of RF and the EMG might result from cross-talk with the vasti, which is a known problem [73]. Considering the hamstrings, especially for S2, according to the correlations, GEO-image/MT-specific models best predicted the activation pattern.

Treadmill walking

Considering treadmill walking, none of the MS-models predicted maximum activation levels. Hence, the model strengths appeared to be sufficient. Mostly, the MS-models which were MT-specific resulted in better predictions of the activation patterns. It was however not straightforward to draw conclusion whether results from an inverse analysis did or did not benefit from advanced subject-specific MS-modeling in healthy adults as the results were subject- and muscle-specific.
As far as the authors are aware, no comparable studies are available. The predicted activation patterns based on the adapted goal criterion [1] were comparable to the results reported by [30].

Countermovement jump

Considering countermovement jumping, model strength obviously becomes an issue. In general, more activation is needed for jumping (and also for isokinetic dynamometry). Therefore, the influence of the goal function is smaller because the solution space will be smaller. Again, the MS-models which were MT-specific result in better predictions of the activation patterns. However, GEO-linear/MT-specific models resulted in lower activation levels, and never saturated in contrast to GEO-image/MT-specific models of S2 for VL and the hamstrings. Hence, GEO-linear/MT-specific models resulted to be more powerful although the correlations indicated that the GEO-image/MT-specific models better predicted the activation patterns. For both subjects, particularly the hamstrings still needed a large activation burst in order to perform the jump. In fact, as only the knee actuators were subject-specific, the bi-articular muscles actuated joints together with non-specific actuators which probably lack strength. Hence, this resulted in higher activation of the specific actuators too. A more accurate estimate of $F^{\mathrm{m}}_{\mathrm{max}}$ might also be beneficial. Again, the authors are not aware of comparable studies.

The importance of evaluating walking and jumping was already mentioned earlier. The MT-

parameters of the knee joint actuators have been functionally scaled based on mono-articular experiments of the knee joint. However, some muscles were bi-articular as they also either articulated the hip joint or the ankle joint. In theory, it is possible that the improved correspondance between measured and modelled knee moments obtained by functional scaling of the MT-actuators of a bi-articular muscles would deteriorate the contribution of these muscles to the hip or ankle moment resulting in compensatory actions of mono-articular muscles. However, our results showed that this was not the case: e.g. at the ankle joint, the functional scaling of the MT-parameters of m. gastrconemii did not corrupt the performance of m. soleus.

7.5 Conclusion

We presented two case studies for which four MS-models including gradually increasing subject-specific features (MS-geometry, MT-parameters) are evaluated for three different movements: isokinetic dynamometry, treadmill walking, and jumping.

We demonstrated that forward simulation of knee joint moment benefits from functionally scaled MT-parameters. The scaling of the MT-parameters also appeared to be more important than the MS-geometry.
Additionnally, we demonstrated that for inverse simulations the effect of functionally scaled MT-parameters of knee joint actuators is less pronounced. However, this can be attributed to the assumption made about muscle recruitement in the goal criterion, and to the model involved during gait and jumping which is a model of the complete lower limb. Yet, the model strength improved when image-based geometry and functionally scaled MT-parameters were combined.

Acknowledgements

The support of the following projects is gratefully acknowledged: project G.0395.09 of the Research Foundation - Flanders, K.U.Leuven's Interdisciplinary Research Program IDO/07/12, and K.U.Leuven-BOF EF/05/006 Center-of-Excellence Optimization in Engineering.

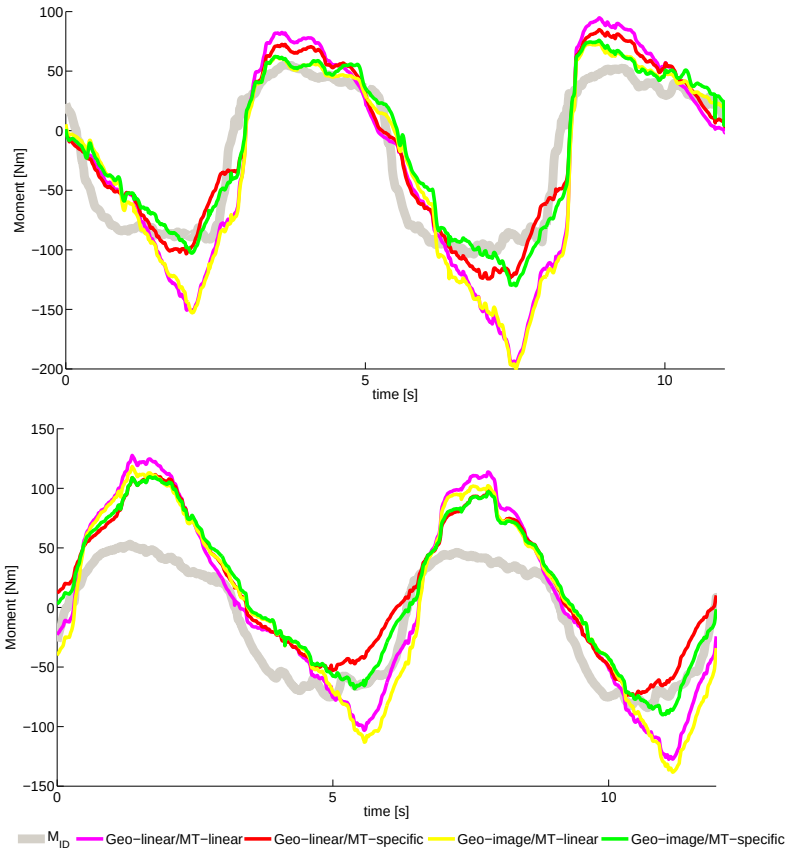

Figure 7.2: Predicted knee joint moments during isokinetic dynamometry for all models. Results for subject 1 are shown on top, results for subject 2 are shown below. Extension moments are negative.

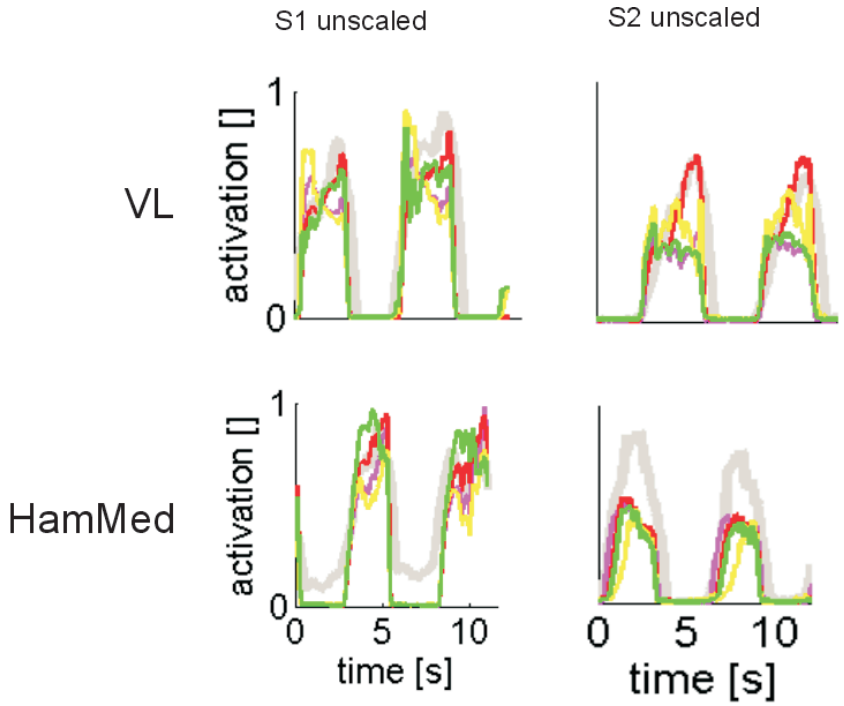

FIGURE 7.3: Predicted activations for isokinetic dynamometry (30°/s) for lateral vastus (VL), and medial hamstrings (HamMed) for subject 1 (S1) and subject 2 (S2). Unscaled results results are shown. The reference EMG is given in light grey, green: GEO-image/MT-specific, yellow: GEO-image/MT-linear, red: GEO-linear/MT-specific, magenta: GEO-linear/MT-specific.

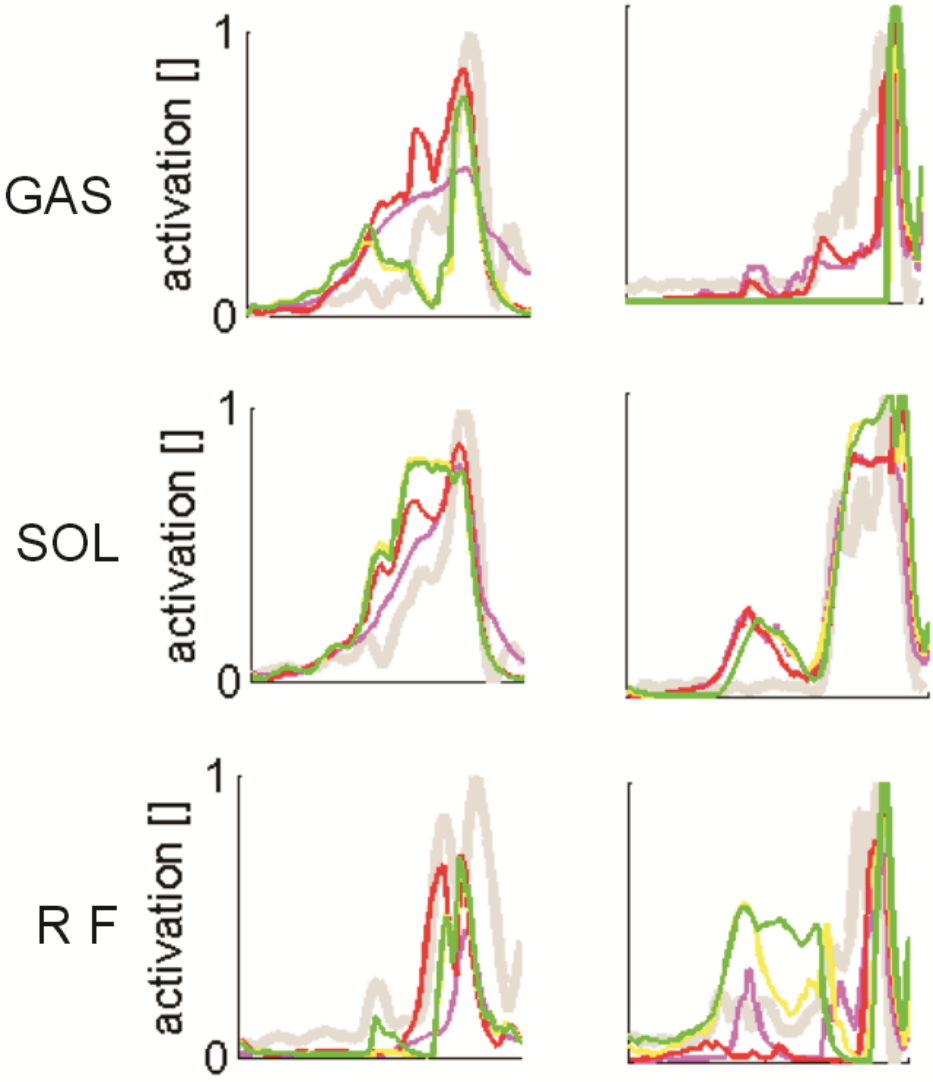
GAS
SOL
R F
activation []
1
0

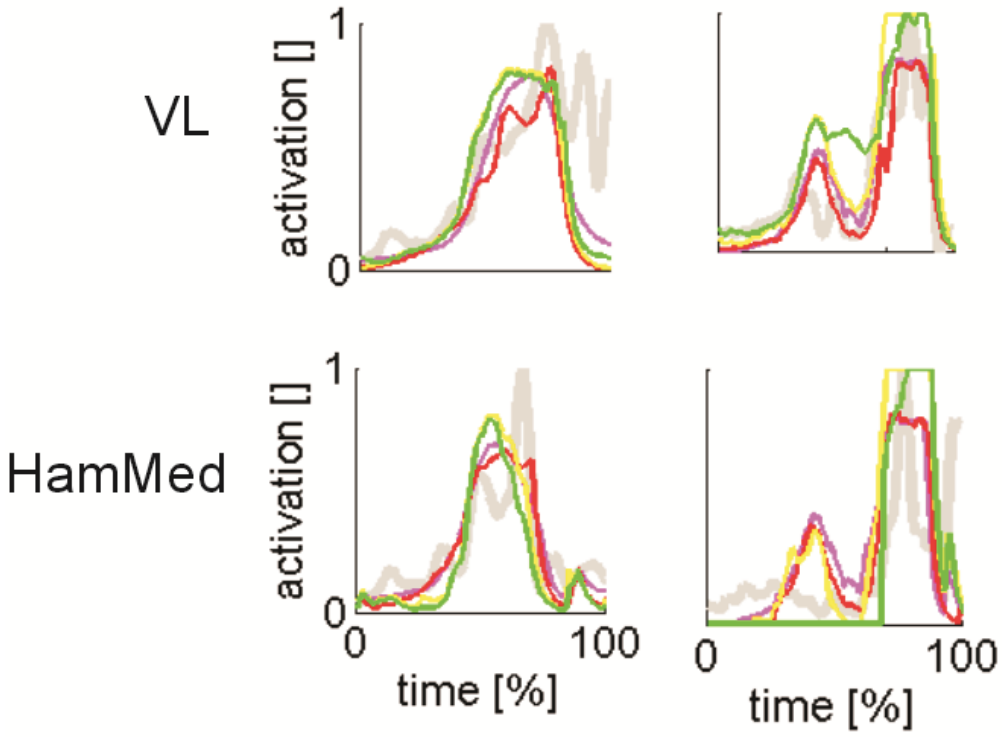

FIGURE 7.4: Predicted activations for countermovement jumping for rectus femoris (RF), lateral vastus (VL), gastrocnemius (GAS), soleus (SOL), and medial hamstrings (HamMed) for subject 1 (S1) and subject 2 (S2). Unscaled results are shown. The reference EMG is given in light grey, green: GEO-image/MT-specific, yellow: GEO-image/MT-linear, red: GEO-linear/MT-specific, magenta: GEO-linear/MT-specific.

7.6 Supplementary Material

Algorithm for subject-specific estimation of optimal fiber length and tendon slack length

The details on the algorithm proposed for subject-specific estimation of the optimal fiber length and the tendon slack length of the knee joint actuators are submitted for publication elsewhere. The experimental joint moments are obtained through isometric dynamometry [104], and a minimum set is selected.

Here, we provide the rationale and some implementation issues of the methodology. The algorithm aims at estimating subject-specific values of the most sensitive MT-parameters according to [29]. Simulation moments which rely on the MT-parameters and experimental moments are fitted. Hence, the MT-parameters are altered. The parameters included are the optimal fiber length $L^{\mathrm{m}}_{\mathrm{opt}}$ and the tendon slack length $L^{\mathrm{t}}_{\mathrm{s}}$ of four knee extensors (rectus femoris RF, vastus lateralis VL, medialis VM, intermedius VI), and four knee flexors (biceps femoris long head BFL, semimembranosus SM, gastrocnemius medialis GM and lateralis GL). The maximal isometric force $F^{\mathrm{m}}_{\mathrm{max}}$ and the optimal pennation angle are set to generic values [32]. Note that if appropriate techniques are available, $F^{\mathrm{m}}_{\mathrm{max}}$ can be determined image-based (e.g. [100]).

1. Rationale

Implicit to Hill-type models, $L^{\mathrm{m}}_{\mathrm{opt}}$ and $L^{\mathrm{t}}_{\mathrm{s}}$ are correlated. Hence, if one of both parameter values changes, by definition of the model, the other value has to change too if the muscle's operating range has to be preserved. Considering a discrete combination of $L^{\mathrm{m}}_{\mathrm{opt}}$ and $L^{\mathrm{t}}_{\mathrm{s}}$, in its neighborhood many other discrete combinations can be found that (i) the respective L_{m} satisfies the Hill-model equations and (ii) guarantee muscle activity in the muscle's operating range. The optimization problem underlying the estimation is a non-linear problem which typically suffers from local optima. However, the better the feasible set (the set of all possible solutions) is defined together with the goodness of the initial guess from where the optimization start, the higher the chances to get close to the global optimum, the exact solution of the problem.

Therefore, a two-phased algorithm was proposed: in phase I the feasible set and a hot start for the optimization in the second phase are obtained, in phase II the non-linear optimization problem is solved.

1.1 Algorithm phase I

For a discrete number of combinations of $L_{\mathrm{opt}}^{\mathrm{m}}$ and $L_{\mathrm{s}}^{\mathrm{t}}$ in an a priori defined neighborhood of the initial combinations, the Hill-model equations are solved. Hence, the states being the muscle fiber lengths are calculated for two extreme positions (one in flexion, one in extension) for the respective actuator. A first selection of combinations is made based on the physiological operating range of the actuator: whenever the normalized state exceeds the borders of the physiological operating range, the combination is excluded from the feasible set. For the remaining combinations, states calculated for the model in the reference position (zero activation, 0° hip/knee/ankle flexion) are compared to respective fiber lengths as presented in literature for cadavers [112]. An uncertainty on the fiber lengths is taken into account based on the sum of the reported standard deviations between cadavers and the coefficient of variation reflecting the regional fiber heterogeneity. Again, all the parameter combinations outside the borders of the uncertainty are removed from the feasible set. For the remaining combinations, the respective states are calculated in accordance to the measurement kinematics. The total joint moment is obtained for all combinations of feasible parameters sets. The hot start results from the parameter combinations which minimize the difference between the experimentally obtained joint moments and the joint simulation moments. The mathematical description of the feasible set is illustrated in figure 6.2.

1.1 Algorithm phase II

The non-linear optimization problem aims at finding parameters that result in the best fit between a vector (here five isometric moments) of simulation moments and a vector of experimentally obtained moments by changing the MT-parameters so that the parameter values fulfill the imposed constraints. The activations are obtained via EMG. The constraints are (i) the borders of the feasible set, (ii) physiologically inspired constraints e.g. the length of an extensor in a more flexed position should be larger than the length of the extensor in a less flexed position, and (iii) anatomically inspired constraints e.g. the functionality of some muscles as lateral and medial gastrocnemii is equivalent which is reflected in the MT-parameters. The optimization variables are defined as transformation of $L^{\mathrm{m}}_{\mathrm{opt}}$ and $L^{\mathrm{t}}_{\mathrm{s}}$ in order exploit the correlation between the model at one side and for the numerical efficiency (calculation time) at the other side.

2. Implementation details

In this section, some details on the implementation of phase II are provided.

2.1 Optimization variables

The vector of optimization variables contains:

- The normalized fiber lengths at every measurement condition for each actuator.
- The transformations of $L^{\mathrm{m}}_{\mathrm{opt}}$ and $L^{\mathrm{t}}_{\mathrm{s}}$ per actuator being ($\frac{L^{\mathrm{s}}_{\mathrm{t}}}{L^{\mathrm{m}}_{\mathrm{opt}}}$ and δ which represents the maximal distance of a feasible combination to the line (see figure 6.2).

2.2 Goal criterion

The goal criterion is a weighted bi-objective criterion:

$$\min_{\boldsymbol{x}} \quad w \ \left\|\mathbf{F}_{\mathrm{t},jk} - \mathbf{F}_{\mathrm{m},jk}\ cos\ \alpha_{jk}\right\|_{\infty} + (1-w)\ \left\|\mathbf{M}\mathrm{sim} - \mathbf{M}\mathrm{exp}\right\|_{\infty}, \tag{7.1}$$

with $\boldsymbol{x}$ the vector of optimization variables, w the weighing factor, $\mathbf{F}_{\mathrm{t},jk}$ the tendon force at a condition $k = 1 \ldots K$ for muscle $j = 1 \ldots J$, $\mathbf{F}_{\mathrm{m},jk}$ the muscle force at a condition k for muscle i, α_{jk} the pennation angle at condition k of muscle j, $\mathbf{M}$sim the joint moments as resulting from the simulations which depend on $L^{\mathrm{m}}_{\mathrm{opt}}$ and $L^{\mathrm{t}}_{\mathrm{s}}$ and $\mathbf{M}$exp the joint moments as resulting from the isometric dynamometer experiments.

2.3 Constraints

The normalized states are constrained by an upper and lower bound, which force the state to lie within a physiological operating range. Additionally, the normalized states for extensors are forced to decrease as the joint goes into extension and vice versa for the flexors. The tendon should be at least at his slack length. The parameter transformations should lie within the feasible set.

Supplementary figures

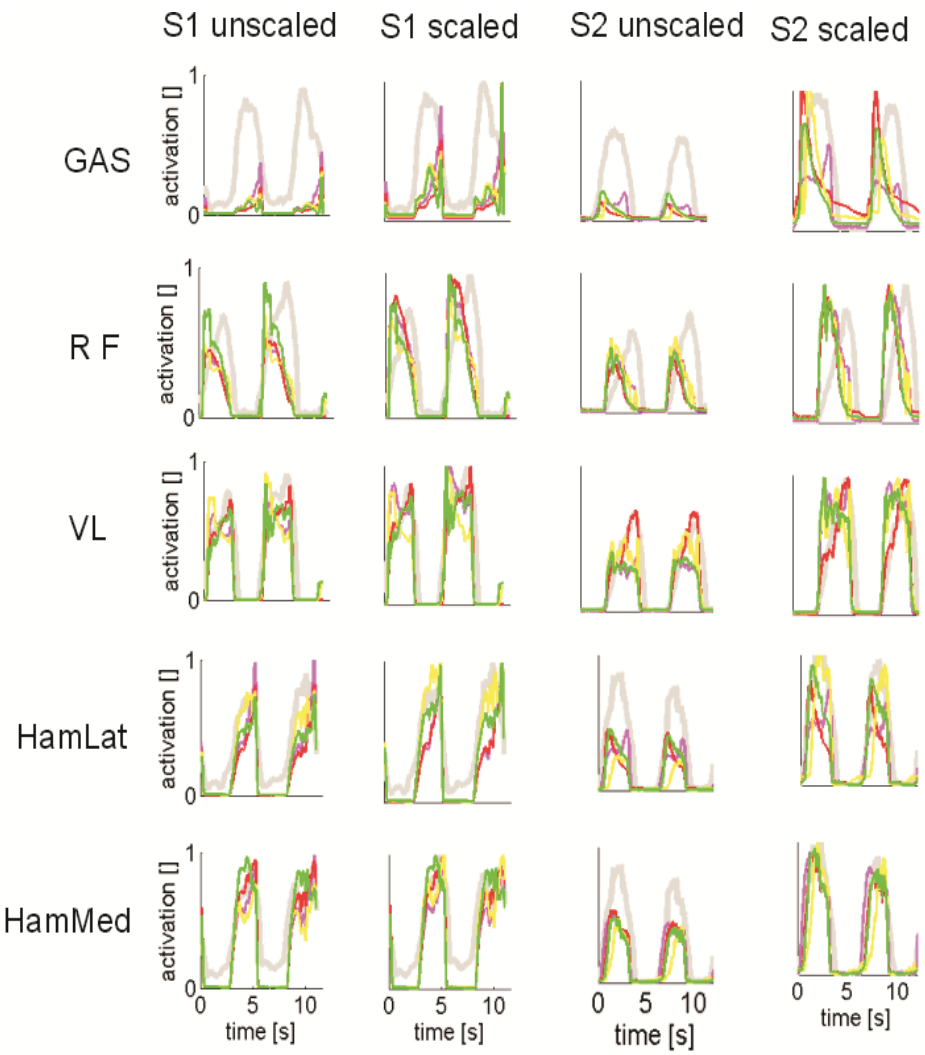

Figure 7.5: Predicted activations for isokinetic dynamometry (30°/s) for rectus femoris (RF), lateral vastus (VL), gastrocnemius (GAS), and medial and lateral hamstrings (HamMed, HamLat) for subject 1 (S1) and subject 2 (S2). Unscaled results as well as scaled results are shown.The reference EMG is given in light grey, green: GEO-image/MT-specific, yellow: GEO-image/MT-linear, red: GEO-linear/MT-specific, magenta: GEO-linear/MT-specific.

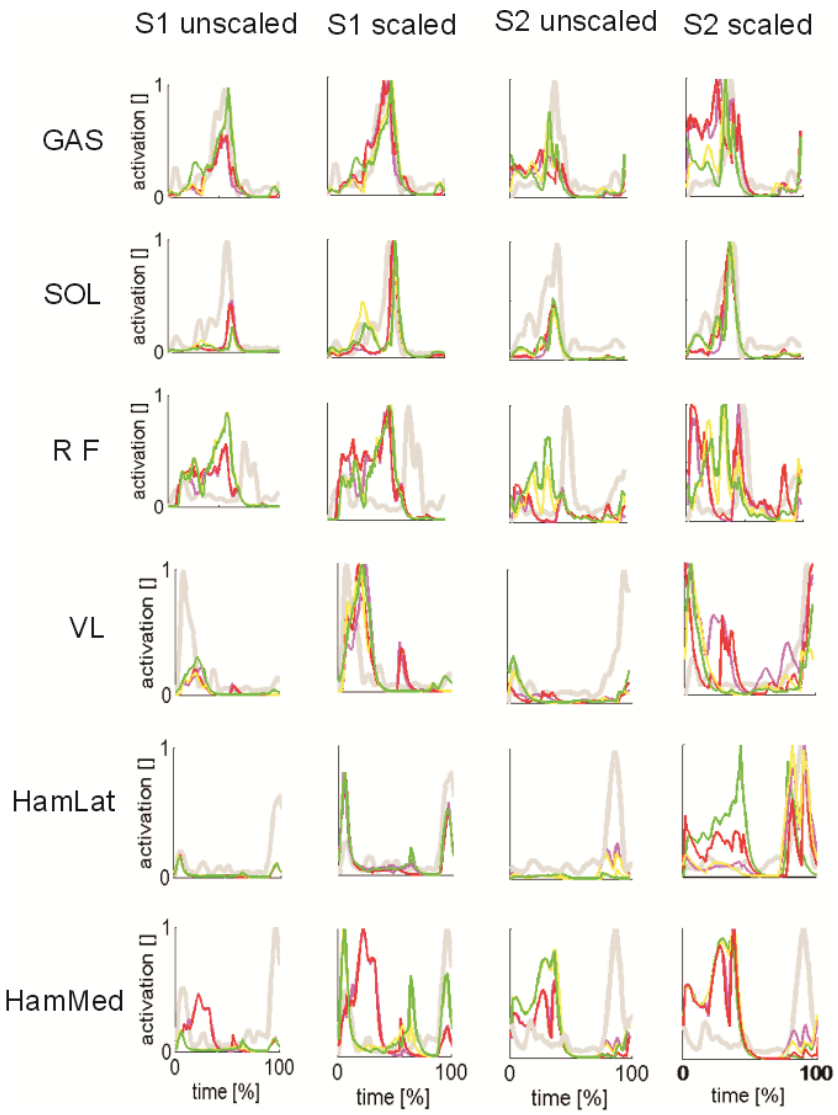

FIGURE 7.6: Predicted activations treadmill walking (4km/h) for rectus femoris (RF), lateral vastus (VL), gastrocnemius (GAS), soleus (SOL), and medial and lateral hamstrings (HamMed, HamLat) for subject 1 (S1) and subject 2 (S2). Unscaled results as well as scaled results are shown. The reference EMG is given in light grey, green: GEO-image/MT-specific, yellow: GEO-image/MT-linear, red: GEO-linear/MT-specific, magenta: GEO-linear/MT-specific.

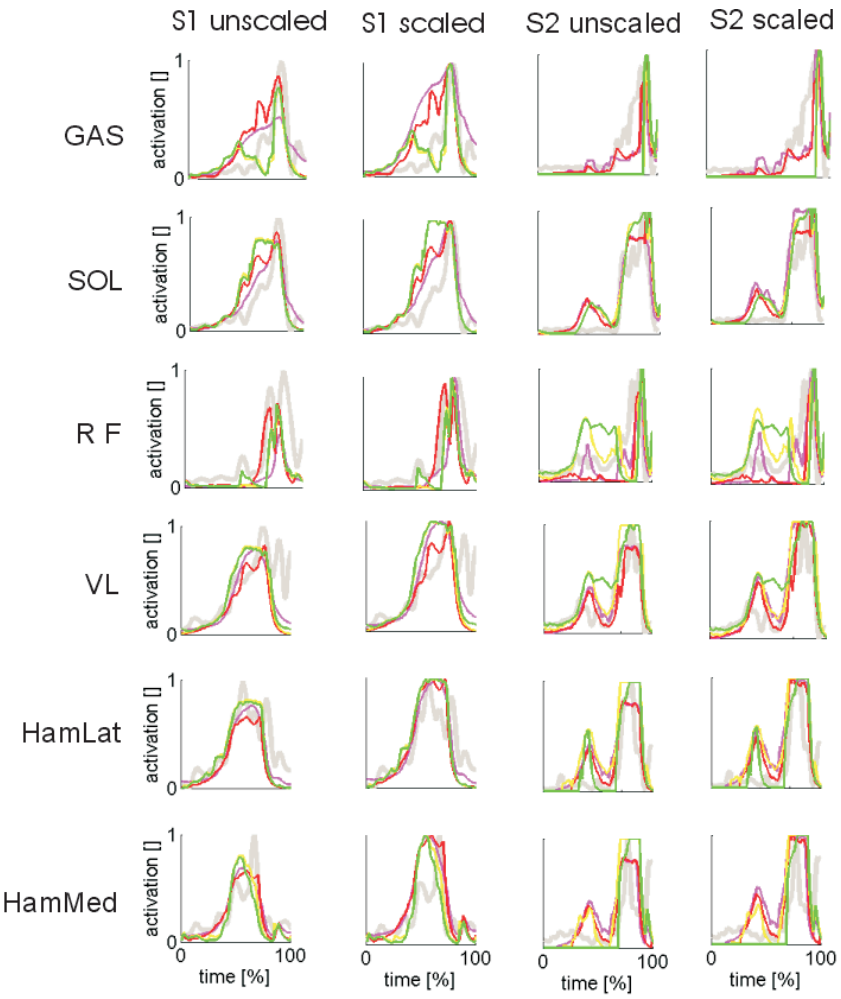

Figure 7.7: Predicted activations for countermovement jumping for rectus femoris (RF), lateral vastus (VL), gastrocnemius (GAS), soleus (SOL), and medial and lateral hamstrings (HamMed, HamLat) for subject 1 (S1) and subject 2 (S2). Unscaled results as well as scaled results are shown.The reference EMG is given in light grey, green: GEO-image/MT-specific, yellow: GEO-image/MT-linear, red: GEO-linear/MT-specific, magenta: GEO-linear/MT-specific.

Chapter 8

Conclusions and suggestions for future work

The aim of this thesis was to identify subject-specific muscle-tendon parameters of Hill-type muscle-tendon models. The focus was on the actuators of the knee joint. Dynamic motion analyses mostly rely on muscle-tendon parameters obtained from cadaver studies and these values are scaled to the subject's anthropometry. The accuracy of dynamic simulations of human motion analyses benefits from the incorporation of subject-specific estimated muscle-tendon parameters. This corresponds to functional parameter scaling.

Five contributions are made in this thesis:

1. Selection based on performance and validation of an algorithm to estimate functional knee axes of rotation using experimental data.

2. Development of an extended dynamometer setup for more accurate calculations of the knee joint reaction moments.

3. Description of the inter-dependency of the muscle-tendon parameters of the knee joint actuators.

4. Formulation of an algorithm to estimate the subject-specific muscle-tendon parameters of the knee joint actuators and its evaluation in simulation.

5. Validation of musculoskeletal models including subject-specific estimated muscle-tendon parameters of the knee joint actuators based on experimental data.

8.1 Contribution 1

The estimation of muscle-tendon parameters is based on experimental dynamometry. The estimation procedure obviously benefits from accurate experimental data as these are used to fit simulation data. However, dynamometry suffers from unreliability mainly due to misalignment between the dynamometer's axis of rotation, and the (knee) joint axis of rotation. This implies that data resulting from the standard dynamometer do not reflect the moment generated by the joint actuators around the joint's axis of rotation. To deal with this issue, the goal was to find the best estimate of the knee joint's axis of rotation which, given the marker-based positions of the segments, boils down to the estimation of a functional axis of rotation which best explains the relative motion of tibia to femur for a recorded (range of) motion. Many algorithms have been proposed in literature (e.g. [37; 41; 71; 87]), but it was not known which algorithm performed best on experimental data. Therefore, the best performing algorithms in a simulation environment ([37; 41]) were implemented and their performance was tested in an experimental environment being isokinetic dynamometry. Validation was based on the equivalent axes describing the relative displacement of tibia(bone) to femur(bone) between two positions as observed in MR-images. Additionally, geometry-based axes including the transepicondylar axis which is most frequently used (also for alignation during dynamometry), were compared to the equivalent axes. Alltogether, this resulted in the conclusion that functional axes of rotation estimated based on the sphere fitting technique of [41] are the best representations of the actual knee joint axis of rotation, and that functional axes of rotation in general are better representatives of the actual knee joint axis of rotation than geometry-based axes of rotation.

This result is important in light of any research in which knee joint kinematics and dynamics should be properly calculated, as these depend on the joint's axis of rotation.

8.2 Contribution 2

Dynamometer data are obtained via an extended setup rather than via standard dynamometry. This approach guarantees an improved accuracy of the experimental data, since a full 3D inverse dynamic analysis can be performed based on measured marker trajectories, and reaction forces and moments. The calculation of the joint dynamics rely on a model including a functional axis of rotation instead of the transepicondylar axis. It is the combination of the tracking of marker trajectories, the measurement of reaction forces and moments (which is critical to enable a 3D

inverse dynamic analysis), and the functional definition of the knee joint axis that distinguish the approach from previous extensions of a dynamometer set-up [5; 46; 55; 101].

The established improvement in accuracy was found to be in the range of 10Nm to 25Nm for isometric dynamometry. The magnitude of the improvements confirms the importance of obtaining accurate experimental measurement data, in particular in view of parameter estimation.

8.3 Contribution 3

The tendon slack length and the optimal muscle fiber length of the knee joint actuators are the most crucial muscle-tendon parameters for human motion analysis. In this thesis, it has been revealed that these parameters are not independent from each other. The inter-dependency appeared to be approximatly linear after applying a non-linear transformation of these parameters.

In its own right, this finding opens perspectives in muscle-tendon parameter scaling.

8.4 Contribution 4

The algorithm proposed in chapter 6 aims at estimating the tendon slack length and the optimal muscle fiber length of the knee joint acuators (according to the sensitivity analysis in chapter 3). The algorithm comprises two phases. The first phase results in the description of the feasible set (relying on the interdependency of the parameters) and the choice of a hot start for the local optimization in the second phase. Also, a transformation of the parameters has been introduced, different from the transformation proposed by Garner and Pandy [42]. The evaluation of the algorithm has been performed in a simulation environment. Both the effect of the initial guesses of the parameters and of measurement noise has been evaluated.

Comparison with the algorithm of Garner and Pandy [42] (in simulation) shows a pronounced higher robustness of the new algorithm to initial parameter guesses and to measurement noise.

8.5 Contribution 5

The last contribution in this thesis is the validation of the parameter estimation in an experimental environment. The validation is based on data obtained for power athletes, hence for a specific sub-

group in the population. The evaluated motions are treadmill walking, isokinetic dynamometry, and jumping. Dynamometry allows us to evaluate the performance of the knee joint acuators. Walking and jumping allow us to evaluate whether an improvement at one joint would cause reduced performance at the other joints, as joints are coupled through bi-articular muscles. The performance of models including different levels of subject-specific information have been evaluated. For walking, all models performed similarly. However, the inclusion of estimated parameters for the knee joint actuators was found to be more crucial than the inclusion of subject-specific geometric features during dynamometry and jumping for power athletes.

This work involved the first validation of MS-models including functional scaling and image-based geometry.

In contrast to the two previously presented methods of Garner and Pandy [42] and Lloyd and Besier [63], the proposed estimation procedure covers the whole process from sensitivity analysis, identifiability, validation in a simulation environment and evaluation on experimental data. Above, due to the numerical efficient formulation, only a limited set of experiments is needed in contrast to [42; 63], hence the experimental load for the subjects is also reduced.

8.6 Suggestions for future work

Many suggestions can be made concerning research in biomechanics including motion analysis. However, in light of this thesis my suggestions are the following:

- **Extending the experimental data for the parameter estimation with isokinetic (or rather non-isometric) experiments.**
  The parameter estimation procedure proposed in this thesis relies on isometric experiments. Hence no dynamics are involved. By combining isometric and isokinetic experimental data, dynamics are included and the experimental set becomes richer, and hence more information on the parameters becomes available. However, the complexity of the optimization increased, as a consequence numerical cost rises, and a last issue is the increase in the uncertainty on the measurements mainly due to the uncertainty on muscle activations. Nevertheless, the inclusion of isokinetic experiments might become essential when estimating the parameters of hip actuators, because more actuators are involved than for the knee joint.

- **Subject-specific estimation of parameters of hip and ankle actuators.**

The accuracy of dynamic motion simulations will obviously benefit from an elaborated subject-specific description. In the lower limb, the ankle and the hip joints are of particular interest. In order to enable subject-specific estimation of the actuators of these joints, the same general procedure can be followed as for the knee joint, starting with a sensitivity analysis.

The main challenge for the ankle joint will be the estimation of the ankle's axis of rotation. Some algorithms have been proposed, but none has been validated [58; 106]. As the ankle comprises a double joint, things become even more complex than for the knee joint. Moreover, the range of motion of the ankle is smaller, segments are smaller, and not all joint segments can be tracked. The design of the experimental setup can be equivalent to the design as described in chapter 5, including tracking of the kinematics and registration of reaction forces and moments. Dynamometery of ankle joint has already been shown to be unreliable [6].

The main challenges for the hip joint will be the experimental setup and the modeling of the actuators. As the hip joint has three degrees of freedom, descisions will have to be made concerning fixation, stabilization of the subject, excitation etc. The actuators are modeled as line segments. However, many actuators as e.g. the glutei have different functional zones, or bundles. The modeling approach of these models might have to be reconsidered, and every functional zone might have to be attributed different characteristics. For the modeling of the hip joint center of rotation, in fact many algorithms are available in literature, mostly these are generalizations of the algorithms for functional knee axis estimation [37; 41].

When all three lower limb joints are taken into account, the introduction of bi-articular experiments (obtaining moment-angle relation at two joints simultaneously) can also be a next step. This way, more information on bi-articular muscles can be obtained.

- **The quantification of muscle activations during experiments.**
  Muscle activations are often obtained through surface electromyography. This results in following problems: only the activation of superficial muscles can be measured, and only a qualitative measure of the actual activation is obtained which is than scaled.

  Concerning the limited number of measurable muscles, it might be valuable to investigate whether it is possible to exploit the similarity in EMG profiles of functionally related muscles

(e.g. [27; 48]).

Concerning the quantification of the activation level, theire is a problem of chosing a reference value. Therefore, instead of opting for some particular normalization procedure [43], it could be of interest to actually form an idea about the maximum activation level possible.

- **Studying the sensitivity of the force-length-velocity characteristics.**
  Results from dynamic motion analyses as reported in literature rely on different force-length-velocity characteristics. The choice for a particular one is based on the numerical efficiency. However it is not known to which extend the characteristics influence the results. Hence, a sensitivity analysis of the force-length-velocity characteristics could give proper insight in this matter.

- **Evolving towards an *in vivo* reference model.**
  My last suggestion is to gradually evolve towards subject-specific musculoskeletal modeling. Because the complete measurement campaign is rather extensive, reference models could be helpful. The next step could be the building of an *in vivo* reference model which could replace the model of Delp et al. [32]. This *in vivo* reference model can be built for example for a male, and a female for which all data are collected from experiments. Hence, geometry is image-based, muscle-tendon characteristics are functionally scaled, joint axes and centers of rotation are described functionally. When using this model, researchers or other users can in relation to geometry, focus on adapting the model for observed subject-specific abnormalities. Concerning muscle-tendon parameters the scaling of the optimal fiber length and tendon slack length should rely on the intrinsic correlation between these parameters while respecting the operating ranges.

Bibliography

[1] Ackerman M., van den Bogert AJ. Optimality principles for model-based prediction of human gait. *J Biomech*, vol. 43, pp. 1055-1060, 2010.

[2] Ackland DC., Kin Y-C., Pandy MG. Sensitivity of model predictions of muscle function to changes in moments arms and muscle-tendon properties: a Monte-Carlo analysis. J Biomech, vol. 45, pp. 1463-1471, 2012.

[3] Akbarshahi M., Schache AG., Fernandez JW., Baker R., Banks S., Pandy MG. Non-invasive assessment of soft-tissue artifacts and its effect on knee joint kinematics during functionally activity. *J Biomech*, vol. 43, pp. 1292-1301, 2010.

[4] Anderson F., Pandy MG. Static and dynamic optimization solution for gait are practically equivalent. *J Biomech*, vol. 34, pp. 153-161, 2001.

[5] Arampatzis A., Karamanidis K., De Monte G., Stafilidis S., Morey-Klapsing G., Bruggemann GP, Differences between measured and resultant joint moments during voluntary and artificially elicited isometric knee extension contractions. *Clin Biomech*, vol. 19, pp. 277-283, 2004.

[6] Arampatzis A., Morey-Klapsing G., Kramanidis K., De Monte G., Stafilidis S., Bruggemann GP. Differences between measured and resultant joint moments during isometric contractions at the ankle joint. *J Biomech*, vol. 38, pp. 885-892, 2005.

[7] Arnold EM., Ward SR., Lieber RL., Delp SL. A model of the lower limb for analysis of human movement. *Ann Biomed Eng*, vol. 38, pp. 269-279, 2010.

[8] Arnold EM., Delp SL. Fiber operating lengths of human lower limb muscles during walking. *Philos Trans R Soc Lond B Biol Sci*, vol. 366, pp. 1530-1539, 2011.

[9] Atkinson G., Nevill AM. Statistical methods for assessing measurement error (reliability) in variables relevant to sports medicine. *Sports Med*, vol. 26, pp. 217-238, 1998.

[10] Babault N., Pousson M., Michaut A., Ballay Y., Van Hoecke Y.. EMG activity and voluntary activation during knee-extensor concentric torque generation. *Eur J Appl Physiol*, Vol. 86, pp. 541-547, 2002.

[11] Balsa-Canto E., Alonso AA., Banga JR. Computational procedures for optimal experimental design in biological systems. *IET Syst Biol*, vol. 2, pp. 163-172, 2007.

[12] Balsa-Canto E., Alonso AA., Banga JR. An iterative identification procedure for dynamic modeling of biomechanical networks. *BMC Syst Biol*, vol. 4, 2010.

[13] Bilodeau M., Schindler-Ivens S., Williams DM., Chandran R., Sharma SS. EMG frequency content changes with increasing force and during fatigue in the quadriceps femoris muscle of men and women. *J Electromyogr Kines*, vol. 13, pp. 83-92, 2003.

[14] Biodex.com, december 2013, *www.biodex.com*.

[15] Boyd S., Vandenberghe L., editors. Convex optimization. *Cambridge University Press*, 2004.

[16] Brand RA., Pederson DR., Friedrich JA. The sensitivity of muscle force predictions to changes in physiologic cross-sectional area. *J Biomech*, vol. 19, pp. 589-596, 1986.

[17] Bray J., Cragg P., Macknight A., Mills R. Human Physiology. *Blackwell Science, Ltd.*, fourth edition, 1999.

[18] Bruggemann JP., Arampatzis A., Emrich F., Potthast W. Biomechanics of double transtibial amputee sprinting using dedicated sprinting prostheses. *Sports Technology*, doi 10.1002/jst.63.

[19] Burden AM., Trew M., Baltzopoulos V. Normalisation of gait EMGs: a re-examination. *J Electromyogr Kines*, vol. 13, pp. 519-532, 2003.

[20] Byrd RH, Nocedal J., Waltz RA. KNITRO: an integrated package for nonlinear optimization. In: Large-scale nonlinear optimization. New York: Springer-Verlag, pp. 3559, 2006.

[21] Cerveri P., Pedotti A., Ferrigno G. Robust recovery of human motion from video using Kalman filters and virtual humans. *Hum Mov Sci*, vol. 41, pp. 377-404, 2003.

[22] Cheze L., Fregly BJ., Dimnet J. Determination of joint functional axes from noisy marker data using finite helical axis. *Hum Mot Sci*, vol. 17, pp. 1-15, 1998.

[23] Chiari L., Della Croche H., Leardini A., Cappozzo A. Human movement analysis using stereophotogrammetry. Part2: Instrumental errors. *Gait Posture*, vol. 21, pp. 197-211, 2005.

[24] Craig JJ. Introduction to robotics: mechanics and control. *Addison-Wesley.* Reading, 1986.

[25] Crowninshield RD., Brand RA. A physiologically based criterion of muscle force prediction in locomotion. *J Biomech*, vol. 14, pp. 793-801, 1981.

[26] Cutts A.. Sarcomere length changes in muscles of the human tigh during walking. *J Anat*, vol. 166, pp. 77-84, 1989.

[27] Davis B., Vaughan C. Phasic behavior of EMG signals during gait: use of multivariate statistics. *J Electromyogra Kinesiol*, vol 3, pp. 51-60, 1993.

[28] De Groote F., De Laet T., Jonkers I., De Schutter J. Kalman smoothing improves the estimation of joint kinematics and kinetics in marker-based human gait analysis. *J Biomech*, vol. 41, pp. 3390-3398, 2008.

[29] De Groote F., Van Campen A., Jonkers I., De Schutter J. Sensitivity of dynamic simulations of gait and dynamometer experiments to Hill muscle parameters of knee flexors and extensors. *J Biomech*, vol. 43, pp. 1876-1883, 2010.

[30] De Groote F., Demeulenaere B., Swevers J., De Schutter J., Jonkers I. A physiology based inverse dynamic analysis of musculotendon forces during human motion. *CMBBE*, vol. 15, pp. 1093-1102 ,2012.

[31] Della Croce U., Leardini A., Chiari L., Capozzo A. Human movement analysis using stereophotogrammetry Part 4: assessment of anatomical landmark misplacement and its effects on joint kinematics. *Gait Posture*, vol. 21, pp. 226-237, 2005.

[32] Delp S., Loan P., Hoy M., Zajac F., Topp E., Rosen J. An interactive graphics-based model of the lower extremity to study orthopeadic surgical procedures. *IEEE TBME*, vol. 37, pp. 757-767, 1990.

[33] Delp SL., Anderson FC., Arnold AS., Loan JP., Habib A., John CT., Guendelman E., Thelen DG. OpenSim: opensource software to create and analyze dynamic simulations of movement. *IEEE TBME*. vol. 54, pp. 1940-1950, 2007.

[34] Drouin JM., Valovich-McLeod TC., Shultz SJ., Gansneder BM., Perrin DH. Reliability and validity of the Biodex system 3 pro isokinetic dynamometer velocity, torque and position measurement. *Eur J Appl Physiol*, vol. 91, pp. 22-29, 2004.

[35] Eckhoff D.G., Dwyer T.F., Bach J.M., Spitzer V.M., Reinig K.D.. Three-Dimensional Morphology of the Distal Part of the Femur Viewed in Virtual Reality. *J Bone Joint Surg*, vol. 83, pp. 43-50, 2001.

[36] Edwards WB., Taylor D., Rudolphi TJ., Gillette JC., Derrick TR. Effects of stride length and running mileage on a probabilistic stress fracture model. *Med Sci Sports Exerc*, vol. 41, pp. 2177-2184, 2009.

[37] Ehrig RM., Taylor WR., Duda GN., Heller MO. A survey of formal methods for determining functional axes. *J Biomech*, vol. 40, pp. 2150-2157, 2007.

[38] Fregly BJ., Boninger ML., Reinkensmeyer DJ. Personalized neuromusculoskeletal modeling to improve treatment of mobility imparments: a perspective from European research sites. *J Neuroeng Rehabil*, vol. 30, pp. 757-767, 2012.

[39] Friedrich JA., Brand RA. Muscle fibre architecture in the human lower limb. *J Biomech*, vol. 23, pp. 91-95, 1990.

[40] Galban CJ., Maderwald S., Uffmann K., de Greiff A., Ladd ME. Diffusive sensitivity to muscle architecture: a magnetic resonance diffusion tensor imaging study of the human calf. *Eur J Appl Physiol*, vol. 93, pp. 253-262, 2004.

[41] Gamage SSHU., Lasenby J. New least squares solutions for estimating the average centre of rotation and the axis of rotation. *J Biomech*, vol. 35, pp. 87-93, 2002.

[42] Garner BA., Pandy MG, Estimation of musculotendon properties in the human upper limb. *Ann Biomed Eng*, vol. 31, pp. 207-220, 2003.

[43] Halaki M., Ginn K. Normalization of EMG signals: to normalize or not to normalize and what to normalize to? Computational Intelligence in Electromyography Analysis - A Perspective on Current Applications and Future Challenges, Dr. Ganesh R. Naik (Ed.), ISBN: 978-953-51-0805-4, InTech, 2012, DOI: 10.5772/49957.

[44] Halvorson K., Lesser M., Lundberg A. a new method for estimating the axis of rotation and the center of rotation. *J Biomech*, vol. 32, pp. 1221-1227, 1999.

[45] Heller MO., Mehta M., Taylor WR, Kim DY., Speirs A., Duda GN, Perka K. Influence of prosthesis design and implantation technique on implant stresses after cementless revision THR. *J Orthop Surg Res*, vol. 13, pp. 6-20, 2011.

[46] Herzog W., The relation between the resultant moments at a joint and the moments measured by an isokinetic dynamometer. *J. Biomech*, vol. 21, pp. 5-12, 1988.

[47] Herzog W., Leonard TR. Force enhancement following stretching of skeletal muscle: a new mechanism. *J Exp Biol*, vol. 205, pp. 1275-1283, 2002.

[48] Hof AL., Elzinga H., Grimmius W., Halbertsma JPK. Speed dependence of averaged EMG profiles in walking. *Gait Posture*, vol. 16, pp. 78-86.

[49] Hoy MG., Zajac FE., Gordon ME. A musculoskeletal model of the human lower extremity: the effect of muscle, tendon, and moment arms on the moment-angle relationship of musculotendon actuators at the hip, knee, and ankle. *J Biomech*, vol. 23, pp. 157-169, 1990.

[50] Huxley AF. Muscle structure and theories of contraction. *Prog. Biophys. Chem.*, vol. 7, pp. 255-318, 1957.

[51] Impellizzeri F., Bizzine M., Rampinini E., Cereda F., Maffiuletti NA. Reliability of isokinetic strength imbalance ratios measured using Cybex NORM dynamometer. *Clin Physiol Imaging*, vol. 28, pp. 113-119, 2008.

[52] Jansen K., De Groote F., Massaad F., Meyns P., Duysens J., Jonkers I., Similar muscles contribute to horizontal and vertical acceleration of center of mass in forward and backward walking: implications for neural control. J Neurophysiol, vol. 107, pp. 3385-3395, 2012.

[53] Johal P., Williams A., Wragg P., Hunt D., Gedroyc W. Tibio-femoral movement in the livingknee. A study of weight bearing and non-weight bearing knee kinematics using 'interventional' MRI. *J Biomech*, vol. 38, pp. 269-276, 2005.

[54] Julier SJ., Uhlmann JK. Unscented filtering and nonlinear estimation. *Proc IEEE*, vol. 92, pp. 401-422, 2004.

[55] Kaufman KR., An K-N., Chao EYS. A comparison of intersegmental joint dynamics to isokinetic dynamometer measurements. *J Biomech*, vol. 28, pp. 1243-1256, 1998.

[56] Klein Horsman MD., Koopman HFJM., van der Helm FCT., Poliacu Prose L., Veeger HEJ. Morphological muscle and joint parameters for musculoskeletal modelling of the lower extremity. *Clin Biomech*, vol. 22, pp. 239-247, 2007.

[57] Leardini A., Chiari L., Della Croce H., Cappozzo A. Human movement analysis using stereophotogrammetry. Part3: Soft tissue artifact assessment and compensation. *Gait Posture*, vol. 21, pp. 212-225, 2005.

[58] Leitch J., Stebbins HJ., Zavatsky AB. Subject-specific axes of the ankle joint complex. *J Biomech*, vol. 43, pp. 2923-2928, 2010.

[59] Lieber RL. Skeletal Muscle Structure and Function: Implications for Rehabilitation and Sports Medicine. *Willians and Wilkins*, 1992.

[60] Lieber RL., Loren GJ., Friden J. In vivo measurement of human wrist extensor muscle sarcomere length changes. *J Neurophysiol*, vol. 71, pp. 874-881, 1994.

[61] Lin DC., Nichols TR. Parameter estimation in a crossbridge muscle model. *Trans ASME*, vol. 125, pp. 132-140, 2003.

[62] Ljung L. System identification: theory for the user. Prentice-Hall, Inc. 1999.

[63] Lloyd DG., Besier TF. An EMG-driven musculoskeletal model to estimate muscle forces and knee joint moments in vivo. *J Biomech*, vol. 36, pp. 765-776, 2003.

[64] Luchetti L, Cappozzo A., Cappello A., Della Croche H. Skin movement assessment and compensation in the estimation of knee-joint kinematics. *J Biomech*, vol. 31, pp. 977-984, 1998.

[65] Lund H., Sondergaard K., Zachariassen T., Christensen R., Bulow P., Henriksen M., Bartels EM., Danneskiold-Samsoe B., Bliddal H. Learning effect of isokinetic measurements in healthy subjects, and reliabililty and comparability of Biodex and Lido dynamometers. *Clin Physiol Funct Imaging*, vol. 25, pp. 75-82, 2005.

[66] MacWilliams BA. A comparison of four functional methods to determine centers and axes of rotation. *Gait Posture*, vol. 28, pp. 673-679, 2008.

[67] Maganaris CN., Paul JP. Tensile properties of the in vivo human gastrocnemius tendon. *J Biomech*, vol. 35, pp. 1639-1646, 2002.

[68] Millard M., Uchida T., Seth A., Delp SL. Flexing computational muscle: modeling and simulation of musculotendon dynamics. *J Biomech Eng*, vol. 135, 021004-1 - 021004-11, 2013.

[69] Modenese L., Phillips ATM., Bull AMJ. An open source lower limb model: Hip joint validation. *J Biomech*, vol. 44, pp. 2185-2193, 2011.

[70] Moles CG., Mendes P., Banga JR. Parameter Estimation in Biochemical Pathways: A comparison of global optimization methods. *Genome Res*, vol. 13, pp. 24672474, 2003.

[71] Most E., Axe J., Rubash H., Li G. Sensitivity of the knee joint kinematics calculation to selection of flexion axes. *J Biomech*, vol. 37, pp. 1743-1748, 2004.

[72] Mungiole M., Martin PE. Estimating segment inertial properties: comparison of magnetic resonance imaging with existing methods.*J. Biomech*, vol. 23, pp. 1039-1046, 1990.

[73] Nene A., Byrne C., Hermens H. Is rectus femoris really a part of quadriceps? Assessment of rectus femoris function during gait in able-bodied adults. *Gait Posture*, vol. 20, pp. 1-13, 2004.

[74] Neptune RR., Wright IC., van den Bogert AJ. The influence of orthotic devices and vastus medialis strength and timing on patellofemoral loads during running. *Clin Biomech*, vol. 15, pp. 611-618, 2000.

[75] Neptune RR., Kautz SA. Muscle activation and deactivation dynamucs: the governing properties in fast cycling human movement performance? *Exerc Sports Sci Rev*, vol. 29, pp. 76-81, 2001.

[76] Nocedal J., Wright SJ. Numerical optimization. *Springer*, 2000.

[77] Out L., Vrijkotte TGM., van Soest AJK., Bobbert MF. Influence of the parameters of a human triceps surae model on the isometric torque-angle relationship. *J Biomech Eng*, vol. 118, pp. 17-25, 1996.

[78] Pipeleers G., Demeulenaere B., Jonkers I., Spaepen P., Van der Perre G., Spaepen A., Swevers J., De Schutter J. A convex optimization approach to dynamic musculoskeletal analysis. *OPTE*, vol. 9, pp. 213-238, 2008.

[79] Raasch C., Zajac FE., Ma B., Levine W. Muscle coordination of maximum-speed pedaling. *J Biomech*, vol. 30, pp. 595-602, 1997.

[80] Raikova RT., Prilutsky BI. Sensitivity of predicted muscle forces to parameters of the optimization-based human leg model revealed by analytical and numerical analysis. *J Biomech*, vol. 34, pp. 1243-1255, 2001.

[81] Redl C., Gfoehler M, Pandy MG. Sensitivity of muscle force estimates to variations in muscle-tendon properties. *Hum Mov Sci*, vol. 26, pp. 306-319, 2007.

[82] Sangnier S., Tourny-Chollet C. Comparison of the decrease in strength between hamstrings and quadriceps during isokinetic fatigue testing in semiprofessional soccer players. *Int J Sports Med*, vol. 28, pp. 952-957, 2007.

[83] Schenkendorf R., Kremling A., Mangold M. Optimal experimental design with the sigma point method. *IET Syst Biol*, vol. 3, pp. 10-23, 2009.

[84] Scheys L., Jonkers I., Loeckx D., Maes F., Spaepen A., Suetens P. Image based musculoskeletal modeling allows personalized biomechanical analysis of gait. *Lecture Notes in Computer Science*, vol. 4072, pp. 58-66, 2006.

[85] Scheys L., Spaepen A., Suetens P., Jonkers I. Calculated moment-arm and muscle-tendon lengths during gait differ substantially using MR based versus rescaled generic lower-limb musculoskeletal models. *Gait Posture*, vol. 28, pp. 640-648, 2008.

[86] Scheys L., Desloovere K., Spaepen A., Suetens P., Jonkers I. Calculating gait kinematics using MR-based kinematic models. *Gait Posture*, vol. 33, pp. 158-164, 2011.

[87] Schwartz MH., Rozumalski. A new method for estimating joint parameters from motion data. *J Biomech*, vol. 38, pp. 107-116, 2005.

[88] Shrout PE., Fleiss JL. Intraclass correlations: uses in assessing rater reliability. *Psychiol Bull*, vol 86, pp. 420-428, 1979.

[89] Schutte L. Using musculoskeletal models to explore strategies for improving performance in electrical stimulation-induced leg cycle ergonometry. *Stanford university*, 1993.

[90] Schutte LM., Rodgers MM., Zajac FE., Glaser RM. Improving the efficacy of electrical stimulation-induced leg cycle ergometry: an analysis based on a dynamic musculo-skeletal model. *IEEE Trans Rehabil Eng*, vol. 1, pp. 109-125, 1993.

[91] Scovil CY., Ronsky JL. Sensitivity of a Hill-based muscle model to perturbations in model parameters. *J Biomech*, vol. 39, pp. 2055-2063, 2006.

[92] Sheehan FT., The finite helical axis of the knee joint (a non-invasive in vivo study using fast-PC MRI). *J Biomech*, vol. 40, pp. 1038-1047, 2007.

[93] Shultz R., Kedgley AE., Jenkyn TR. Quantifying skin motion artifact error of the hindfoot and the forefoot marker cluster with the optical tracking of a multi-segment foot model using single-plane fluoroscopy. *Gait Posture*, vol. 34, pp. 44-48, 2011.

[94] Soderkvist I., Wedin P-A. Determining the movements of the skeleton using well-configured markers. *J Biomech*, vol. 26, pp. 1473-1477, 1993.

[95] Sole G., Hamren J., Milosavljevic S., Nicholson H., Sullivan SJ. Test-retest reliability of isokinetic knee extension and flexion. *Arch Phys rehabil*, vol. 88, pp.626-631, 2007.

[96] Spoor C., Veldpaus F. Rigid body motion calculated from spatial coordinates of markers. *J Biomech*, vol. 13, pp. 929-936, 1980.

[97] Symons TB., Vandervoort AA., Rice CL., Overend TJ., Marsh GD. Reliability of a single-session isokinetic and isometric strength measurement protocol in older men. *J Gerontol A Biol Sci Med Sci.*, vol. 60A, pp. 114-119, 2005.

[98] Taddei F., Martelli S., Valente G., Leardini A., Benedetti MG., Manfrini M., Viceconti M. Femoral loads during gait in a patient with massive skeletal reconstruction. *Clin Biomech*, vol. 27, pp. 273-280, 2012.

[99] Thelen DG. Adjustment of muscle mechanics model parameters to simulate dynamic contractions in older adults. *J Biomech Eng*, vol. 125, pp. 70-77, 2003.

[100] Tsai L-C., Colletti PM., Powers CM. Magnetic resonance imaging-measured muscle parameters im-proved knee moment prediction of an EMG-driven model. *Med Sci Sports Exerc*, vol. 44, pp. 305-312, 2012.

[101] Tsaopoulos DE., Baltzopoulos V., Richards PJ., Maganaris CN. Mechanical correction of dynamometer moment for the effects of segment motion during isometric knee-extension tests. *J Appl Physiol.*, vol. 111, pp. 68-74, 2011.

[102] Van Campen A. Sensitiviteit van dynamische simulaties van gaan en dynamometrische experimenten voor spier-peesparameters. *Unpublished master thesis*, KU Leuven, 2009.

[103] Van Campen A., De Groote F., Bosmans L., Scheys L., Jonkers I., De Schutter J. Functional knee axis based on isokinetic dynamometry data: Comparison of two methods, MRI validation, and effect on knee joint kinematics. A. Van Campen, F. De Groote, L. Bosmans, L. Scheys, I. Jonkers, J. De *J Biomech*, vol. 44, pp. 2595-2600, 2011.

[104] Van Campen A., De Groote F., Jonkers I., De Schutter J. An extended dynamometer set-up to improve the accuracy of knee joint moment assessment. *TBME*, vol. 66, pp. 1202-1208, 2013.

[105] Van Campen A., Pipeleer G., De Groote F., Jonkers I., De Schutter J. A new method for estimating subject-specific muscle-tendon parameters of the knee joint actuators: a simulation study. *Int J Numer Methods Eng* , submitted for review.

[106] van den Bogert A., Smith GD., Nigg BM. In vivo determination of the anatomical axes of the ankle joint compex: an optimization approach. *J Biomech*, vol. 27, pp. 1477-1488, 1994.

[107] van den Bogert A., Gerritsen KGM., Cole GK. Human muscle modelling from a user's perspective. *J Electromyogr Kines*, vol. 8, pp. 119-124, 1998.

[108] van den Bogert A., Ackermann M. Effect of a prosthetic limb on sprint running performance. Cape Town: International Society of Biomechanics. 2009.

[109] van den Bogert A., Reinschmidt C., Lundberg A. Helical axes of skeletal knee joint motion during running. *J Biomech*, vol. 41, pp. 1632-1638, 2008.

[110] Van den Hof PMJ., Van Doren JFM., Douma SG. Identification of parameters in large scale physical model structures, for the purpose of model-based operations. *Model-based control.* Springer, 125-143, 2009.

[111] Walker PS., Rovick JS., Robertson DD. The effect of knee brace hinge design and placement on joint mechanics. *J Biomech*, vol. 21, pp. 965-974, 1988.

[112] Ward SR., Eng CM., Smallwood LH., Lieber RL. Are current measurements of lower extremity muscle architecture accurate? *Clin Orthop Relat Res*, vol. 467, pp. 1074-1082, 2009.

[113] Wickiewicz TL., Roy RR.,Powell PL., Edgerton VR. Muscle architecture of the human lower limb. *Clin Orthop Rel Res*, vol. 179, pp. 275-283, 1983.

[114] Williams WO. Huxley's model of muscle contraction with compliance. *J Elast*, vol. 105, pp. 365-380, 2011.

[115] Winby CR., Lloyd DG.,Kirk TB. Evaluation of different analytical methods for subject-specific scaling of musculotendon parameters. *J Biomech*, vol. 41, pp. 1682-1688, 2008.

[116] Winters J., Stark L. Estimated mechanical properties of synergistic muscle involved in movements of a variety of human joints. *J Biomech*, vol. 21, pp. 1027-1041, 1988.

[117] Winters TM., Takahashi M., Lieber RL., Ward SR. Whole muscle length-tension relationships are accurately modeled as scaled sarcomeres in rabbit hindlimb muscles. *J Biomech*, vol. 44, pp. 109-115, 2011.

[118] Wu G., Siegler S., Allard P., Kirtley C., Leardini A., Rosenbaum D., Whittle M., D'Lima DD., Cristofolini L., Witte H., Schmid O., Stokes I. ISB recommendation on definitions of joint coordinate system of various joints for the reporting of human joint motion - part 1: ankle, hip and spine. *J Biomech*, vol. 35, pp. 543-548, 2002.

[119] Yamaguchi GT., Zajac FE. A planar model of the knee joint to characterize the knee extensor mechanism. *J Biomech*, vol. 22, pp. 1-10, 1989.

[120] Zajac FE. Muscle and tendon: properties, models, scaling, and application to biomechanics and motor control. *Crit Rev Biomed Eng.*, vol. 17, pp. 359-411, 1989.

List of publications

1. Van Campen A., De Groote F., Van Rossom S., Bosmans L., Jonkers I., De Schutter J. The added value of the estimation of subject-specific muscle-tendon parameters of the knee joint actuators in musculoskeletal modelling: two case studies. *Journal of Biomechanics*.

2. Van Campen A., Pipeleers G., De Groote F., De Schutter J. A new method for estimating subject-specific muscle-tendon parameters of the knee joint actuators: a simulation study. *Numerical methods in biomedical engineering*.

3. Bosmans L., Valente G., Wesseling M., Van Campen A., De Groote F., De Schutter J., Jonkers I. Sensitivity of predicted muscle forces during gait to anatomical variability in musculotendon geometry. *Journal of Biomechanics*.

4. Van Campen A., De Groote F., Jonkers I., De Schutter J. An extended dynamometer set-up to improve the accuracy of knee joint moment assessment. *IEEE Transaction on Biomedical Engineering*, vol. 60, pp. 1202-1208, 2013.

5. Van Campen A., De Groote F., Bosmans L., Scheys L., Jonkers I., De Schutter J. Functional knee axis based on isokinetic dynamometry data: comparison of two methods, MRI validation, and effect on knee joint kinematics. *Journal of Biomechanics*, vol. 44, pp. 2595-2600, 2011.

6. De Groote F., Van Campen A., Jonkers I., De Schutter J. Sensitivity of dynamic simulations of gait and dynamometer experiments to Hill muscle model parameters of knee flexors and extensors. *Journal of Biomechanics*, vol. 43, pp. 1876-1883, 2010[1].

[1] *According to the master thesis of Anke Van Campen, KU Leuven, 2009*